Al-Mukhtar Journal of Basic Sciences

Volume
Issue
2023

Published by OMU

Al-Mukhtar Journal of Basic Sciences

Peer-reviewed scientific journal, Volume Twenty-Two, Issue Two, 2023

Published by Omar Al-Mukhtar University, Al-Bayda, Libya

A peer-reviewed journal published by Omar Al-Mukhtar University,

Al Bayda, Libya

Peer-reviewed scientific journal, Volume Twenty-Two, Issue Two, 2023

Email: ljbs.sci@omu.edu.ly

EDITORS & STAFF

Al-Mukhtar Journal of Basic Sciences 21: (2), 2023

Al-Mukhtar Journal of Basic Sciences 21 (2): 01-08, 2023
Doi: https://doi.org/10.54172/5zhts957

Research Article **Open Access**

Phytochemical Screening and Antibacterial Activity of Moringaoleifera Leaf Extract Western Libya

Safa E. Rahuma[1], Munira M. Ashrif [*2]

***Corresponding author:** m.ashrif@zu.edu.ly, Department of Chemistry, Faculty of Science, University of Zawia, Zawia, Libya.

Second Author: safaelta-beb@gmail.com Department of Chemistry, Faculty of Education Zaltan, Sabratha University, Zaltan, Libya.

Received:
20 December 2022

Accepted:
24 October 2023

Publish online:
31 December 2023

Abstract

Moringa oleifera (M. oleifera) is one of the Moringaceae family. M. oleifera plant parts retain a precious pharmacological effect. Its leaves are utilized commonly because of having enormous nutrients as nutraceuticals. Moreover, its compresses various effects such as biological and antimicrobial effect as antibacterial or antifungal. Additionally, M. oleifera investigationin was carried out either in vivo or in vitro to conclude that their leaves component has pharmacological effect. This current study had confirmed therapeutic effect of Moringa Oleifera leaf extract and its antibacterial activity. There is critical need for more advanced research about use and pharmaceutical effects of Moringa Oleifera leaves in improvement of various drugs and useful foods. This study aimed to investigate phytochemical ingredients and antibacterial effect of Moringa Oleifera leaf extract and the uses of Moringa Oleifera leaf extract either traditionally or pharmacologically conclouded.

Keywords: *Moringaoleifera*, Antibacterial activity, Phytochemical screening, Libya.

INTRODUCTION

The drumstick tree, or *Moringaoleifera* Lam., is a member of the Moringaceae family and is extensively dispersed in various regions, including tropical and desert nations, as well as in India and Africa. It was primarily used for food and medicine (Al_husnan & Alkahtani, 2016). *Moringaoleifera* has numerous qualities that may be used for food, medicine, and other industrial and home applications (Falowo et al., 2018; Padayachee & Baijnath, 2020), particularly its leaves, which may be eaten raw, roasted, or dried and kept for a long time without losing any of their nutritional value. In addition to using the leaves for food and feed, they may also be used as functional foods or nutraceuticals since they naturally contain phytochemicals such as flavonoids, carotenoids, and glucosinolates (Amaglo et al., 2010; Sultana et al., 2009). The main phytochemicals found in moringa leaves are astragalin, isoquercetin, and crypto-chlorogenic acid, which have anti-oxidant, anti-hypertension, and anti-inflammation characteristics (Verma et al., 2009; Vongsak et al., 2012).

Based on the bioactive components and their antioxidant activity, several in vitro experiments have largely supported the biological activity of these plant extracts (Leone et al., 2015; Sultana et al., 2009). Its strong antioxidant properties are principally brought on by its high phenolic content. Due to these therapeutic advantages, several pharmaceutical preparations from this plant have been manufactured and sold in both the Indian and global markets.(Mehra et al., 2020; Sahakitpichan et al., 2011) Different sections of *M. oleifera* have antibacterial potentials that can be used to purify

water, eliminate biofilm threats, and eradicate pathogenic microbes. The long-term use of *M. oleifera* and its ethno-pharmacological characteristics have proven its safety. *M. oleifera* has also been employed for bio-enhancement and as nanoparticles in medication administration in addition to its antibacterial action (Arora et al., 2013). Fidrianny et al. study mentioned that *M. oleifera* is commonly named Sanjana and drumstick. The name Moringa originated from murungai; a Tamil word that means twisted pod (Dhakad et al., 2019; Fidrianny et al., 2021) study illustrated that the cultivation of Moringa has different reasons according to its nutritional content or medicinal uses (Djemoui et al., 2019). *M. oleifera* has medicinal effects documented by (Djemoui et al., 2019). study, such as hypoglycemic effect, antioxidant, antibacterial, antifungal, and wound healing due to anti-inflammatory activity (Djemoui et al., 2019). (Amaglo et al., 2010) reported that the leaves, in particular, can be used in a salad, roasted, or kept as dry powder for a prolonged time without losing nutritive constituents (Amaglo et al., 2010).

Moringa leaves were reported by (Maheshwari et al., 2014). to have elevated amounts of protein that could be utilized as food. Also, they mentioned that *Moringa oleifera* contains a high amount of provitamin A.(Tshabalala et al., 2020). traced the source of the cardiovascular benefit and body energizing to the omega-3 and omega-6 polyunsaturated fatty acid content of Moringa. It can be used for obese patients due to low calorific value (Kashyap et al., 2022; Maheshwari et al., 2014)

They also illustrated calcium contents and digestible protein that is higher than milk. (Kasolo et al., 2010). mentioned moringa leaves' high content of potassium, magnesium, and copper. Iron content is 28 times of spinach, proved (Fuglie, 1999; Kasolo et al., 2010). Interestingly, Mbikay approved that fat-soluble vitamins like D and E and water-soluble like folic acid, nicotinic acid, and vitamin care also exist in *M. oleifera* (Mbikay, 2012). Stevens et al. mentioned that leaves are not toxic when taken in large amounts, so it is found to be safer and healthier for consumption (Stevens et al., 2013). Bacterial species develop drug resistance to common antibacterial agents. So, medicinal plants such as Moringa leaves could be used as alternative treatments for infectious diseases (Luqman et al., 2012).

Rios & Recio's studies reported the need for more studies on the antibacterial activity of essential oils or compounds like alkaloids, flavonoids, diterpenes, and triterpenes to justify the use of medicinal plants (Rios & Recio, 2005), while Abdallah mentioned that metabolites of *Moringa oleifera* leaves, such as alkaloids, flavonoids, and saponins have wonderful pharmacological effects as antibacterial and anti-microbial properties and interestingly as anticancer on (Berkovich et al., 2013). study (Abdallah, 2011; Berkovich et al., 2013).

MATERIALS AND METHODS

Collection and Identification of Plant Material

Moringaoleifera tree leaves were collected. The leaves were washed under distilled water for dust and foreign particle removal. After that, the leaves were air-dried in an oven at 60ºC. The dried leaves were added to a mixer to be ground into fine powder. The fine powder was stored in a refrigerator to avoid heat and light exposure and kept for further use.

Preparation of Plant Material

About 10g of the fine powdered *Moringaoleifera* leaves were suspended in 100 mL of ethanol and shaken well. The suspensions were kept at room temperature for 24 hours. The suspensions were then filtered. The solvent was removed by heat treatment at 80 ºC to concentrate the extract. The extracts were stored in a refrigerator at 4ºC for further analysis (Abadallah & Ali, 2019).

Phytochemical Screening

The collected plant extracts were subjected to qualitative phytochemical analysis for identification of various bioactive chemical constituents (alkaloids, volatile oils, saponins, flavonoids, steroids, tannins, and terpenoids) conducted using standard laboratory methods as described by (Edeoga et al., 2006; Sofowora, 1993)**.**

Test Isolates

Clinical *Staphylococcus aureus*, *Streptococcus pyogenes*, and *Pseudomonas aeruginosa* isolates were collected for testing the antibacterial activity of *Moringaoleifera*. As described by Chees brough, gram staining and microbiological analysis were used in recognizing the isolates by utilizing differential media and biochemical tests.

Antibacterial activity testing

0.1 ml of each organism culture was inoculated onto the plates' surface by a sterile swab stick. The plates were incubated for 24 hours at 37ºC, after which the inhibition zones were calculated using a meter ruler.

All the experiments were repeated three times, and the mean was recorded.

RESULTS

Phytochemical Screen

1. Tannins**:** A green color and gelatinous precipitate resulted upon adding 1 ml of 1% Lead acetate to 1 ml of the moringa leaf extract in a test tube. This result confirmed the existence of tannins.
2. Saponins: Durable white precipitate resulted when 1-3 ml of mercury chloride was added to 5 ml of leaf extract which was judged as an indicator of saponins existence.
3. Flavonoids: A yellow shade that signified flavonoids resulted when moringa leaf extract was added to diluted ammonia and concentrated sulphuric acid.
4. Terpenoids (Salkowskitest): No brown color resulted when 1 ml of leaf extract was added to chloroform, one drop of concentrated sulphuric acid, and one drop of anhydrous acetic acid.
5. Resins: Turbidity resulted when the leaf extract was added to the ethyl alcohol (95%) solution
6. Volatile oils: A shiny pink layer on filter paper formed after UV light exposure after the filtration of leaf extract, indicating volatile oils' content.
7. Alkaloids: A grey color confirmed alkaloids' presence when adding leaf extract to 2 ml of Marquis Reagents.
8. Glycosides: A few drops of Fehling reagent were added to 1 ml of leaf extract.

(Table 1) lists the phytochemical components of moringa leaf extracts.

Table: (1). Illustrate the phytochemical constituent of moringa leaf extract.

Phytochemical constitutes	Result
Alkaloids	++
Saponins	+
Tannins	+++
Flavonoids	+
Terpenoids	-
Resins	+++
Volatile oils	+++
Glycosides	++

Symbol:+=Existence of phytochemical, -=Absence of phytochemical. (+++)high, (++) medium, (+) poor, (-)no found

The results indicate the presence of saponins, resins, tannins, alkaloids, flavonoids, glycosides and volatile oils, and the absence of terpenoids.

Antibacterial Activity:

The antibacterial activity of *Moringa Oleifera* leaf extract is summarized in (Table 2).

The inhibition zones emphasized that it depends on the type of bacteria and concentration of *Moringa Oleifera* leaf extract. The highest zone of inhibition is demonstrated by *Pseudomonas aeruginosa* (17 mm) in concentrated extract and (14mm) in diluted extract.

Interestingly, the case of *Staphylococcus aureus* and Streptococcus pyogenes reported zero results which indicates their negative results and the antibacterial activity of Moringa Oleifera leaf extract.

Table: (2). Demonstrate the antibacterial activity of MoringaOleifera leaves extract

Name		Result
Staphylococcusaureus	Concentrated	0
	Diluted	0
Streptococcus pyogenes	Concentrated	0
	Diluted	0
Pseudomonasaeruginosa	Concentrated	17
	Diluted	14

DISCUSSION

Chhetri *et al*. study reported that bioactive constituents can be taken from plant parts like seeds, roots, stems, leaves, and flowers (Chhetri et al., 2008). The results of our study showed the existence of bioactive components in moringa leaf extracts. Our study revealed the presence of alkaloids, volatile oils, saponins, resins, etc., in the ethanol extract of the leaves as in (Table1**)**. The outcome of the current study is in a parallel line with previous studies that screened the phytochemical composition of moringa leaves. Moringa leaves were proven to include numerous phytochemicals (Edeoga et al., 2006; Madziga et al., 2010).

The phytochemicals have remarkable pharmaceutical effects that are used in drugs for treating sclerosis, diabetes, skin antiseptic, diarrhea, colitis, and cancer.(Aboaba et al., 2011; Madziga et al., 2010). studies illustrated that Alkaloids, for example, are extensively used as anticancer agents, aesthetics, and central nervous stimulants. Alkaloids also have metabolic effects and control development in living systems (Aboaba et al., 2011; Madziga et al., 2010).(Mir et al., 2013). mentioned the role of saponins as one of the phytochemicals in cholesterol lowering. Tannins containing plants are commonly used as mouthwashes, and eye washes, as mentioned by (Abadallah & Ali, 2019; Mir et al., 2013).

They also mentioned that terpenoids are effective as antimicrobial, anti-inflammatory, and immunemodulatory agents and in the case of cancer. (Abadallah & Ali, 2019) explained the result of moringa leaf extracts' antibacterial activity achieved in our study against the clinical isolates of *Staphylococcus aureus*, Streptococcus pyogenes, and pseudomonas (Abadallah & Ali, 2019).

The outcome of our study was in line with (Saadabi & Zaid, 2011) results that reported that the extracts of *moringaoleifera* have an impeding effect on pathogenic bacteria like *Pseudomonas aeruginosain* and Escherichia coli (Saadabi & Zaid, 2011). The result of this study concludes that ethanol extracts of *moringaoleifera* showed a maximum zone of inhibition (17 mm) against *Pseudomo-*

nas aeruginosainas in (Table 2). This conclusion also describes the study by (Al-Bakri & Afifi, 2007) who mentioned moringa leaf extract constraining the growth of *E. coli, Klebsiella pneumoniae,* and *P.aeruginosa* (Al-Bakri & Afifi, 2007). Numerous investigations have shown that *M. oleifera* leaves have antibacterial properties. As an illustration, a study on plant extracts prepared in different solvents found the ether extract of leaves of *M. oleifera* was the most active ingredient against the ambient and clinical isolates of Proteus mirabilis, a well-known cause of urinary tract infections (Arun & Rao., 2001). Several studies on the antifungal activity of *M. oleifera* leaves against Trichophytonrubrum, T. mentagrophytes, Epidermophytonfloccosum, and Microsporum documented that the crude extracts as well as essential oils from *M. oleifera* leaves reveal antifungal activity (Abalaka et al., 2012; Chuang et al., 2007). (Patel et al., 2014) study showed *M. oleifera* leaf extracts in ethanolic and aqueous forms were effective against the yeast Saccharomyces cerevisiae and the fungus Candida tropicalis, but not against *C. albicans*. Little is known about the antibacterial activity of *M. oleifera* roots. Nevertheless, a few investigations have revealed this plant's roots to have anti-microbial properties(Patel et al., 2014). Additionally, in vitro tests on several *M. oleifera* root bark extracts against *S. aureus, E. coli, Salmonella gallinarum, P. aeruginosa*, and others showed that ethyl acetate and acetone extracts have the highest activity in comparison to other solvents (Raj et al., 2011). Similar to this, only a small amount of research—a few early reports—has been done on the antibacterial properties of *M. oleifera's* stem bark. Studies demonstrate the existence of active organic extracts with variable degrees of activity in *M. oleifera* root extract's antibacterial efficacy against several human diseases (Chhetri et al., 2008).

CONCLUSION

The current study showed that *moringa oleifera* leaf extracts have an antibacterial activity that impedes bacterial growth. The results express that ethanol extract of *moringa oleifera* leaf is effective against bacterial strains.

The antibacterial effect may be due to bioactive constituents such as alkaloids, saponins, flavonoids, and tannins. Therefore, the study results emphasized the *moringa oleifera* leaf components and its therapeutic prospects as an antibacterial agent.

Duality of interest: In relation to this paper's publication, the authors state that they have no conflicts of interest.

Author contributions: Practical experimentation was conducted with Safa E. Rahuma assistance. Munira M. Ashrif contributed in writing, reviewing, and debating the paper.

Funding: No specific grant from a public or commercial funding agency was received for this research.

REFERENCES

Abadallah, M., & Ali, M. (2019). Antibacterial activity of Moringa oleifera leaf extracts against bacteria isolated from patients attending general Sani Abacha specialist hospital damaturu. *J. Allied Pharm. Sci, 1*, 61-66.

Abalaka, M., Daniyan, S., Oyeleke, S., & Adeyemo, S. (2012). The antibacterial evaluation of Moringa oleifera leaf extracts on selected bacterial pathogens. *Journal of Microbiology research, 2*(2), 1-4.

Abdallah, E. M. (2011). Plants: An alternative source for antimicrobials. *Journal of applied pharmaceutical science*(Issue), 16-20.

Aboaba, O. O., Ezeh, A. R., & Anabuike, C. L. (2011). Antimicrobial activities of some Nigerian spices on some pathogens. *Agriculture and Biology Journal of North America, 2*(8), 1187-1193.

Al-Bakri, A. G., & Afifi, F. U. (2007). Evaluation of antimicrobial activity of selected plant extracts by rapid XTT colorimetry and bacterial enumeration. *Journal of Microbiological Methods, 68*(1), 19-25.

Al_husnan, L. A., & Alkahtani, M. D. (2016). Impact of Moringa aqueous extract on pathogenic bacteria and fungi in vitro. *Annals of Agricultural Sciences, 61*(2), 247-250.

Amaglo, N. K., Bennett, R. N., Curto, R. B. L., Rosa, E. A., Turco, V. L., Giuffrida, A., Curto, A. L., Crea, F., & Timpo, G. M. (2010). Profiling selected phytochemicals and nutrients in different tissues of the multipurpose tree Moringa oleifera L., grown in Ghana. *Food Chemistry, 122*(4), 1047-1054.

Arora, D. S., Onsare, J. G., & Kaur, H. (2013). Bioprospecting of Moringa (Moringaceae): microbiological perspective. *Journal of pharmacognosy and phytochemistry, 1*(6), 193-215.

Arun T, Rao PCH. (2011).Phytochemical screening and antibacterial activity of Moringa oleifera Lam. against Proteus mirabilis from urinary tract infected patients. *International Journal of PharmTech Research*;3(4):2118–23.

Berkovich, L., Earon, G., Ron, I., Rimmon, A., Vexler, A., & Lev-Ari, S. (2013). Moringa Oleifera aqueous leaf extract down-regulates nuclear factor-kappaB and increases cytotoxic effect of chemotherapy in pancreatic cancer cells. *BMC complementary and alternative medicine, 13*, 1-7.

Chhetri, H. P., Yogol, N. S., Sherchan, J., Anupa, K., Mansoor, S., & Thapa, P. (2008). Phytochemical and antimicrobial evaluations of some medicinal plants of Nepal. *Kathmandu university journal of science, engineering and technology, 4*(1), 49-54.

Chuang, P.-H., Lee, C.-W., Chou, J.-Y., Murugan, M., Shieh, B.-J., & Chen, H.-M. (2007). Anti-fungal activity of crude extracts and essential oil of Moringa oleifera Lam. *Bioresource technology, 98*(1), 232-236.

Dhakad, A. K., Ikram, M., Sharma, S., Khan, S., Pandey, V. V., & Singh, A. (2019). Biological, nutritional, and therapeutic significance of Moringa oleifera Lam. *Phytotherapy Research, 33*(11), 2870-2903.

Djemoui, D., Saidi, M., Rahmani, Z., & Djemoui, A. (2019). Influence of phenolic compounds on antioxidant capacity of leaves extracts of Moringa oleifera from Tamanrasset region. *Journal of Fundamental and Applied Sciences, 11*(1), 280-293.

Edeoga, H., Omosun, G., & Uche, L. (2006). Chemical composition of Hyptis suaveolens and Ocimum gratissimum hybrids from Nigeria. *African journal of Biotechnology, 5*(10).

Falowo, A. B., Mukumbo, F. E., Idamokoro, E. M., Lorenzo, J. M., Afolayan, A. J., & Muchenje, V. (2018). Multi-functional application of Moringa oleifera Lam. in nutrition and animal food products: A review. *Food research international, 106*, 317-334.

Fidrianny, I., Kanapa, I., & Singgih, M. (2021). Phytochemistry and pharmacology of moringa tree: an overview. *Biointerface Res Appl Chem, 11*(3), 10776-10789.

Fuglie, L. J. (1999). The miracle tree: Moringa oleifera, natural nutrition for the tropics.

Kashyap, P., Kumar, S., Riar, C. S., Jindal, N., Baniwal, P., Guiné, R. P., Correia, P. M., Mehra, R., & Kumar, H. (2022). Recent advances in Drumstick (Moringa oleifera) leaves bioactive compounds: Composition, health benefits, bioaccessibility, and dietary applications. *Antioxidants, 11*(2), 402.

Kasolo, J. N., Bimenya, G. S., Ojok, L., Ochieng, J., & Ogwal-Okeng, J. W. (2010). Phytochemicals and uses of Moringa oleifera leaves in Ugandan rural communities.

Leone, A., Fiorillo, G., Criscuoli, F., Ravasenghi, S., Santagostini, L., Fico, G., Spadafranca, A., Battezzati, A., Schiraldi, A., & Pozzi, F. (2015). Nutritional characterization and phenolic profiling of Moringa oleifera leaves grown in Chad, Sahrawi Refugee Camps, and Haiti. *International journal of molecular sciences, 16*(8), 18923-18937.

Luqman, S., Srivastava, S., Kumar, R., Maurya, A. K., & Chanda, D. (2012). Experimental assessment of Moringa oleifera leaf and fruit for its antistress, antioxidant, and scavenging potential using in vitro and in vivo assays. *Evidence-Based Complementary and Alternative Medicine, 2012*.

Madziga, H., Sanni, S., & Sandabe, U. (2010). Phytochemical and elemental analysis of Acalypha wilkesiana leaf. *Journal of American Science, 6*(11), 510-514.

Maheshwari, K., Yadav, R., Malhotra, J., Dhawan, N., & Mohan, L. (2014). Fascinating nutritional, prophylactic, therapeutic and socio-economic reconcile attributable to drum stick tree (Moringa oleifera Lam.). *Glob. J. Med. Res. B: Pharm. Drug Discov. Toxicol. Med, 14*, 11-22.

Mbikay, M. (2012). Therapeutic potential of Moringa oleifera leaves in chronic hyperglycemia and dyslipidemia: a review. *Frontiers in pharmacology, 3*, 24.

Mehra, R., Kumar, H., Kumar, N., & Kaushik, R. (2020). Red rice conjugated with barley and rhododendron extracts for new variant of beer. *Journal of Food Science and Technology, 57*, 4152-4159.

Mir, M. A., Sawhney, S., & Jassal, M. (2013). Qualitative and quantitative analysis of phytochemicals of Taraxacum officinale. *Wudpecker Journal of Pharmacy and Pharmocology, 2*(1), 1-5.

Padayachee, B., & Baijnath, H. (2020). An updated comprehensive review of the medicinal, phytochemical and pharmacological properties of Moringa oleifera. *South African Journal of Botany, 129*, 304-316.

Patel, P., Patel, N., Patel, D., Desai, S., & Meshram, D. (2014). Phytochemical analysis and antifungal activity of Moringa oleifera. *International Journal of Pharmacy and Pharmaceutical Sciences, 6*(5), 144-147.

Raj, A. J., Gopalakrishnan, V. K., Yadav, S. A., & Dorairaj, S. (2011). Antimicrobial activity of Moringa oleifera (Lam.) root extract. *Journal of Pharmacy Research, 4*(5), 1426-1427.

Rios, J.-L., & Recio, M. C. (2005). Medicinal plants and antimicrobial activity. *Journal of ethnopharmacology, 100*(1-2), 80-84.

Saadabi, A. M., & Zaid, I. A. (2011). An in vitro antimicrobial activity of Moringa oleifera L. seed extracts against different groups of microorganisms. *Australian Journal of Basic and Applied Sciences, 5*(5), 129-134.

Sahakitpichan, P., Mahidol, C., Disadee, W., Ruchirawat, S., & Kanchanapoom, T. (2011). Unusual glycosides of pyrrole alkaloid and 4′-hydroxyphenylethanamide from leaves of Moringa oleifera. *Phytochemistry, 72*(8), 791-795.

Sofowora, A. (1993). Medicinal plants and traditional medicine in Africa. Spectrum Books Limited. *Ibadan, Nigeria*, 1-153.

Stevens, G., Baiyeri, K., & Akinnnagbe, O. (2013). Ethno-medicinal and culinary uses of Moringa oleifera Lam. in Nigeria. *Journal of medicinal plants research, 7*(13), 799-804.

Sultana, B., Anwar, F., & Ashraf, M. (2009). Effect of extraction solvent/technique on the antioxidant activity of selected medicinal plant extracts. *Molecules, 14*(6), 2167-2180.

Tshabalala, T., Ndhlala, A., Ncube, B., Abdelgadir, H., & Van Staden, J. (2020). Potential substitution of the root with the leaf in the use of Moringa oleifera for antimicrobial, antidiabetic and antioxidant properties. *South African Journal of Botany, 129*, 106-112.

Verma, A. R., Vijayakumar, M., Mathela, C. S., & Rao, C. V. (2009). In vitro and in vivo antioxidant properties of different fractions of Moringa oleifera leaves. *Food and Chemical Toxicology, 47*(9), 2196-2201.

Vongsak, B., Sithisarn, P., & Gritsanapan, W. (2012). HPLC quantitative analysis of three major antioxidative components of Moringa oleifera leaf extracts. *Planta Medica, 78*(11), PJ15.

Al-Mukhtar Journal of Basic sciences 21 (2): 09-15, 2023
Doi: https://doi.org/10.54172/0pm5gm25

Research Article **Open Access**

The Conduct of Statistical Models when Parameters Are Perturbed From Their True Values

Tarek Elghazali* **and Mohammed Elnazali**

***Corresponding author** tarek.elghazali@uob.edu.ly Department of Statistics, University of Benghazi, Benghazi, Libya

Second Author: mohammed.elnazali@uob.edu.ly Department of Statistics, University of Benghazi, Benghazi, Libya

Received:
02 April 2023

Accepted:
31 July 2023

Publish online:
31 December 2023

Abstract

This paper aims to investigate the so-called non-linear properties of the skeleton of a non-linear autoregressive process, i.e., if $X_t - f(X_{t-1}) = \varepsilon_t$. Setting the variance of $\varepsilon_t = 0$, the skeleton of the process is obtained. Having fitted a self-exciting threshold autoregressive (SETAR) model to data and obtained a 95% confidence interval for parameters, we study the behaviour of non-linear properties, e.g., a limit cycle, amplitude dependency frequency, etc. We mainly consider a limit cycle for values of parameters at various locations within the confidence interval, or we may just slightly perturb model parameters from their true values.

Keywords: SETAR models, A limit point, A limit cycle, Simulation.

INTRODUCTION

A Self–Exciting Threshold Autoregressive (SETAR) Model: Tong (1983) proposed a self-exciting threshold autoregressive (SETAR) Model in his study of river flow data, which takes the form

$$X_t = \begin{cases} b^{(1)} X_{t-1} + \varepsilon_t^{(1)} & \text{if } X_{t-d} \le r \\ b^{(2)} X_{t-1} + \varepsilon_t^{(2)} & \text{if } X_{t-d} > r \end{cases} \qquad (1)$$

where $\varepsilon_t^{(1)}, \varepsilon_t^{(2)}$ are each a strict white-noise process, $b^{(1)}$, $b^{(2)}$ are constants, and d the delay parameters, respectively. The multiple threshold model takes the formula

$$X_t = b^{(j)} X_{t-1} + \varepsilon_t^{(j)} \text{ if } X_{t-d} \in R^{(j)}; j = 1,2,\dots,l$$

Where $R^{(1)}$, $R^{(2)}$,..., $R^{(l)}$ are given subset of the real line R, which define a partition of R into disjoint intervals $(-\infty, r_0]$, $[r_0, r_1]$,..., $[r_{l-1}, \infty)$, with $R^{(1)}$ denoting the interval $(-\infty, r_0]$ and $R^{(l)}$ denoting the interval $[r_{l-1}, \infty)$ (Priestley, 1988).

Jones and Cox (1978) discussed the general first order non-linear model

$$X_t - f(X_{t-1}) = \varepsilon_t \qquad (2)$$

where $f(.)$ is some general non-linear function, and ε_t is a sequence of independent variables. Model (1) can be used as a piecewise linear approximation to Model (2).

Similarly, a SETAR model of order $k > 1$ is given by

$$X_t = b_0^{(j)} + \sum_{i=1}^{k} b_i^{(j)} X_{t-i} + \varepsilon_t^{(j)} \text{ if } \underline{X}_{t-1} \in R^{(j)};\ j = 1,2,\ldots,l \qquad (3)$$

Where $R^{(j)}$ is a given region of k-dimensional Euclidean space $R^{(k)}$, and X_{t-1} $=(X_{t-1},X_{t-2},\ldots,X_{t-k})^T$ is the state vector at time $t-1$. Model (3) can be regarded as a piecewise linear approximation to the general k^{th} order non-linear AR model

$$\underline{X}_{t-1} - f(\underline{X}_{t-1}) = \varepsilon_t \qquad (4)$$

A Limit Cycle: According to Tong (1983), a limit cycle in discrete time can be defined as follows: Given a non-linear difference equation $X_t - f(X_{t-1}) = 0$, here $X_t = (X_{t-1},X_{t-2},\ldots,X_{t-p})$ is the state vector at time t, and f is a vector valued function, let $f^{(j)}$ denote the j^{th} iterate of f. Any vector of dimension p, which satisfies $f^{(jm)}(X) \to V$ as $j \to \infty$, is said to be a stable periodic point with a period m, with respect to domain $D \in R^p$. In this case $V_1, f^{(1)},\ldots, f^{(p-1)}(V_1)$, are all district stable limit points (Priestley, 1988).

The stable limit cycle is nothing but a set of vectors $(V_1,V_2,\ldots,V_{p-1})$. A limit cycle does depend only on the parameter of the system and the initial conditions of the system. A limit cycle is said to be stable if it does not change with changing the initial conditions of the system. A stable limit cycle is the only one that can be observed in practice being one of the models of behaviour to which the system, then, it is said to be robust. A limit cycle with an infinite period is known as chaos, which is very dependent on the initial values of the system. SETAR models can give rise to a limit cycle behaviour where the white-noise is suppressed, or equivalently, when it has zero variance (Tong, 1990).

MATERIALS AND METHODS

A Simulation Study: The aim of this study is to see whether, if we slightly change the parameters of a model that is known to have a limit cycle of a specific period, over their 95% bootstrap confidence intervals, the model would still have a limit cycle with a reasonable period, or would a period vary considerably as parameter values wander over their bootstrap confidence intervals. We consider simulation on two well-known models due to Tong and Lim (1980), which are known to have stable limit cycles each of period 9. The two models are

$$X_t = \begin{cases} 0.62 + 1.25X_{t-1} - 0.43X_{t-2} + \varepsilon_t^{(1)} & \text{if } X_{t-2} \le 3.25 \\ 2.25 + 1.52X_{t-1} - 1.24X_{t-2} + \varepsilon_t^{(2)} & \text{if } X_{t-2} > 3.25 \end{cases} \quad (5)$$

$$X_t = \begin{cases} 0.546 + 1.032X_{t-1} - 0.173X_{t-2} + 0.171X_{t-3} - 0.431X_{t-4} \\ +0.332X_{t-5} - 0.284X_{t-6} + 0.210X_{t-7} + \varepsilon_t^{(1)} & \text{if } X_{t-2} \le 3.16 \\ 2.632 + 1.492X_{t-1} - 1.32X_{t-2} + \varepsilon_t^{(2)} & \text{if } X_{t-2} > 3.16 \end{cases} \quad (6)$$

Our simulation consists of the following steps:

Step1. The bootstrap confidence interval of each parameter is constructed by using 50 replications, except for the delay parameter, where instead of constructing a bootstrap confidence interval, we allow the delay parameter to take the values 1, 2, 3, 4, and 5.

Step2. Starting from the lower limit of the bootstrap confidence interval of each parameter, and increasing by values, we simulate 1000 observations from each one of the skeletons of Models 5 and 6. The last 1000 observations are tested for a limit cycle with a possible maximum period of up to 500.

Step3. The experiment is terminated when the new perturbed value of each parameter reaches roughly the upper limit of its bootstrap confidence interval.

Step4. The above steps were repeated for each parameter in the skeleton of Models 5and 6.

We could, if we wished, instead of constructing the bootstrap confidence interval of each parameter in Step 1, just perturb the model parameters from their true value; therefore, Step 1 is not an essential step.

It should be mentioned that, in this study, we do not investigate each limit cycle in detail (i.e., how many sub-limit cycles it has or whether it is stable or not). We mainly investigate the existence of a limit cycle and its period. In cases where a no–limit cycle of a period less than or equal to 500 exists, we assume either it has a period greater than 500, or it is a chaos.

RESULTS

The value of each parameter, as it wanders over roughly its 95% bootstrap confidence interval, and the period of the corresponding limit cycle (if any) are given in Tables 1 to 7. Cases, where no limit cycle of a period less than, or equal to, 500 exists are denoted by $*$.

When the same limit cycle occurs in a sub-interval rather than at a single point within the bootstrap confidence interval of each parameter, the lower and upper limits of the sub-interval are given in each table. A single point is given as a sub-interval with equal upper and lower limits. Due to the

similarity in the results for Models (5-6) and the lack of space, we give here only the results for Model 5. The other results can be obtained from the authors.

Table: (1). The limit cycles occurred due to small changes in the constant–term in the first region for the skeleton of Model 5.

Bootstrap Confidence Interval		Period
Lower Limit	Upper Limit	
0.474	0.584	1
0.585	0.585	12
0.586	0.588	11
0.589	0.592	10
0.593	0.600	9
0.601	0.610	8
0.611	0.638	9
0.639	0.739	8

Table: (2). The limit cycles occurred due to small changes in the first-coefficient in the first region for the skeleton of Model 5.

Bootstrap Confidence Interval		Period
Lower Limit	Upper Limit	
1.202	1.238	1
1.239	1.239	13
1.240	1.241	10
1.242	1.243	9
1.244	1.247	8
1.248	1.257	9
1.258	1.310	8
1.311	1.363	9

Table: (3). The limit cycles occurred due to small changes in the second-coefficient in the first region for the skeleton of Model 5.

Bootstrap Confidence Interval		Period
Lower Limit	Upper Limit	
-0.597	-0.464	1
-0.463	-0.463	25
-0.462	-0.462	12
-0.461	-0.461	77
-0.460	-0.450	*
-0.449	-0.417	9

Table:(4). The limit cycles occurred due to small changes in the constant-term in the second region for the skeleton of Model 5.

Bootstrap Confidence Interval		Period
Lower Limit	UpperLimit	
2.134	2.214	8
2.215	2.274	9
2.275	2.364	8
2.365	2.374	51
2.375	2.474	*
2.475	2.484	98
2.485	2.494	144
2.495	2.504	169
2.505	2.514	103
2.515	2.524	81
2.525	2.534	47
2.535	2.574	12

Table:(5). The limit cycles occurred due to small changes in the first-coefficient in the second region for the skeleton of Model 5.

Bootstrap Confidence Interval		Period
Lower Limit	Upper Limit	
1.340	1.410	10
1.411	1.484	9
1.485	1.510	8
1.511	1.530	9
1.531	1.553	8
1.554	1.554	34
1.555	1.555	51
1.556	1.556	17
1.557	1.557	70
1.558	1.566	*

Table: (6). The limit cycles occurred due to small changes in the second-coefficient in the second region for the skeleton of Model 5.

Bootstrap Confidence Interval		Period
Lower Limit	Upper Limit	
-1.367	-1.343	10
-1.342	-1.275	9
-1.274	-1.250	8
-1.249	-1.231	9
-1.230	-1.205	8
-1.204	-1.204	25
-1.203	-1.203	442
-1.202	-1.193	*

Table: (7). The limit cycles occurred due to small changes in the threshold value in for the skeleton of Model 5.

Bootstrap Confidence Interval		Period
Lower Limit	Upper Limit	
3.184	3.218	8
3.219	3.273	9
3.274	3.312	8
3.313	3.363	9
3.364	3.405	10
3.406	3.431	11
3.432	3.445	12
3.446	3.451	13
3.452	3.452	14
3.453	3.461	1

DISCUSSION

Examination of Tables 1–7 drew the following conclusion:

1). The most frequent limit cycles that occur are the original limit cycle of the models that has a period of 9 and limit cycles with periods of a multiple of 9 or with periods close to 9.

2). The two models appear to retain the original limit cycle of period 9 in the neighbourhood of each true parameter value, which suggests that the original limit cycle of each one of the two models is robust.

3). Model 5 appears to be more sensitive to minor changes in some parameters than others.

4). Where the same limit cycle is exhibited among the sub-intervals within the bootstrap confidence interval of each parameter, the ones where the original limit cycle occurred are the largest.

CONCLUSION

It should be noted that these results are specific to Model 5. Moreover, we have used only one initial value in simulated data from the skeletons of Model 5, which does not guarantee the stability of the limit cycles found during the experiment.

For future work, we suggest using more models with different initial values before these results can be generalized. In addition, it would be interesting to repeat this study using skeletons of bootstrap models rather than skeletons of initial models like the ones adopted in our experiment. In other words, it would be attractive to see if fitted, a SETAR model gave rise to a limit cycle behaviour of a specific period, whether the corresponding bootstrap model would give rise to the same limit cycle, and how sensitive it is to small changes in the bootstrap model parameters.

Duality of interest: The authors declare that they have no duality of interest associated with this manuscript.

Author contributions: Contribution is equal between authors.

Funding: No specific funding was received for this work.

REFERENCES

Jones, D. A., and Cox, D. R. (1978). Nonlinear autoregressive processes. *Proceedings of the Royal Society of London. A. Mathematical and Physical Sciences*, 360(1700):71–95.

Priestley, M. B. (1988). Non-linear and non-stationary time series analysis. London: Academic Press.

Tong, H. (1983). Threshold models in non-linear time series analysis. Lecture notes in statistics, no. 21.

Tong, H. (1990). Non-linear time series: a dynamical system approach. Oxford university press.

Tong, H., and Lim, K. S. (1990). Threshold autoregression, limit cycles and cyclical data. Journal of the Royal Statistical Society: Series B (*Methodological*), 42(3):245-268.

Al-Mukhtar Journal of Basic sciences 21 (2): 16-29, 2023
Doi: https://doi.org/10.54172/ecympv33

Research Article **Open Access**

On β-Generalized Open and Closed Sets in Neutrosophic Topological Spaces

Rukaia M. Rashed

***Corresponding author:** r.rasheed@zu.edu.ly
Department of Mathematics, Faculty of Education, Al-Zawia University, Libya)

Received:
14 May 2023

Accepted:
24 October 2023

Publish online:
31 December 2023

Abstract

This article demonstrates a class of neutrosophic closed sets named neutrosophic generalized βg −closed sets, discusses their essential characteristics in neutrosophic topological spaces, and analyses some new interesting theorems based on the newly introduced set. It also discusses its relationship between basic open and closed sets in neutrosophic topological spaces.

Keywords: Neutrosophic sets, neutrosophic topology, neutrosophic generalized βg −closed sets, and neutrosophic generalized βg −open sets.

INTRODUCTION

The concept of nutrosophic sets was first introduced by Floretin Smarandache (Floretin S.2010) in 1999, which is a generalization of intuitionistic fuzzy sets by Atanassov (Atanassov K. 1986). In (Dhavaseelan R. & Jafari S.2017), a generalized neutrosophic closed set (in short, N_gCS) is defined, and using this generalized neutrosophic continuous, generalized neutrosophic irresolute functions are defined.

Recently in (Dhavaseelan R., Jafari S. & Hani Md. 2018, Dhavaseelan R. & Hani Md. 2019), the perception of generalized α-contra continuous and neutrosophic almost α-contra-continuous functions are introduced.

In 1999, the neutrosophic sets and neutrosophic topological spaces by Salama A. A. and Alblowi S. A. were extended (Rena T. & Anila S.2018). Furthermore, the basic sets like neutronsophic open sets (NOS), neutrosophic semiopen sets (NSOS) neutrosophic pre-open sets (NPOS), neutrosophic α open sets ($N_\alpha OS$), neutrosophic regular open sets (N-ROS), neutrosophic β open sets ($N_\beta OS$), and neutrosophic b open sets (N-bOS) are introduced in neutrosophic topological spaces and their properties are studied by various authors (Pushpaiatha A.& Nandhini T.2019). This paper introduces the new concept of neutrosophic closed sets called generalized neutrosophic β closed and open sets and some of their basic properties with examples.

1- PRELIIMINARIES:

In the following section, we assume that (X, τ) is the neutrosophic topological space, let A be a neutrosophic set in X and it is an open set. Then we symbolize it by $NSO(A)$, and the com-

plement of A is termed a neutrosophic closed set in X, also symbolized by $NSC(A)$. Also, the neutrosophic interior is denoted by $Nint(A)$, neutrosophic closure is denoted by $Ncl(A)$, and the empty band whole sets are denoted by 0 & 1 respectively.

Definition 1.1 (Abd El Monsef M.E. 1980)
A sub set A of topological space (X,τ) is called β −open (or semi pre open[6] if $A \subset cl\left(int(cl(A))\right)$.

Definition 1.2 (Levine N. 1970)
A sub set A of topological space (X,τ) is called a generalized closed set ($g-$ closed for short) if $cl(A) \subseteq U$, whenever $A \subseteq U$ and U is an open set. The complement of $g-$ closed set is called a g −open set.

Definition 1.3 (Dunham W. 1982)
If A is a subset of a space (X,τ), then
1- The generalized closure of A is defined as the intersection of all g −closed sets in X containing A and is denoted by $gcl(A)$ where$gcl(A) = \cap\{F: F\ is\ g-closed\ \&\ A \subseteq F\}$.
2- The generalized interior of A is defined as the union of all g −open sets in X contained in A and is denoted by $gint(A)$ where
$gint(A) = \cup\{G: G\ is\ g-open\ \&\ G \subseteq A\}$.

Definition 1.4 (Pushpaiatha A. & Nandhini T.2019)
For subset A of topological space (X,τ), then
1- The β −closure of A is the intersection of all $\beta-$ closed set that contain A. They are denoted by $\beta cl(A)$.
2- The $\beta-$ interior of A is the union of all $\beta-$ open sets contained in A. They are denoted by $\beta int(A)$.

Definition 1.5 (Salama A.A. & Alblowi S.A. 2012)
Let X be a non-empty fixed set, A neutrosophic set $NS-(A)$ is an object having the form $A = \{\langle X, \mu_A(x), \delta_A(x), V_A(x)\rangle : x \in X\}$ where $\mu A(x), \delta_A(x)$ & $V_A(x)$ represent the degree of membership, degree of indeterminacy, and the degree of nonmembership respectively of each element $x \in X$ to the set A. A neutrosophic set $A = \{\langle X, \mu_A(x), \delta_A(x), V_A(x)\rangle : x \in X\}$ can be identified as an ordered triple $\langle \mu_A, \delta_A, V_A\rangle$ in $]0,1[$ or X.

Definition 1.6 (Salama A.A. and Alblowi S.A. 2012)
Let $A = \langle \mu_A, \delta_A, V_A\rangle$ be a NS on X, then the complement $C(A)$ may be defined as
1- $C(A) = \{\langle x, 1-\mu_A(x), 1-\delta_A(x), 1-V_A(x)\rangle : x \in X\}$.

2- $C(A) = \{\langle x, V_A(x), \delta_A(x), \mu_A(x)\rangle : x \in X\}$.
3- $C(A) = \{\langle x, V_A(x), 1-\delta_A(x), \mu_A(x)\rangle : x \in X\}$.

Note that for any two neutrosophic sets A & B

4- $C(A \cup B) = C(A) \cap C(B)$.

5- $C(A \cap B) = C(A) \cup C(B)$.

Definition 1.7 (Salama A.A. & Alblowi S.A. 2012)

For any two neutrosophic sets

$A = \{\langle x, \mu_A(x), \delta_A(x), V_A(x)\rangle : x \in X\}$, and

$B = \{\langle x, \mu_B(x), \delta_B(x), V_B(x)\rangle : x \in X\}$ we may have

1- $A \subseteq B \Leftrightarrow \mu_A(x) \leq \mu_B(x)$,

$\delta_A(x) \geq \delta_B(x)$, $V_A(x) \geq V_B(x), \forall x \in X$.

2-

$A \cap B =$

$\langle x, \mu_A(x) \wedge \mu_B(x), \delta_A(x) \vee \delta_B(x), V_A(x) \vee V_B(x)\rangle$

3-

$A \cup B =$

$\langle x, \mu_A(x) \vee \mu_B(x), \delta_A(x) \wedge \delta_B(x), V_A(x) \wedge V_B(x)\rangle$

Definition 1.8 (Salama A.A. and Alblowi S.A. 2012)

A neutrosophic topology (in short, NT) on $X \neq \emptyset$ is a family τ of N −sets in X satisfying the laws given below

1- $0_N, 1_N \in \tau$.

2- $W_1 \cap W_2 \in \tau$ being $W_1, W_2 \in \tau$.

3- $\bigcup W_i \in \tau$ for the arbitrary family

$\{W_i : i \in A\} \subseteq \tau$.

In this case the pair (X, τ) is a neutrosophic topological space (NTS) and any neutrosophic set in τ is known as a neutrosophic open set (NOS) in X. A neutrosophic set A is a neutrosophic closed set (NCS) if and only if its complement $C(A)$ is a neutronsophic open set in X.

Definition 1.9

A neutrosophic A in a neutrosophic topological space (X, τ) is said to be

1- A neutrosophic β-open set $(N_\beta OS)$ if $A \subseteq Ncl\left(Nint\left(Ncl(A)\right)\right)$.

2- A neutrosophic β-closed set$(N_\beta CS)$ if $Nint\left(Ncl\left(Nint(A)\right)\right) \subseteq A$.

Remark 1.1

Note that $Ncl\big(C(A)\big) = C\big(Nint(A)\big)$ &

$Nint\big(C(A)\big) = C\big(Ncl(A)\big)$.

Proposition 1.1 (Salama A.A. and Alblowi S.A. 2012)

Let (X, τ) be NTS and A, B be two neutrosophic sets in X, then the following properties hold:

(a) $Nint(A) \subseteq A$, (b) $A \subseteq Ncl(A)$,

(c) $A \subseteq B \Longrightarrow Nint(A) \subseteq Nint(B)$,

(d) $A \subseteq B \Longrightarrow Ncl(A) \subseteq Ncl(B)$,

(e) $Nint\big(Nint(A)\big) = Nint(A) \wedge Nint(B)$, (f) $Ncl(A \cup B) = Ncl(A) \vee Ncl(B)$,

(g) $Nint(1_N) = 1_N$, (h) $Ncl(0_N) = 0_N$.

Proposition 1.2 (Salama A.A. & Alblowi S.A. 2012)
For any neutrosophic set A in (X,τ) we have
(a) $Ncl(C(A)) = C(Nint(A))$,
(b) $Nint(C(A)) = C(Ncl(A))$.

Proposition 1.3 (Salama A.A. & Alblowi S.A. 2012),
For all, $A\ B$ two neutrosophic sets then the following are true
(a) $C(A \cap B) = C(A) \cup C(B)$,
(b) $C(A \cup B) = C(A) \cap C(B)$.

Definition 1.10 (Salama A.A.& Alblowi S.A. 2012)
Let A be an NS in an $NTS\ (X,\tau)$, there for
1-
$Nint(A) = \cup\{G: G\ is\ a\ NOS\ in\ X\ and\ G \subseteq A\}$
is termed as neutrosophic interior
($Nint$ for short) of A.
2-
$Ncl(A) = \cap\{G: G\ is\ an\ NCS\ in\ X\ and\ G \supseteq A\}$
is termed as neutrosophic closure (Ncl for short) of A.

Definition 1.11 (Pushpaiatha A. & Nandhini T. 2019)
$A\ NS\ \ A$ in $NTS\ X$ is so called a neutron
sophic generalized closed set denoted by
N_gCS if for any $NOS\ \ U$ in X such that
$A \subseteq U$, then $Ncl(A) \subseteq U$. Moreover, its complement is named a neutrosophic generalized open set and referred to N_gOS.

Definition 1.12 (Dhavaseelan R. & Jafari S. 2017)
Let (X,τ) be NTS and B be a NS in X, then neutrosophic generalized closure is defined as
$N_gcl(B) = \cap\{G: G\ is\ a\ GNCS\ in\ X\ and\ B \subseteq G\}$
.
$N_gint(B) =$
$\cup\{U: U\ is\ a\ GNOS\ in\ X\ and\ U \subseteq B\ \}$
.

Proposition 1.4 (Salama A.A. & Alblowi S.A. 2012),
For any generalized neutrosophic set A
the following are holds:
$0_N \subseteq A$, $0_N \subseteq 0_N$, $A \subseteq 1_N$, $1_{N \subseteq 1_N}$

Proposition 1.5 (Salama A.A. & Alblowi S.A. 2012)
Let (X,τ) be a $GNTS$ and A, B be two neutrosophic sets in X. Then the following properties hold:
(a) $Gint(A) \subseteq A$, (b) $A \subseteq GNcl(A)$, (c) $A \subseteq B \Longrightarrow GNint(A) \subseteq GNint(B)$,
(d) $A \subseteq B \Longrightarrow GNcl(A) \subseteq GNcl(B)$,
(e)$GNint((A \cap B)) = GNint(A) \wedge GNint(B)$,

(f) $GNcl\big((A \cup B)\big) = GNcl(A) \vee GNcl(B)$,
(g) $GNint(1_N) = 1_N \quad , \quad GNcl(0_N) = 0_N$.

Proposition 1.6 (Salama A.A.& Alblowi S.A. 2012)
For any generalized neutrosophic set A in (X, τ) we have
(a) $GNcl\big(C(A)\big) = C\big(GNint(A)\big)$,
(b) $GNint\big(C(A)\big) = C\big(GNcl(A)\big)$.

Definition 1.13
Let A be a neutrosophic set of a neutrosophic topological space (X, τ), then the neutrosophic β-interior and the neutrosophic β-closure are defined as
$N_\beta int(A) = \bigcup\{U : U \; is N\beta OS \; in \; X \; \& U \subseteq A\}$,
$N_\beta cl(A) = \bigcap\{F : F \; is \; N\beta CS \; in \; X \; \& \; A \subseteq F\}$.

Proposition 1.7
Let A be an a neutrosophic set in X, then
1- $N_\beta cl(A) = A \cup Nint\Big(Ncl\big(Nint(A)\big)\Big)$.
2- $N_\beta int(A) = A \cap Ncl\Big(Nint\big(Ncl(A)\big)\Big)$.

Proof:
1- We need to prove that $N_\beta cl(A) \subseteq A \cup Nint\Big(Ncl\big(Nint(A)\big)\Big)$ &
$A \cup Nint\Big(Ncl\big(Nint(A)\big)\Big) \subseteq N_\beta cl(A)$
Since $N_\beta cl(A) \subseteq N_\beta CS(A) \Longrightarrow$
$Nint\Big(Ncl\Big(Nint\big(N_\beta cl(A)\big)\Big)\Big) \subseteq N_\beta cl(A)$
$\Longrightarrow A \cup Nint\Big(Ncl\big(Nint(A)\big)\Big)$
$\subseteq A \cup Nint\Big(Ncl\Big(Nint\big(N_\beta cl(A)\big)\Big)\Big)$
$\subseteq A \cup N_\beta cl(A) = N_\beta cl(A). \qquad \longrightarrow (1)$
On the other hand, since we have
$Nint\Big(Ncl\Big(Nint\big((A)\big)\Big)\Big) \cup$
$Nint\Big(Ncl\Big(Nint\big((A)\big)\Big)\Big)$

$\subseteq Nint\Big(Ncl\Big(Nint\big((A \cup Ncl(A)\big)\Big)\Big)\Big)$
$= Nint\Big(Ncl\Big(Nint\big(Ncl(A)\big)\Big)\Big)$
$= Nint\Big(Ncl\Big(Nint\big((A)\big)\Big)\Big)$
$\subseteq A \cup Nint\Big(Ncl\Big(Nint\big((A)\big)\Big)\Big). \qquad \longrightarrow (2)$
From (1) & (1) we get

$N_\beta cl(A) = A \cup Nint\left(Ncl\left(Nint(A)\right)\right)$.

2- The proof of this case similar to paragraph 1.

2- β- Generalized Closed and Open Sets in Neutrosophic Topological Spaces:

In this section we interduce concepts of the neutrosophic closure, neutrosophicβ β-interior and β-generalized closed and open sets and its respective open set in neutrosophic topological spaces and discuss some of their properties.

Definition 2.1 (Rukaia M. Rashed 2020)

A sub set A of a topological space (X,τ) is called a β-generalized closed set $(g\beta - closed)$ if $\beta cl(A) \subseteq U$ whenever $A \subseteq U$ and $U \in \beta O(X)$.

Definition 2.2 (Rukaia M. Rashed 2020)

A subset A of a topological space (X,τ) is said to be a generalized β −open ($g\beta$ −open for short) set if $U \subseteq \beta int(A)$ where ever $U \subseteq A$ and U is closed. The complement of generalized β −open set is said to be generalized β −closed. The family of all $g\beta$ −open (resp. $g\beta$ −closed) sets of X is denoted by $G\beta O(X)$ (resp.$PG\beta C(X)$).

Proposition 2.1

Let (X,τ) be a neutrosophic topological space, then the union of any two $N_\beta OS$ in a $NTSX$ is a $N_\beta OS$.

Proof:

Let A & B be two $N_\beta OS$, therefore

$A \subseteq Ncl\left(Nint\left(Ncl(A)\right)\right)$ &

$B \subseteq Ncl\left(Nint\left(Ncl(B)\right)\right) \Rightarrow$

$A \cup B \subseteq$

$Ncl\left(Nint\left(Ncl(A)\right)\right) \cup Ncl\left(Nint\left(Ncl(B)\right)\right)$

$= Ncl\left(Nint\left(Ncl(A)\right) \cup Nint\left(Ncl(B)\right)\right)$

$\subseteq Ncl\left(Nint\left(Ncl(A) \cup Ncl(B)\right)\right)$

$= Ncl\left(Nint\left(Ncl(A \cup B)\right)\right)$, then

$A \cup B \subseteq Ncl\left(Nint\left(Ncl(A \cup B)\right)\right)$,

so that $A \cup B$ is a $N_\beta OS$ in X.

Remark 2.1

The intersection of any two $N_\beta OS$ of an NTS does not have to be a $N_\beta OS$ as in this example.

Example 2.1

Let $X = \{a, b\}$ & $\tau = \{0_N, 1_N, A, B, M, N\}$ is a NTS on X where

$A = \langle x, (.3, .4), (.2, .1), (.7, .5)\rangle$,

$B = \langle x, (.2, .5), (.3, .4), (.4, .5)\rangle$,

$M = \langle x, (.3, .5), (.3, .4), (.4, .5)\rangle$,

$N = \langle x, (.2, .4), (.2, .1), (.7, .5)\rangle$, and let

$K_1 = \langle x, (.8, .4), (.1, .2), (.5, .7) \rangle$,
$K_2 = \langle x, (.5, .6), (.2, .5), (.3, .3) \rangle$.Then $Ncl\left(Nint\left(Ncl(K_1)\right)\right) = 1_N$,
$Ncl\left(Nint\left(Ncl(K_2)\right)\right) = 1_N$, therefor
K_1 & K_2 are $N_\beta OS$ in X. But
$K_1 \cap K_2 = \langle x, (.5, .4), (.1, .2), (.5, .7) \rangle$ is
not $N_\beta OS$ in X.

Proposition 2.2

Let A be any neutrosophic set in a neutrosophic topological space X, and let $A \subseteq B \subseteq Ncl(A)$, then B is a $N_\beta OS$ set in X.

Proof:

Since A is a $N_\beta OS$ set so that
$A \subseteq Ncl\left(Nint\left(Ncl(A)\right)\right) \Longrightarrow$
$Ncl(A) \subseteq Ncl\left(Ncl\left(Nint\left(Ncl(A)\right)\right)\right)$
$= Ncl\left(Nint\left(Ncl(A)\right)\right) \Longrightarrow$
$Ncl(A) \subseteq Ncl\left(Nint\left(Ncl(A)\right)\right)$, since
$A \subseteq B \subseteq Ncl(A)$, then
$B \subseteq Ncl\left(Nint\left(Ncl(A)\right)\right)$. Also $A \subseteq B \Longrightarrow$
$Ncl\left(Nint\left(Ncl(A)\right)\right) \subseteq Ncl\left(Nint\left(Ncl(B)\right)\right)$,
hence $B \subseteq Ncl\left(Nint\left(Ncl(B)\right)\right)$, then B is a $N_\beta OS$ set in X.

Proposition 2.3

Let(X, τ) be a neutrosophic topological space, and A be a neutrosophic set of X. Then A is $N_\beta CS$ if and only if $C(A)$ is a $N_\beta OS$.

Proof:

Suppose that A is a $N_\beta CS$ in X. Then $Nint\left(Ncl\left(Nint(A)\right)\right) \subseteq A$, taking the compliment of both sides, then we have

$C(A) \subseteq C\left(Nint\left(Ncl\left(Nint(A)\right)\right)\right) =$
$Ncl\left(Nint\left(Ncl\left(C(A)\right)\right)\right) \Longrightarrow$

$C(A) \subseteq Ncl\left(Nint\left(Ncl\left(C(A)\right)\right)\right)$, therefore
$C(A)$ is $N_\beta OS$ in X.
On the other hand, suppose that $C(A)$ is $N_\beta OS$ in X. So that
$C(A) \subseteq Ncl\left(Nint\left(Ncl\left(C(A)\right)\right)\right)$, taking the complement of both sides we have

$C\left(Ncl\left(Nint\left(Ncl(C(A))\right)\right)\right) \subseteq A \Longrightarrow$
$Nint\left(Ncl(Nint(A))\right) \subseteq A.$
Then A is a
$N_\beta CS$ in X.

Proposition 2.4

The intersection of any two $N_\beta CS$ of an
NTS, is also $N_\beta CS$.

Proof

Suppose that A & B are two $N_\beta CS$ in X. So $Nint\left(Ncl(Nint(A))\right) \subseteq A$ &
$Nint\left(Ncl(Nint(B))\right) \subseteq B$, then
$Nint\left(Ncl(Nint(A))\right) \cap$
$Nint\left(Ncl(Nint(B))\right) \subseteq A \cap B \Longrightarrow$

$Nint\left(Ncl(Nint(A \cap B))\right) \subseteq A \cap B$. Then
$A \cap B$ is a $N_\beta CS$.

Remark 2.2

Note that the union of any two $N_\beta CS$ in X is not a $N_\beta CS$ as in the following example:

Example 2.2

Let $X = \{a\}$ & $\tau = \{0_N, 1_N, A, B\}$ be a
NTS on X where $A = \langle x, (.2), (.5), (.3)\rangle$,
$B = \langle x, (.1), (.5), (.7)\rangle$, and let
$K_1 = \langle x, (.0), (.5), (.8)\rangle$,
$K_2 = \langle x, (.1), (.2), (.3)\rangle$. Then
$Nint(K_1) = 0_N$ & $Nint(K_2) = 0_N$.
Therefore, K_1,
K_2 are $N_\beta CS$, but $K_1 \cup K_2$ is not $N_\beta CS$.

Proposition 2.5

Every NCS in X is a $N_\beta CS$.

Remark 2.3

The converse of the above proposition is not true in the general, as in the following example:

Example 2.3

Let $X = \{a, b, c\}$ & $\tau = \{0_N, 1_N, A, B\}$ is a NTS on X where
$A = \langle x, (.5, .1, .1), (.6, .7, .6), (.3, .9, .4)\rangle$,
$B = \langle x, (.0, .1, .5), (.4, .6, .5), (.7, .9, .8)\rangle$,
and let

$K = \langle x, (.2,0,.3), (.4,.2,.2), (.9,.9,.1) \rangle$.
Then K is a $N_\beta CS$ but not a NCS.

Proposition 2.6

Let A be a $N_\beta CS$, and $Nint(A) \subseteq B \subseteq A$, then B is a $N_\beta CS$.

Proof

Suppose that A is a $N_\beta CS$, so
$Nint\left(Ncl\left(Nint(A)\right)\right) \subseteq A$, then we have
so $Nint\left(Ncl\left(Nint(A)\right)\right) \subseteq Nint(A)$, and we have $Nint(A) \subseteq B$. Then, it follows that $Nint\left(Ncl\left(Nint(A)\right)\right) \subseteq B$, and $B \subseteq A \Longrightarrow$
$Nint\left(Ncl\left(Nint(B)\right)\right) \subseteq$
$Nint\left(Ncl\left(Nint(A)\right)\right)$,

so $Nint\left(Ncl\left(Nint(B)\right)\right) \subseteq B$, then B is a
$N_\beta CS$.

Proposition 2.7

For any NS A in TS τ, the subsequent features stand:
1- $N_{\beta g} int\left(\overline{A}\right) = N_{\beta g} int(A)$.
2- $N_{\beta g} cl\left(\overline{A}\right) = N_{\beta g} cl(A)$.

Proof

The proof will be evident by symbolic definition,
$Neg\beta cl(A) =$
$\cap\{F: A \subseteq F, F \text{ is a } Ne - g\beta CS\}$
1- $Ne - g\beta cl(A) =$
$\cap\{\overline{F}: \overline{A} \subseteq \overline{F}, \overline{F} \text{ is a } Ne - g\beta C(S)\}$
$= \cup\{U: A \supseteq U, U \text{ is a } Ne - g\beta OS\}$
$= Ne - g\beta int\left(\overline{A}\right)$.
2- This feature has undeniable proof analogous to feature (1).

Proposition 2.8

For any $N_{\beta g} OS$ A in TS τ, then this set is $N_\beta OS$ (corresponding $N_{\beta g} OS$).

Proof

Similar to the proof of the previous theorem.

Definition 2.3

A neutrosophic A in a neutrosophic topological space X is said to be a neutrosophic β-generalized closed set $\left(N_{\beta g} CS\right)$ if
$N_\beta cl(A) \subseteq U$ whenever $A \subseteq U$ and U is a
NOS in X. The complement $C(A)$ of a
$N_{\beta g} CSA$ is a $N_{\beta g} OS$ in X.

Definition 2.4

A neutrosophic A in a neutrosophic topological space X is said to be a neutrosophic β-generalized open set $(N_{\beta g}OS)$ if
$U \subseteq N_\beta int(A)$ whenever $U \subseteq A$ and U is a N-closed set.

Example 2.4

Let $X = \{a, b\}$ and $\tau = \{0_N, 1_N, A, B\}$
where $A = \langle x, (.5,.6), (.3,.2), (.4,.1)\rangle$ &
$B = \langle x, (.4,.4), (.4,.3), (.5,.4)\rangle$ then τ is a neutrosophic topology. Hence let
$M = \langle x, (.5,.4), (.4,.4), (.4,.5)\rangle$ be any NS
in X then $M \subseteq A$ where A is a NOS in X. Now $N_\beta cl(M) =$
$\cap\{F : F\ is N_\beta CS\ in\ X\ \&\ M \subseteq F\} = C(B) \subseteq A$, or $N_\beta cl(M) = M \cup C(B) = C(B) \subseteq A$.
Therefore M is a $N_{\beta g}CS$ in X.
$C(A) = \langle x, (.4,.1), (.3,.2), (.5,.6)\rangle$,
$C(B) = \langle x, (.5,.4), (.4,.3), (.4,.4)\rangle$, so A is
$N_\beta CS$ if $Nint\left(Ncl\left(Nint(A)\right)\right) \subseteq A$
$\Longrightarrow Nint\left(Ncl\left(Nint(A)\right)\right) = o_N \subseteq A$,
also $Nint\left(Ncl\left(Nint(B)\right)\right) = B \subseteq B$
$\Longrightarrow A\ \&\ B$ are neutrosophic β-closed sets.
Now, $N_\beta cl(M) = A \nsubseteq U = C(B)$, so that M is not $N_{\beta g}CS$.

Example 2.5

Let $X = \{a, b\}, \tau = \{0_N, 1_N, A, B\}$ is an
$NTS, A = \langle x, (.5,.3), (.5,.7), (.5,.7)\rangle$&
$B = \langle x, (.4,.3), (.6,.7), (.6,.7)\rangle$ are NS in X, if $M = \langle x, (.4,.6), (.4,.4), (.4,.4)\rangle$, then M is $N_{\beta g}CS$ but does not $N_\beta CS$ in X, since
$Nint\left(Ncl\left(Nint(M)\right)\right) = A \nsubseteq M$.

Proposition 2.9

Every $NCS\ A$ is a $N_{\beta g}CS$ in X but not conversely in general.

Proof

Let $A \subseteq U$ where U is a NOS in X,
Now $N_\beta cl(A) = \left(N_\beta O(A)\right)^C =$
$\left(A \subseteq Ncl\left(Nint\left(Ncl(A)\right)\right)\right)^C =$
$\left(A \subseteq Ncl(A)\right)^C = \left(A \cup Ncl(A)\right)^C =$
$(A \cup A)^C = A^C \subseteq U^C \Longrightarrow A \subseteq U$,
by hypothesis therefore A is $N_{\beta g} - CS$.

Proposition 2.10

Every $N_\beta CS\ A$ is a $N_{\beta g}CS$ in X but the converse is not true in general.

Proof:

Let $A \subseteq U$, where A is$N_\beta CS, U$ is a $N_\beta OS$ in X, then $N_\beta C(A) = \left(N_\beta O(A)\right)^c$ $= \left(A \subseteq Ncl\left(Nint(Ncl(A))\right)\right)^c$ $= N_\beta C(A) = A \subseteq U$ (by previous *Proposition)*. Then we have $N_\beta C(A) \subseteq U$, hence A is an $N_{\beta_g} CS$ in X.

Proposition 2.11

Every $NOS, N_\beta OS$ are $N_{\beta_g} OS$ but not conversely in general.

Proof*:*

Obvious.

Remarks 2.4

1- The union of any two $N_{\beta_g} CS$ in a $NTSX$ is not a $N_{\beta_g} CS$ in a general case.

2- The intersection of any two $N_{\beta_g} CS$ need not be a $N_{\beta_g} CS$ in a $NTS\ X$ in general.

Example 2.7

Let $X = \{a, b\}$, and $\tau = \{0_N, 1_N, A, B, M\}$ be a neutrosophic topological space on X where $A = \langle x, (.5, .6), (.5, .4), (.5, .4)\rangle$ and $B = \langle x, (.2, .3), (.8, .7), (.8, .7)\rangle$, $M = \langle x, (.6, .7), (.4, .3), (.4, .3)\rangle$. Let $L_1 = \langle x, (.1, .5), (.9, .5), (.9, .5)\rangle$, $L_2 = \langle x, (.5, .2), (.5, .8), (.5, .8)\rangle$, then L_1 & L_2 are $N_{\beta_g} CS$ in X but $L_1 \cup L_2$ is not an $N_{\beta_g} CS$ since $L_1 \cup L_2 = \langle x, (.5, .5), (.5, .5), (.5, .5)\rangle \subseteq A$ but $N_\beta cl(L_1 \cup L_2) = \langle x, (.6, .7), (.4, .3), (.4, .3)\rangle \not\subseteq A$. Then M & N are $N_{\beta_g} CS_S$ in X but $M \cup N \subseteq B$ and $N_\beta cl(M \cup N) = 1_N \not\subseteq A$.

Example 2.8

Let $X = \{a, b\}$, and $\tau = \{0_N, 1_N, A, B, M\}$ is a neutrosophic topological space on X where $A = \langle x, (.5, .6), (.5, .4), (.5, .4)\rangle$ and $B = \langle x, (.2, .3), (.8, .7), (.8, .7)\rangle$, $M = \langle x, (.6, .7), (.4, .3), (.4, .3)\rangle$. Let $L_1 = \langle x, (.5, .8), (.5, .2), (.5, .2)\rangle$, $L_2 = \langle x, (.8, .6), (.2, .4), (.2, .4)\rangle$, then L_1 & L_2 are $N_{\beta_g} CS$ in X but $L_1 \cap L_2$ is not an $N_{\beta_g} CS$ since $L_1 \cap L_2 = \langle x, (.5, .6), (.5, .4), (.5, .4)\rangle \subseteq A$. But $N_\beta cl(L_1 \cap L_2) = \langle x, (.6, .7), (.4, .3), (.4, .3)\rangle$ $\not\subseteq A$. Then M & N are $N_{\beta_g} CS_S$ in X but

$M \cap N \subseteq B$ and $N_\beta cl(M \cap N) = 1_N \not\subset A$.

Proposition 2.12

Let (X, τ) be a NTS. Then for every $A \in N_{\beta g}C(X)$ and for every $B \in NS(X)$, $A \subseteq B \subseteq N_\beta cl(A)$ implies that $B \in N_{\beta g}C(X)$.

Proof:

Let $B \subseteq U$ and U be a NOS in (X, τ). Then, since $A \in N_{\beta g}C(X), \Longrightarrow$ $N_\beta cl(A) \subseteq U, A \subseteq U$ then, since $B \subseteq N_\beta cl(A) \Longrightarrow$ $N_\beta cl(B) \subseteq N_\beta cl\left(N_\beta cl(A)\right) = N_\beta cl(A)$, so $N_\beta cl(B) \subseteq N_\beta cl(A) \subseteq U$, then $N_\beta cl(B) \subseteq U$, Hence $B \in N_{\beta g}C(X)$.

Example 2.9

Let $X = \{a, b\}, \tau = \{0_N, 1_N, A, B\}$, such that $A = \langle X, (.5, .5), (.5, .5), (.5, .5)\rangle$ $B = \langle X, (.4, .3), (.6, .7), (.6, .7)\rangle$, $S = \langle X, (.3, .2), (.7, .8), (.7, .8)\rangle \Longrightarrow S$ is $N_\beta CS$ in X, why? We have $C(A) = \langle X, (.5, .5), (.5, .5), (.5, .5)\rangle$, $C(B) = \langle X, (.6, .7), (.6, .7), (.4, .3)\rangle$, $C(S) = \langle X, (.7, .8), (.7, .8), (.3, .2)\rangle$ note that $C(S)S$ is not NCS, since $C(S) \notin \tau$.

The $N_\beta OS$ are $A, B, C(A)$ & $C(B)$ since

$A \subseteq Ncl\left(Nint\left(Ncl(A)\right)\right) = C(A)$,

$B \subseteq Ncl\left(Nint\left(Ncl(B)\right)\right) =$ $\langle X, (.5, .5), (.6, .7), (.5, .5)\rangle$,

$C(A) \subseteq Ncl\left(Nint\left(Ncl\left(C(A)\right)\right)\right) = C(A)$ &

$C(B) \subseteq Ncl\left(Nint\left(Ncl\left(C(B)\right)\right)\right) = B$.

The $N_\beta CS$ are $A, B, C(A)$ & $C(B)$, so that S is $N_\beta gCS$ if $N_\beta cl(S) \subseteq U, U$ is $N_\beta OS$ $N_\beta cl(S) = \bigcap\{K: K \text{ is a } N_\beta CS \text{ in } X \& S \subseteq K\} = A \cap B \cap C(A) \cap C(B) = B \Longrightarrow S$ is $N_\beta gCS$.

Proposition 2.13

If A is a NOS and a $N_{\beta g}CS$ in (X, τ), then A is a $N_{\beta g}CS$ in (X, τ).

Proof

Since $A \subseteq A$ and A is a NOS in(X, τ), by hypothesis, $N_\beta cl(A) \subseteq A$. But $A \subseteq N_\beta cl(A)$. There $N_\beta cl(A) = A$. Hence A is a $N_\beta CS$ in (X, τ).

Proposition 2.14

Every neutrosophic closed set in neutrosophic topological space (X, τ) is a neutrosophic generalized β −closed set.

Proof

Let A be a neutrosophic closed set in neutrosophic topological space X, let $A \subseteq U$ be a neutrosophic open set in X. Then by definition and previous proposition, we get $A = Ncl(A)$, $N_S cl(A) \subseteq Ncl(A)$, we get
$N_S cl(A) \subseteq Ncl(A) = A \subseteq U$. Hence A is a neutrosophic generalized semi-closed set in X.

DISCUSSION

The results should be discussed in relation to any hypotheses advanced in the Introduction. Comment on results and indicate possible sources of error. Place the study in the context of other work reported in the literature. Only in exceptional cases should the "Results and Discussion" sections be combined. Refer to graphs, tables and figures by number (for example Figure 5 or Table 5. This helps tie the data into the text in a very effective manner.

CONCLUSION

This paper introduced and studied the notion of β −open and β −closed sets in a neutrosophic topology, and some characterizations of these notions are discussed.
In future research, we will extend these neutrosophic topology concepts by neutrosophic generalized β −continuous and neutrosophic β −generalized continuous in neutrosophic topological spaces. Also, we extend this neutrosophic concept by nets, filters, and neutrosophic βg −compactnes.

Duality of interest: The authors declare that they have no duality of interest associated with this manuscript..

Author contributions: The author did all the work related to the manuscript, including designing the research, collecting information, formulating theories and proofs, and preparing the entire paper.

Funding: There is no funding to support this manuscript

REFERENCES

Abd El Monsef M.E. (1980), Studid on Some Pre-Topological Concepts, P.h.D. Thesis, *Tanta Egypt.*

Abd El Monsef M.E., Mahmoud R. A. and Lashin S. R. (1986), β- closure and interior" Bull. β Fac. *Ed. Ein Shams University*, (10) 235-245.

Abd El-monsef M. E. and Mahoud R. A. (1987), Some Concepts Based on β-Open Sets, *Della J. Scl.* 110(1):58-71.

Arya S. P. and Nour T. (1990), Characteri- zations of S- normal Spaces, *Indian J. Pure Appl. Math.* 21(8):717-719.

A tanassov K.(1986), Intuitionistic Fuzzy Sets, *fuzzy sets and systems*, 87-96.

Dunham W. (1982), A new Closure Opera tor for Non-T_1 Topologies, *Kyungpook Mathematics, J*. Vol. 22, PP.55-60.

Dhavaseelan R. and Jafari S. (2017), Generalized Neutrosophic closed Sets, *Newtrends in neutrosophic theory and applications*, (2), 261-273.

Dhavaseelan R., Jafari S. and Hani Md. PAGE, (2018), Neutrosophic Generalized α-Contra-Continuity, *CREAT. MATH. Inform*, 27(2),133-134.

Dhavaseelan R. and Hani Md. PAGE, (2019), Neutrosophic Almost α Contra -Continuous Function, *Neutrosophic sets and systems*, (29), 71-77.

Floretin Smarandache, (2010), Neutro- sophic sets: A generalization of Intuitionistic Fuzzy Set, *Journal of Defense Resources Management*, 107-116.

Levine N. (1970), Generalized Closed Sets in Topology, *Rend. circ. MathematicsPalermo*, 19(2) 89-96.

Pushpaiatha A. and Nandhini T. (2019), Generalized Closed Sets Via Neutrosophic Topological Spaces, *Malaya Journal of Matematik*, 7(1), 50-54.

Rena Thomas and Anila S. (2018), On Neutrosophic Semi-Preopen Sets and Semi-Pre closed Sets in Neutrosophic Topolgical Spaces, *International Journal of Scientific Researh in Mathematical & Statistical Scinces*, Vol. 5, PP. 138-143.

Rukaia M. Rashed (2020), New Types of β-Generalized and β-Separate Axioms for Topological Spaces, *Journal of Pure & Applied Sciences*, ISSN 2521-9200.

Salama A.A. and Alblowi S.A. (2012), Neutrosophic Set and Neutrosophic Topological Spaces, *IOSR Journal of Mathematics* (IOSR-JM) ISSN: 2278-5728, Volume 3, Issue 4, PP 31-35.

Salama A.A. and Alblowi S.A. (2012), Generalized Neutrosophic Set and Generalized Neutrosophic Topol.

Al-Mukhtar Journal of Basic Sciences 21 (2): 30-38, 2023
Doi: https://doi.org/10.54172/k1188z31

Research Article **Open Access**

Performance Evaluation of the Giga-bit 802.11ac Based WLANs

Ashraf Ali Bourawy*, Abdalmunam Abdalla

***Corresponding author:** abourawy@omu.edu.ly, Department of Computer Science, Faculty of Science, Omar AL-Mukhtar University, Libya.

Second Author: abdalmunam.abdalla@omu.edu.ly, Department of Computer Science, Faculty of Science, Omar AL-Mukhtar University, Libya.

Received:
07 August 2023

Accepted:
09 November 2023

Publish online:
31 December 2023

Abstract

Wireless local area networks based on the legacy 802.11-1997 standard brought about a new era in wireless communications, enabling users to utilize the Internet anytime, anywhere. About two decades later, the IEEE 802.11ac amendment was released that broke the Gigabit-Ethernet barrier for wireless local area networks (WLANs). This amendment introduced improvements to the first and second layers (PHY and MAC) of the standard. The very high throughput was accomplished by improving the modulation mechanism, adding more spatial streams, utilizing broader channels, exploiting beam forming techniques, and allowing for better frame aggregation. In this article, a simulation evaluation is conducted to investigate the performance of the 802.11ac considering the enhancements introduced by this amendment. The main metric used in this study is the system throughput. In addition, the average delay metric is also considered for investigation. Different simulation scenarios are considered to examine the previously mentioned features and enhancements. Results showed that the system throughput of 802.11ac increases with larger channel sizes, improved modulation schemes, and more spatial streams. The frame aggregation has indicated to be an effective mechanism for alleviating unwanted overheads, which consequently increased the overall throughput.

Keywords: 802.11ac; modulation schemes; spatial streams; frame aggregation.

INTRODUCTION

Wireless communication technology offers the convenience of wireless communication services and enables individuals worldwide to stay mobile. Utilizing the IEEE 802.11 wireless standards, Wireless local area networks (WLANs) have undergone ongoing development year after year (Rochim *et al*., 2020). WLANs are extensively utilized for various device types, with easy deployment options. Besides its usage in accessing the Internet, different applications use the WLANs, such as autonomous vehicles, surveillance, and audio/video delivery for real-time services. These applications involve users' mobility, which entails the probability of a high collision rate and potentially causing performance drops (Coronado *et al*., 2023).

The data rates of the original 802.11 standard have been improved by the 802.11a/b/g amendments. The IEEE 802.11n standard was established in 2009, exploiting the MIMO technology that achieved higher throughput rounding to 0.6 Gbps. The IEEE 802.11ac (IEEE, 2013) amendment has succeeded in accomplishing a very high throughput (VHT), which exceeds the Giga-bit base-

line. Accomplishing this VHT level was obtained according to several enhancements such as using more spatial streams, considering broader channels, increasing the modulation, and coding schemes, utilizing the new feature of multi-user MIMO, and frame aggregation techniques (IEEE, 2013).

Additionally, two essential frame aggregation methods are proposed by the amendment to be used by the MAC layer while transmitting data frames. These two methods are known as Aggregate MAC service data unit (A-MSDU) and Aggregate MAC protocol data unit (A-MPDU). The utilization of frame aggregation methods considerably decreases the overhead by allowing multiple frames to share the physical header and inter-frame spacing during channel access. Moreover, the frame size has increased, as stated by the amendment, to enable more data packets coming from upper layers to be aggregated. The frame aggregation mechanism, however, is set to be compulsory in 802.11ac, making the MAC layer transmits all its MPDUs as aggregate MPDUs (A-MPDUs) (Gast, 2013; IEEE, 2013).

Essentially, the 802.11ac builds upon the significant advancements made in 802.11n. Various techniques are employed in 802.11ac to increase data rates by utilizing MIMO technology. Instead of dealing with a single receiver, the 802.11ac proposed the MU-MIMO mechanism, which allows the access point to send to multiple users simultaneously. This is a groundbreaking feature that sets 802.11ac apart from its predecessors (Gast, 2013).

This paper aims to evaluate the new enhancements proposed by the 802.11ac and investigate their impact on the performance. Simulation methodology is utilized to conduct this study considering several scenarios which cover the features introduced in the 802.11ac. Broader channels, elevated modulation schemes, increased spatial streams, and frame aggregation are the enhancements investigated in this paper. Throughput and average delay are the metrics used in this study for performance evaluation. The evaluated performance indicated that the 802.11ac achieved better throughput when employing the new key features.

RELATED WORK

Extensive research has been proposed in the literature that investigated the operational effectiveness of the IEEE 802.11 wireless networks. Tuifaiga *et al*. presented a study that compares the performance of IEEE 802.11ac wireless LAN in Windows and Linux Ubuntu (Tuifaiga *et al*., 2021). The study showed that IPv4 outperforms IPv6 in terms of several performance metrics. UDP has higher throughput than TCP, and Linux performs better than Windows. The theoretical limit of 1.3Gbps for 802.11ac was not reached with an 80 MHz channel size. Another study by (ElKassabi *et al*., 2022) explored the practical deployment of WiFi standards in outdoor smart city environments. The study compared the 802.11ax, 802.11ac, and 802.11n in terms of performance. The results indicated that both IEEE 802.11ax and IEEE 802.11ac outperformed the performance of the IEEE 802.11n. Surprisingly, the distance between the transmitter and receiver was the criterion which made the 802.11ac perform better when a certain distance was exceeded. De Carvalho *et al*. evaluated the performance of wireless equipment in Wi-Fi (IEEE 802.11ac) using WPA2 PTP links (de Carvalho *et al*., 2020). TCP and UDP performance metrics were measured. The 802.11ac outperformed 802.11n in terms of TCP throughput, jitter, and datagram loss. The results suggested further investigations across different standards, equipment, and environments. Alternatively, a Markovian model was presented to predict AP throughput based on network topology and demands (Stojanova *et al*., 2021). Simulations showed a 10% mean error. The model is tailored for IEEE 802.11 standards with channel bonding, providing insights for channel assignment. Guidelines for static channel

bonding were derived considering node characteristics. The authors of (Natkaniec *et al*., 2023) analyzed the coexistence of 802.11ax stations with other legacy stations. The study investigated the effect on system performance caused by the BSS coloring, A-MPDU, and A-MSDU aggregations. Simulation results showed that implementing BSS coloring increased throughput by up to 43%, but legacy devices disrupted its functioning. Fukuda *et al*. focused on IEEE 802.11ax and its impact on communication performance in dense campus wireless LANs (Fukuda *et al*., 2022). They conducted experiments using multiple terminals to measure the throughput under various channel configurations and coexistence scenarios with other standards. Findings indicated that 40-MHz channel bonding improved throughput with a small number of terminals, whereas increasing the ratio of 802.11ax stations coexisting with 802.11ac stations enhanced the overall performance. The challenge of combining 802.11ad and 802.11ac interfaces in future WLAN devices was addressed by (Aggarwal *et al*., 2022). The authors proposed MuSher, an agile MPTCP scheduler that improves throughput in WLAN/Internet settings and speeds up traffic recovery.

Similarly, Chen *et al*. focused on the challenges of rate adaptation (RA) in IEEE 802.11ac networks (Chen *et al*., 2021). The authors identified limitations in current RA solutions, such as the lack of joint rate and bandwidth adaptation, scalability, and online learning capability. To overcome these limitations, they proposed an experience-driven rate adaptation (EDRA), which incorporates deep reinforcement learning. The evaluation results demonstrated that EDRA outperformed the default RAs by up to 821.4% (Intel) and 242.8% (Linux) in various scenarios. The research of (Khan *et al*., 2017) discussed the high system throughput of IEEE 802.11ac networks in a MIMO channel. It considered key MAC and PHY layer features and identified trends and trade-offs. The work in (Muhammad *et al*., 2021) presented a performance evaluation of 802.11ax (Wi-Fi 6). The research conducted empirical tests to investigate metrics such as throughput and jitter, and their relationship with parameters like payload length and environmental variables. The results showed that 802.11ax achieved higher throughput compared to its predecessor 802.11ac, and exhibited improved channel utilization due to its higher modulation and coding scheme. Confined to the 160-MHz channel, Kolahi *et al*. evaluated the performance of WLAN 802.11ac for IPv4, IPv6, UDP, and TCP protocols (Kolahi *et al*., 2023). Results indicated that the client-server setup using UDP and IPv4 achieved the highest throughput at 1124 Mbps, surpassing the results for IPv6. However, the achieved throughput is lower than the theoretical maximum of 1700 Mbps. Another study (Gupta *et al*., 2020) explored an integrated fiber-wireless network combining a 10-Gigabit passive optical network and IEEE 802.11ac WLAN. The focus was on enhancing network throughput and meeting quality of service requirements. The proposed approach incorporated a deficit dynamic bandwidth allocation algorithm at the optical line terminal to ensure improved QoS parameters. Simulation results demonstrated positive enhancements in all measured performance metrics. The authors of (Rochim *et al*., 2020) compared the performance of the sixth-generation wireless protocol IEEE 802.11ax with the previous fifth-generation protocol IEEE 802.11ac, both operating at 5 GHz. Different modulation schemes and payload sizes, as well as the number of users, were considered for comparison. Results indicated that in the case of dense stations, 802.11ax performed better than 802.11ac. However, the 802.11ax experienced a slightly longer delay response time.

Buta *et al*. presented an implementation and evaluation of the sub-band MVDR algorithm for IEEE 802.11ac signals (Buta *et al*., 2020). The algorithm demonstrated a good performance and effectively directed the array of antennas as required. Additionally, it improved data transmission quality, as indicated by lower bit error rates compared to non-beamforming scenarios under the same signal-to-noise ratio conditions. On the other hand, many studies focused on the impact of frame aggregation on network operation. Karmakar *et al*. conducted a survey examining the effect on application performance caused by the concepts of high throughput WLANs (Karmakar *et al*., 2017). It covered

IEEE 802.11n and IEEE 802.11ac standards, highlighting features like frame aggregation, MIMO, and channel bonding. The survey emphasized the need for research on evaluating the performance of upper layers in HT-WLANs and developing efficient link adaptation mechanisms. The authors of (Suzuki *et al*., 2021) proposed an optimization problem to maximize throughput in IEEE 802.11 networks using frame aggregation. They introduced a scheme that determined optimal subframe sets for both A-MPDU and A-MSDU, resulting in a significant improvement in throughput. Another work by (Yazid *et al*., 2016) discussed the frame aggregation techniques and their effects on 802.11ac system performance. It also emphasized the importance of cross-layer communications between the PHY and MAC layers to optimize wireless bandwidth utilization. Simulation results demonstrated the benefits provided by the frame aggregation in improving network performance. Guo *et al*. focused on optimizing IEEE 802.11-based wireless networks, specifically for Linear Wireless Ad-hoc Networks (Guo *et al*., 2022). The study identified the impact of the linear multi-hop characteristic on frame aggregation and the RTS/CTS handshake. Based on this analysis, a variable frame aggregation method and an adaptive RTS/CTS control algorithm were proposed to improve network performance in Linear-WANETs. Simulation results validated the effectiveness of the algorithm, demonstrating the significance of adjusting frame aggregation and RTS/CTS mechanisms to enhance overall system performance. Using simulations, the authors of (Khalil *et al*., 2020) demonstrated that the 802.11ac standard could achieve throughputs of around 600 Mbit/s, approaching the data rates specified in the IEEE 802.11ac standard. The study presented the performance of hybrid frame aggregation, which achieved higher throughputs compared to A-MPDU or A-MSDU aggregations. Additionally, the study analyzed the most suitable modulation and coding schemes based on the distance between the station and the access point, finding that QPSK modulation performed better than 256-QAM for longer ranges.

MATERIALS AND METHODS

The Jemula 802.11ac simulator was used to assess the various aspects of 802.11ac (Jumela Team, 2016). It is an open-source Java library that serves as an event-driven stochastic simulation kernel for real-time systems. The simulator comprises three primary packages: kernel, statistics, and plot. Our simulation involved different channel configurations (20 MHz, 40 MHz, 80 MHz, and 160 MHz) and examined various modulation schemes, including QPSK, 16-QAM, 64-QAM, and 256-QAM. We also investigated the impact of varying the number of spatial streams (1, 2, 4, and 8). Table 1 summarizes the physical and MAC layer parameters (IEEE, 2013) as well as the frame aggregation parameters employed in the simulation. Multiple scenarios were created, with each scenario run for 20 seconds. The average values were obtained by executing every scenario for ten times to ensure the reliability and robustness of the obtained results.

Table:(1). Simulation Parameters.

Para.	Val.
Time of slot	9 μs
CW_{min}	16
CW_{max}	1024
Prop $_{Delay}$	1 μs
T_{SIFS}	16 μs
T_{DIFS}	34 μs
MAC Header length	36 bits
Max MSDU length	2304 bytes
Max MPDU length	11454 bytes
BLK_ACK length	64 bytes
ACK length	14 bytes
Min P_ HDR Time	40 μs
Max P_HDR Time	68 μs

RESULTS AND DISCUSSION

In this study, we intended to examine how various features implemented in 802.11ac impacted the overall throughput of the system. We assess the combined throughput of the network and evaluate the effects of these features utilizing different scenarios.

Scenario 1: Channel Bandwidt:

In order to investigate the impact of using broader channels, we vary the channel bandwidth, taking the values of 20, 40, 80, 160 MHz. The payload is also varied between 500 and 2000 octets. However, other parameters are fixed to focus only on the channel bandwidth effect. Modulation is fixed at 16-QAM, one spatial stream is used, and number of stations is set to 10. As shown in Figure 1, the system throughput increases by about 10 Mbps as the channel bandwidth is doubled. The increase in throughput can be interpreted easily when considering the formula of Shannon for channel capacity. That is when the bandwidth is widened, the channel can handle more data transfer, thus increasing the throughput. Nonetheless, another factor must be considered; the SNR, which plays a crucial role in the channel capacity formula.

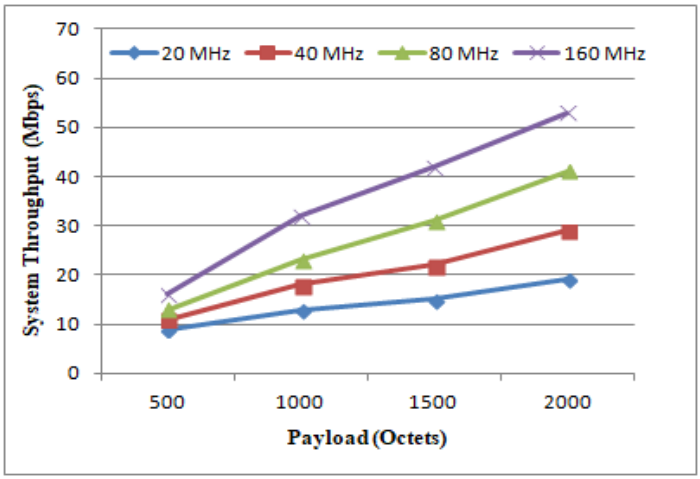

Figure: (1). Impact of channel bandwidth.

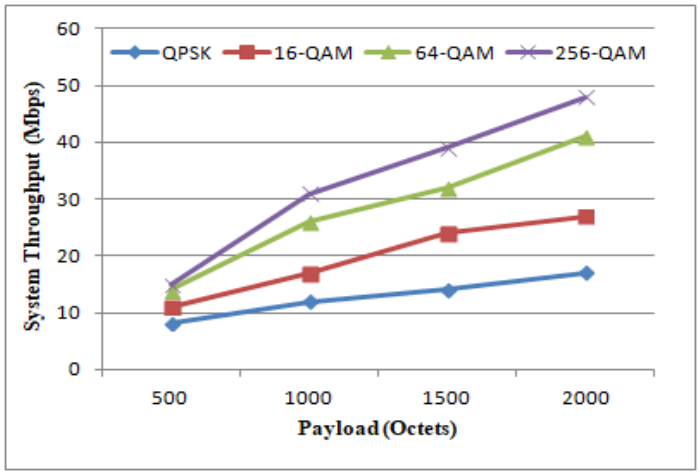

Figure: (2). Impact modulation schemes.

Scenario 2: Modulation Schemes

Modulation schemes are varied in this scenario (QPSK, 16-QAM, 64-QAM, and 256-QAM) to explore their influence on system throughput. For simplicity, we fix the spatial stream to one, the

number of stations is ten, and the channel bandwidth is 40 MHz. The system throughput increases with the increase of modulation and coding schemes, as illustrated in Figure 2. It is clearly understood and expected result because as the modulation scheme increases, the number of bits per symbol increases. This leads to conveying more data bits, which consequently increases the system throughput. It is worth to mention that the 256-QAM is newly proposed by the 802.11ac, which achieved about 10 Mbps higher that of the 64-QAM.

Scenario 3: Spatial Streams

To evaluate the impact of spatial streams on system throughput, we varied the number of spatial streams with values 1, 2, 4, and 8 and plotted it against the payload size. We fixed the number of stations to 10, the modulation scheme is 16-QAM, and we used the 40 MHz channel. The system throughput is increased significantly with the increase of spatial streams, as depicted in Figure 3.

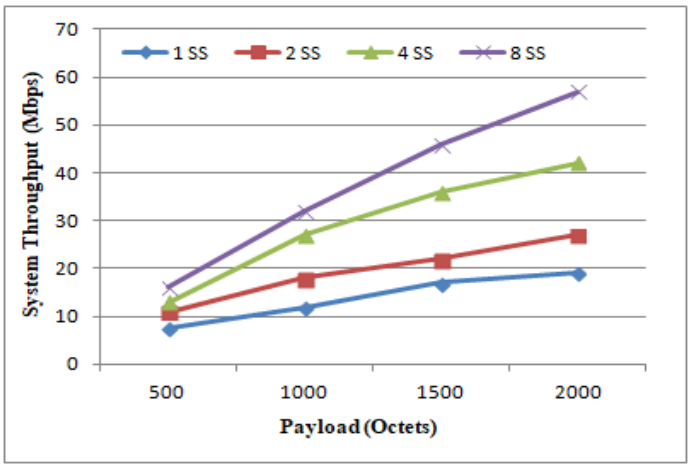

Figure: (3). Impact of spatial streams (SS).

It is clearly seen that the throughput is increased more than threefold when considering 8 spatial streams rather than 1 spatial stream. This is a great enhancement of the 802.11ac.

Scenario 4: MCS impact on average delay

Modulation and coding schemes are varied in this scenario to investigate the average delay in delivering data packets. Payload is fixed to 1500 octets, 20 MHz and 40 MHz channels are considered with spatial streams is set to 1. The average delay experienced by data transmission is decreased as the modulation and coding scheme increases, as shown in Figure 4. This decrement is observed in both channel bandwidths (20 and 40 MHz). However, the 40 MHz channel experiences a higher average delay than the 20 MHz channel. This can be attributed to the higher number of packets transmitted in case of using a wider channel.

Scenario 5: Impact of Frame Aggregation

The impact of employing the aggregate MPDUs is the aim of this scenario. We vary the number of the 2000 octets MPDUs that are aggregated into an A-MPDU. The 100 Mbps and 150 Mbps physical rates are used. The number of stations is fixed to 12 stations. The 40 MHz channel, along with 16-QAM is utilized. According to the results depicted in Figure 5, as the number of aggregated MPDUs increases, the throughput also increases. This can be taken as an evidence of the efficiency of frame aggregation mechanisms. This increase in throughput can be attributed to the reduction in the amount of overheads entailed by the MAC and PHY layers. However, after aggregating 64 or more MPDUs, the throughput reaches a plateau and no significant increase is observed. We argue

that when dealing with larger frames, higher physical rates are needed to accomplish better enhancements in system throughput.

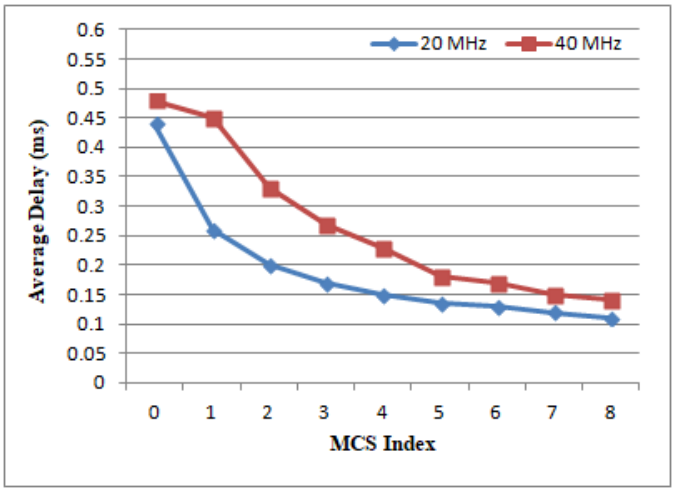

Figure: (4). Impact of MCS on average delay.

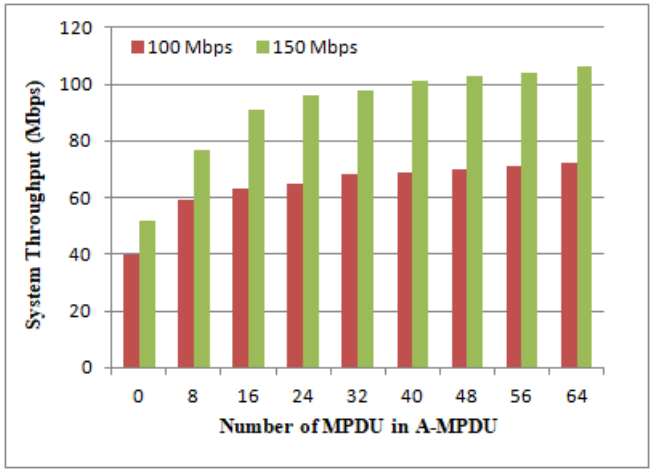

Figure: (5). Impact of Aggregate MPDU.

CONCLUSION

This study analyzed various aspects of the IEEE 802.11ac amendment. Our simulation scenarios focused on exploring wider channel bandwidths, modulation schemes, and multiple spatial streams, which are critical features of the amendment. The results demonstrated that these features significantly increase the system throughput, thereby improving overall performance. Additionally, we assessed the average delay as a metric to gain insights into the impact on data packet transmission. Based on simulation findings, it has been demonstrated that frame aggregation is a valuable approach for improving channel utilization. By reducing overhead, frame aggregation enhances the efficiency of the MAC protocol. However, it is essential to carefully consider the relationship between frame sizes and the physical data rate to ensure optimal performance.

Duality of interest: The authors declare that they have no duality of interest associated with this manuscript.

Author contributions: Ashraf Bourawy brought up the research topic and conducted the simula-

tion scenarios. In addition, Abdalmunam contributed in setting up the simulation scenarios and parameters. Abdalmunam Abdalla surveyed the literature and wrote the introduction and related work. Ashraf Bourawy extracted the results and wrote the results and discussion part. Both authors contributed to the last version of the manuscript.

Funding: No specific funding was received for this work.

REFERENCES

Aggarwal, S., Saha, S. K., Khan, I., Pathak, R., Koutsonikolas, D., & Widmer, J. (2022). Musher: An agile multipath-tcp scheduler for dual-band 802.11 ad/ac wireless lans. *IEEE/ACM Transactions on Networking, 30*(4), 1879-1894.

Buta, R., Codau, C., Pastrav, A., Palade, T., Dolea, P., & Puschita, E. (2020, November). Performance evaluation of sub-band MVDR beamforming for IEEE 802.11 ac wideband signals. In *2020 International Symposium on Electronics and Telecommunications (ISETC)* (pp. 1-4). IEEE.

Chen, S. C., Li, C. Y., & Chiu, C. H. (2021, May). An experience driven design for IEEE 802.11 ac rate adaptation based on reinforcement learning. In *IEEE INFOCOM 2021-IEEE Conference on Computer Communications* (pp. 1-10). IEEE.

Coronado, E., Valero, V., Cambronero, M. E., & Orozco-Barbosa, L. (2023). Modelling, simulation and performance evaluation of the IEEE 802.11 e protocol with station mobility. *PeerJ Computer Science*, *9*, e1457.

De Carvalho, J. A. P., Pacheco, C. F. R., Reis, A. D., & Veiga, H. (2020). Performance Evaluation of IEEE 802.11 ac WPA2 Laboratory Links. *KnE Engineering*, 182-194.

ElKassabi, I., & Abdrabou, A. (2022, October). An Experimental Comparative Performance Study of Different WiFi Standards for Smart Cities Outdoor Environments. In *2022 IEEE 13th Annual Ubiquitous Computing, Electronics & Mobile Communication Conference (UEMCON)* (pp. 0450-0455). IEEE.

Fukuda, Y., Hatase, T., Satoh, A., Nakamura, Y., & Wada, S. (2022, April). Characterizing the basic performance of IEEE 802.11 ax using actual hardware measurements. In *NOMS 2022-2022 IEEE/IFIP Network Operations and Management Symposium* (pp. 1-4). IEEE.

Gast, M. (2012). *802.11 n: a survival guide*. " O'Reilly Media, Inc.".

Guo, Y., & Li, Z. (2022). Adaptive Frame Aggregation and Rts/Cts Joint Optimization for Ieee 802.11 ac Based Linear-Wanets. *Cts Joint Optimization for Ieee, 802*.

Gupta, A., Goel, H., Bohara, V. A., & Srivastava, A. (2020, December). Performance evaluation of integrated XG-PON and IEEE 802.11 ac based EDCA networks. In *2020 IEEE International Conference on Advanced Networks and Telecommunications Systems (ANTS)* (pp. 1-6). IEEE.

IEEE. (2013). IEEE Standard for Information technology--Telecommunications and information exchange between systems—Local and metropolitan area networks--Specific requirements--

Part 11: Wireless LAN Medium Access Control (MAC) and Physical Layer (PHY) Specifications--Amendment 4: Enhancements for Very High Throughput for Operation in Bands below 6 GHz. *IEEE Std 802.11ac(TM)-2013 (Amendment to IEEE Std 802.11-2012, as amended by IEEE Std 802.11ae-2012, IEEE Std 802.11aa-2012, and IEEE Std 802.11ad-2012)*, 1-425. doi:10.1109/IEEESTD.2013.7797535

Jemula Team. (2016). Jemula 802.11ac simulator. Retrieved from https://sourceforge.net/projects/hewsimulator/

Karmakar, R., Chakraborty, S., & Chattopadhyay, S. (2017). Impact of IEEE 802.11 n/ac PHY/MAC high throughput enhancements over transport/application layer protocols-a survey. *arXiv preprint arXiv:1702.03257*.

Khalil, N., & Najid, A. (2020). Performance analysis of 802.11 ac with frame aggregation using NS3. *International Journal of Electrical and Computer Engineering*, *10*(5), 5368.

Khan, G. Z., Gonzalez, R., Park, E. C., & Wu, X. W. (2017, February). Analysis of very high throughput (VHT) at MAC and PHY layers under MIMO channel in IEEE 802.11 ac WLAN. In *2017 19th International Conference on Advanced Communication Technology (ICACT)* (pp. 877-888). IEEE.

Kolahi, S. S., Shaheen, T., Aderson, E., Aljadani, R., & Ceyddique, A. (2023, January). IEEE 802.11 ac WLAN Analysis in 160Mhz Channel. In *2023 International Conference on Information Networking (ICOIN)* (pp. 190-193). IEEE.

Muhammad, S., Zhao, J., & Refai, H. H. (2021, March). An empirical analysis of IEEE 802.11 ax. In *2020 International Conference on Communications, Signal Processing, and their Applications (ICCSPA)* (pp. 1-6). IEEE.

Natkaniec, M., & Bieryt, N. (2023). An Analysis of the Mixed IEEE 802.11 ax Wireless Networks in the 5 GHz Band. *Sensors*, *23*(10), 4964.

Rochim, A. F., Harijadi, B., Purbanugraha, Y. P., Fuad, S., & Nugroho, K. A. (2020, February). Performance comparison of wireless protocol IEEE 802.11 ax vs 802.11 ac. In *2020 international conference on smart technology and applications (ICoSTA)* (pp. 1-5). IEEE.

Stojanova, M., Begin, T., & Busson, A. (2021). A Markov model for performance evaluation of channel bonding in IEEE 802.11. *Ad Hoc Networks*, *115*, 102449.

Suzuki, K., & Yamazaki, S. (2021). Throughput maximization based on optimized frame-aggregation levels for IEEE 802.11 WLANs. *IEEE Communications Letters*, *25*(5), 1725-1728.

Tuifaiga, A. A., Ram, P. A., & Kolahi, S. S. (2021, December). Performance comparison of IPv6 in 802.11 ac WLAN in Windows and Linux environment. In *TENCON 2021-2021 IEEE Region 10 Conference (TENCON)* (pp. 799-804). IEEE.

Yazid, M., Bouallouche-Medjkoune, L., & Aïssani, D. (2016, September). Performance Study of Frame Aggregation Mechanisms in the New Generation WiFi. In *VECoS* (pp. 85-92).

Al-Mukhtar Journal of Basic Sciences 21 (2): 39-51, 2023
Doi: https://doi.org/10.54172/55bvvp02

Research Article

Open Access

A multi-step formable transform decomposition method for solving fractional order Riccati equation

Ahmad A. H. Mtawal

***Corresponding author:**
ahmad.mtawal@uob.edu.ly
Department of Mathematics, Faculty of Education Almarj, Benghazi University, Libya

Received:
15 August 2023

Accepted:
25 October 2023

Publish online:
31 December 2023

Abstract

A multi-step formable transform decomposition method (MFTDM) is suggested in this study to solve the nonlinear fractional-order Riccati problem. It is well understood that a corresponding numerical solution given by the FTDM is only valid for a short period.In the case of integer-order systems, however, the MFTDM solutions are more correct and reliable throughout time and are in very good agreement with the exact solutions. The fractional derivative is described in the Caputo sense. The method is tested on prominent examples, and the results show that it is accurate and efficient when compared to other numerical methods.

Keywords: Caputo derivative; Fractional orderRiccati equation; Multi-step Formable transform decomposition Method.

INTRODUCTION

The formable transform decomposition method (FTDM) is a computational and analytical approach for solving fractional partial differential problems (Saadeh et al., 2023). The method provides the solution in terms of convergent series with easily computable components. In the past years, several academics have concentrated their efforts on the numerical solution of ordinary differential equations of fractional order and various numerical techniques, including the Fourier transform method (Kemle& Beyer, 1997), Homotopy perturbation method (Wang, 2007; Odibat & Momani, 2008; Mtawal & Alkaleeli, 2020), Homotopy analysis method (Canget al., 2009; Zurigatet al., 2010; Freihat, et al., 2014), Residual power series method (Ali et al., 2017), Alternative variational iteration method (Mtawalet al., 2020), Triple Shehu transform method (Alkaleeliet al., 2021; Kapooret al., 2022), the Laplace residual power series method (Burqan, et al., 2022),. Recently, a formable transformation decomposition method (FTDM) was applied by (Al-ZouBi&Zurigat, 2014), it combines the formable integral transform (Saadeh, 2021) and the decomposition method (Momani& Al-Khaled, 2005; Shawagfeh, 2002; Khanet al, 2013; Mahdyet al., 2015). In the present study, we analyze the suitability and value of the MFTDM as a method to obtain the right approximation solutions to the fractional differential equation of the form using a series of intervals.

$$D_{*}^{\beta} y(t) = g(t) - L[y(t)] - N[y(t)], \qquad (1)$$

with $t \geq 0,\ 0 < \alpha \leq 1,$ and subject to the initial condition.

$$y(0) = c. \qquad (2)$$

Where $D_*^{\beta} y(t)$ is the fractional derivative of Caputo?This optimized approach is known as the multi-step formable transform decomposition method.The MFTDM was successfully shown to effectively, quickly, and accurately solve fractional differential equations. There is an enormous class of nonlinear fractional differential equations with approximations that rapidly converge to exact solutions. We provided two examples to show the effectiveness of our results.

PRELIMINARIES

This section describes the essential terminology and notations used in the fractional derivative field (Caputo, 1969; Miller &Roos, 1993; Beyer &Konuralp, 1995; Gorenflo&Mainardi, 1997; Podlubny, 1999). Also covered are the definition and characteristics of the formable integral transform (Kanwal*et al*., 2018; Saadeh& Ghazal, 2021; Saadeh*et al*., 2023).

Definition 2.1. The Riemann-Liouville fractional integral of order $\beta > 0$,ofa function $f \in C_{\rho},\ \rho \geq -1$ is defined as (Miller &Roos, 1993; Beyer &Konuralp, 1995; Gorenflo&Mainardi, 1997; Podlubny, 1999) :

$$J^{\beta} f(t) = \frac{1}{\Gamma(\beta)} \int_0^t (t-\zeta)^{\beta-1} f(\zeta)\, d\zeta .$$

Definition 2.2. Let $f \in C_n^m,\ m \in N \cup \{0\}$. The Caputo fractional derivative of f in the Caputo sense is defined as follows (Caputo, 1969):

$$D_t^{\beta} f(t) = \begin{cases} \dfrac{1}{\Gamma(m-\alpha)} \int_0^t (t-\zeta)^{m-\beta-1} f^{(m)}(\zeta)\ d(\zeta), \\ \qquad\qquad\qquad\qquad m-1 < \beta \leq m, \\ D_t^{\beta} f(t), \qquad\qquad\qquad \beta = m. \end{cases}$$

Definition 2.3.(Saadeh& Ghazal, 2021; Saadeh*et al*., 2023) A function $f : [0,\infty) \to R$ is said to be of exponential order $\beta\ (\beta > 0)$, if there $|f(t)| \leq M\ e^{\beta t}$, for all $t \geq t_0$.

Definition 2.4. The formable integral transform of a continuous function f on the interval $(0,\infty)$ is defined by (Saadeh& Ghazal, 2021; Saadeh*et al*., 2023)

$$F[f(t)] = \frac{s}{u} \int_0^{\infty} \exp\left(-\frac{s\,t}{u}\right) f(t)\, dt$$

$$= A(s,u).$$

The formula for the inverse formable integral transform is

$$f(t) = F^{-1}[A(s,u)]$$

$$= \frac{1}{2\pi i} \int_{a-i\infty}^{a+i\infty} \frac{1}{s} \exp\left(\frac{s\,t}{u}\right) A(s,u)\, ds .$$

A constant's or polynomial's formable integral transform is given by:

$$F[a] = a.$$

$$F\left[t^{m}\right]=\left(\frac{u}{s}\right)^{m} m!, m \in N .$$

$$F\left[t^{\beta}\right]=\left(\frac{u}{s}\right)^{\beta} \Gamma(\beta+1), \beta>0.$$

Theorem 2.1. The Mittag-Leffler function's formable integral transform is provided by(Kanwal*et al*., 2018)

$$A(s,u)=\sum_{i=0}^{\infty} \lambda^{i}\left(\frac{u}{s}\right)^{\beta i+\alpha-1} .$$

Theorem 2.2. Let$f$ be a piecewise continuous function defined on $[0,\infty)$. Then, the formable integral transform of the Riemann-Liouville fractional integral of order $\beta>0$ of the function f is given by (Saadeh& Ghazal, 2021; Saadeh*et al*., 2023)

$$F\left[I_{t}^{\beta} f(t)\right]=\left(\frac{u}{s}\right)^{\beta} A(s,u).$$

Theorem 2.3. Let f be a piecewise continuous function defined on $[0,\infty)$. Then, the formable integral transform of the Caputo fractional derivative of the order $\beta, m-1<\beta \leq m$, of the function f is given by (Saadeh& Ghazal, 2021; Saadeh*et al*., 2023)

$$F\left[D_{t}^{\beta} f(t)\right]=\left(\frac{u}{s}\right)^{\beta}\left[A(s,u)\right] -\left(\frac{u}{s}\right)^{\beta}\left(\sum_{i=0}^{m-1}\left(\frac{u}{s}\right)^{i} f^{(i)}(0)\right).$$

MATERIALS AND METHODS

Despite the fact that the FTDM (Saadeh, 2021) is used to approximate solutions to a wide range of nonlinear problems in terms of convergent series with readily calculated components, it has certain shortcomings: The series solution always converges rapidly in a small region and slowly in a bigger region. In this section, we present the core notions of the MFDTM that we built for numerically solving our problems (1) and (2). It is a simple tweak to regular FTDM that verifies the accuracy of the estimated solution for large time intervals. The solution is expanded over the interval $[0,t]$ by dividing it into i - subintervals $[t_{i-1},t_i]$, $j=1,2,\ldots,i$ of equal length Δt. If t^* is the initial value and $y_j(t)$ is an approximation in each subinterval $[t_{i-1},t_i]$, $j=1,2,\ldots,i$, the equations (1) and (2) can be transformed into the following system:

$$D_{*}^{\beta} y_j(t)=g(t)-L\left[y_j(t)\right]-N\left[y_j(t)\right], \qquad (3)$$

with $t \geq 0,\ 0<\beta \leq 1,\quad j=1,2,\ldots,i$ and subject to the initial condition

$$y_j(t^*)=a,\quad y_j(t^*)=y_{j-1}(t_{j-1})=c_j, \qquad (4)$$

where $D_{*}^{\beta} y_j(t)$ is the Caputo fractional derivative,the source term is $g(t)$, L means the linear differential operator and N means the general nonlinear differential operator.

Using the formable integral (denoted by F in this study) on both sides of Equation (3), we obtain

$$F\left[D_*^{\beta} y_j(t) \right] = F\Big[g(t) - L\left[y_j(t) \right] - N\left[y_j(t) \right] \Big]. \tag{5}$$

Equation (5) can be read using Theorem 2.3 and the initial condition in equation (4) as

$$F\left[y_j(t) \right] = c_j + \left(\frac{u}{s} \right)^{\beta} F\Big[g(t) - L\left[y_j(t) \right] - N\left[y_j(t) \right] \Big]. \tag{6}$$

Using the formable inverse on both sides of Equation (6) yields

$$y_j(t) = F^{-1}\left[c_j \right] + F^{-1}\left[\left(\frac{u}{s} \right)^{\beta} F\left[g(t) \right] - L\left[y_j(t) \right] \right] - F^{-1}\left[\left(\frac{u}{s} \right)^{\beta} F\left[N\left[y_j(t) \right] \right] \right]. \tag{7}$$

Then,

$$y_j(t) = \sum_{i=0}^{n} y_{j,i}(t), \tag{8}$$

The nonlinear term in Equation (7) can be decomposed as follows:

$$N\left[y_{j,i}(t) \right] = \sum_{i=0}^{\infty} A_{j,i}\left(y_{j,0}, y_{j,1}, \ldots, y_{j,i} \right), \tag{9}$$

for some Adomian's polynomials A_i that are given by (Ghorbani, 2009).

$$A_{j,i}\left(y_{j,0}, y_{j,1}, \ldots, y_{j,i} \right) = \frac{1}{i!} \left(\sum_{i=0}^{n} \frac{d^i}{d\lambda^i} N\left(\sum_{k=0}^{\infty} \lambda^i y_{j,i} \right) \right)_{\lambda=0}. \tag{10}$$

Substituting Equations (8) and (9) into Equation (7) yields

$$\sum_{i=0}^{n} y_{j,i}(t) = c_j + F^{-1}\left[\left(\frac{u}{s} \right)^{\beta} F\left[g(t) \right] \right] - F^{-1}\left[\left(\frac{u}{s} \right)^{\beta} F\left[\sum_{i=0}^{\infty} \left(L\left[y_{j,i-1}(t) \right] \right) \right] \right] - F^{-1}\left[\left(\frac{u}{s} \right)^{\beta} F\left[\sum_{i=0}^{\infty} \left(A_{j,i-1} \right) \right] \right]. \tag{11}$$

After considering the comparison in Equation (11), we obtain

$$
\begin{aligned}
&y_{j,0}(t)=c_j,\\
&y_{j,1}(t)=F^{-1}\left[\left(\frac{u}{s}\right)^{\beta}F\left[g(t)\right]\right]\\
&\qquad -F^{-1}\left[\left(\frac{u}{s}\right)^{\beta}F\left[L\left[y_{j,0}(t)\right]\right]\right]\\
&\qquad -F^{-1}\left[\left(\frac{u}{s}\right)^{\beta}f\left[A_{j,0}\right]\right],\\
&y_{j,2}(t)=-F^{-1}\left[\left(\frac{u}{s}\right)^{\beta}F\left[L\left[y_{j,1}(t)\right]\right]\right]\\
&\qquad -F^{-1}\left[\left(\frac{u}{s}\right)^{\beta}F\left[A_{j,1}\right]\right],\\
&\quad\vdots\\
&y_{j,i}(t)=-F^{-1}\left[\left(\frac{u}{s}\right)^{\beta}F\left[L\left[y_{j,i-1}(t)\right]\right]\right]\\
&\qquad -F^{-1}\left[\left(\frac{u}{s}\right)^{\beta}F\left[A_{j,i-1}\right]\right]. \qquad (12)
\end{aligned}
$$

In addition, a power series solution needs the form

$$y_j(t)=\sum_{i=0}^{\infty}y_{j,i}(t),\quad j=1,2,\ldots,i. \qquad (13)$$

Finally, the system (1) solutions have the form

$$y(t)=\begin{cases} y_1(t), & t\in[t_0,t_1],\\ y_2(t), & t\in[t_1,t_2],\\ \vdots & \\ y_i(t), & t\in[t_{i-1},t_i]. \end{cases} \qquad (14)$$

RESULTS

To show the applicability and effectiveness of our approach for solving nonlinear fractional Riccate equations, we explore the following examples: (Al-ZouBi&Zurigat, 2014;Zurigatet al., 2010; Canget al.,2009) :

Example 1.Consider the following nonlinear fractional Riccati equation

$$D_*^{\beta}y(t)=1-y^2(t),\quad t\geq 0,\quad 0<\beta\leq 1, \qquad (15)$$

with the initial condition

$$y(0)=0. \qquad (16)$$

The exact solutions of this equation when $\beta=1$ is $y(t)=\frac{e^{2t}-1}{e^{2t}+1}$. If $y_j(t)$ is an approximation in each subinterval $[t_{i-1},t_i]$, $j=1,2,\ldots,i$, the equations (15) and (16) can be transformed into the following system:

$$D_*^{\beta} y_j(t) = 1 - y_j{}^2(t), \quad j = 1, 2, \ldots, i. \quad (17) \qquad y_j(t^*) = c_j, \quad (18)$$

With initial conditionwith $c_1 = 1.$

Using the formable integral (denoted by F in this study) on both sides of Equation (17), we obtain

$$F\left[D_*^{\beta} y_j(t)\right] = F\left[1 - y_j{}^2(t)\right], \quad (19)$$

Equation (19) can be read using Theorem 2.3 and the initial condition in equation (18) as

$$F\left[y_j(t)\right] = c_j + \left(\frac{u}{s}\right)^{\beta} F\left[1 - y_j{}^2(t)\right]. \quad (20)$$

Using the formable inverse on both sides of Equation (20) yields

$$y_j(t) = F^{-1}\left[c_j\right] + F^{-1}\left[\left(\frac{u}{s}\right)^{\beta} F\left[1 - y_j{}^2(t)\right]\right]. \quad (21)$$

Where $N\left[y_j(t)\right] = y_j^2(t)$ is a nonlinear operator, respectively.The nonlinear term of Eq.(21) can be decomposed as

$$N\left[y_j(t)\right] = y_j^2(t) = \sum_{i=0}^{\infty} A_{j,i}. \quad (22)$$

Adomian polynomials' first few components are provided by

$$A_{j,0} = y_{j,0}^2,$$
$$A_{j,1} = 2 y_{j,0} y_{j,1},$$
$$A_{j,2} = 2 y_{j,0} y_{j,2} + y_{j,1}^2.$$
$$\vdots$$

Assume that the solution of Equation (17) has the following series

$$y_j(t) = \sum_{i=0}^{n} y_{j,i}(t). \quad (23)$$

Substituting Equations (22) and (23) into Equation (21) yields

$$\sum_{i=0}^{n} y_{j,i}(t) = c_j + F^{-1}\left[\left(\frac{u}{s}\right)^{\beta} F\left[1 - \sum_{i=0}^{\infty} A_{j,i}\right]\right]. \quad (24)$$

After considering the comparison in Equation (24), we obtain

$$y_{j,0}(t) = c_j,$$
$$y_{j,1}(t) = F^{-1}\left[\left(\frac{u}{s}\right)^{\beta} F\left[1 - A_{j,0}\right]\right]$$
$$= \frac{\left(1 - c_j^2\right)(t - t^*)^{\beta}}{\Gamma(\beta + 1)},$$
$$y_{j,2}(t) = -F^{-1}\left[\left(\frac{u}{s}\right)^{\beta} F\left[A_{j,1}\right]\right]$$

$$= \frac{-2c_j\left(1 - c_j^2\right)(t - t^*)^{2\beta}}{\Gamma(2\beta + 1)},$$

$$y_{j,3}(t) = -F^{-1}\left[\left(\frac{u}{s}\right)^{\beta} F\left[A_{j,2}\right]\right]$$
$$= \frac{4c_j^2\left(1-c_j^2\right)(t-t^*)^{3\beta}}{\Gamma(3\beta+1)}$$
$$-\frac{\left(1-c_j^2\right)^2\Gamma(2\alpha+1)(t-t^*)^{3\beta}}{\Gamma^2(\beta+1)\Gamma(3\beta+1)}.$$
$$\vdots \qquad (25)$$

The series solution to equation (17) is provided by

$$y_j(t) = c_j + \frac{\left(1-c_j^2\right)(t-t^*)^{\beta}}{\Gamma(\beta+1)}$$
$$-\frac{2c_j\left(1-c_j^2\right)(t-t^*)^{2\beta}}{\Gamma(2\beta+1)} + \frac{4c_j^2\left(1-c_j^2\right)(t-t^*)^{3\beta}}{\Gamma(3\beta+1)}$$
$$-\frac{\left(1-c_j^2\right)^2\Gamma(2\beta+1)(t-t^*)^{3\beta}}{\Gamma^2(\beta+1)\Gamma(3\beta+1)} + \ldots.$$

In this example, the suggested method is applied to the interval $[0,10]$. We selected dividing the interval $[0,10]$ into subintervals with a time step of $\Delta t = 0.5$ .Figures 1 and 2 show the series solution of the MFTDM of the nonlinear fractional Riccati equations (15) and (16) for $\beta = 1, 0.7, 0.9$ and the exact. The graphical results show that the results produced using the MFTDM for $\beta = 1$ very closely correspond to the results of the exact solution.This emphasizes MFTDM applicability to many different kinds of nonlinear fractional differential equations, as well as its reliability and promise when compared to existing methods. Furthermore, as in the preceding instance, the numerical results produced by the MFTDM have the same course for various values of β . All results are obtained using Maple 16.

Example 2. Consider the following nonlinear fractional Riccati equation

$$D_*^{\beta} y(t) = 1 + 2y(t) - y^2(t), \quad t \geq 0, \quad 0 < \beta \leq 1, \quad (26)$$

with the initial condition

$$y(0) = 0. \qquad (27)$$

The exact solutions of this equation when $\beta = 1$ is $y(t) = 1 + \sqrt{2}\tanh\left(\sqrt{2}t + \frac{1}{2}\log\left(\frac{\sqrt{2}-1}{\sqrt{2}+1}\right)\right)$. If $y_j(t)$ is an approximation in each subinterval $[t_{i-1}, t_i]$, $j = 1, 2, \ldots, i$, the equations (26) and (27) can be transformed into the following system:

$$D_*^{\beta} y_j(t) = 1 + 2y_j(t) - y_j^2(t), \quad j = 1, 2, \ldots, i. \quad (28)$$

$$y_j(t^*) = c_j, \quad (29)$$

With initial conditionswith $c_1 = 1$.

Using the formable integral (denoted by F in this study) on both sides of Equation (28), we obtain

$$F\left[D_*^{\alpha} y_j(t)\right] = F\left[1 + 2y_j(t) - {y_j}^2(t)\right], \quad (30)$$

Equation (30) can be read using Theorem 2.3 and the initial condition in equation (29) as

$$F\left[y_j(t)\right] = c_j + \left(\frac{u}{s}\right)^{\beta} F\left[1 + 2y_j(t) - {y_j}^2(t)\right]. \quad (31)$$

Using the formable inverse on both sides of Equation (31) yields

$$\begin{aligned} y_j(t) &= F^{-1}\left[c_j\right] \\ &+ F^{-1}\left[\left(\frac{u}{s}\right)^{\beta} F\left[1 + 2y_j(t)\right]\right] \\ &- F^{-1}\left[\left(\frac{u}{s}\right)^{\beta} f\left[{y_j}^2(t)\right]\right] \end{aligned} \quad (32)$$

Where $L\left[y_j(t)\right] = y_j(t), N\left[y_j(t)\right] = y_j^2(t)$ are linear and nonlinear operators, respectively.The nonlinear term of Eq.(32) can be decomposed as

$$N\left[y_j(t)\right] = y_j^2(t) = \sum_{i=0}^{\infty} A_{j,i}. \quad (33)$$

Adomian polynomials' first few components are provided by

$$A_{j,0} = y_{j,0}^2,$$

$$A_{j,1} = 2y_{j,0}y_{j,1},$$

$$A_{j,2} = 2y_{j,0}y_{j,2} + y_{j,1}^2.$$

$$\vdots$$

Assume that the solution of Equation (28) has the following series

$$y_j(t) = \sum_{i=0}^{n} y_{j,i}(t). \quad (34)$$

Substituting Equations (33) and (34) into Equation (32) yields

$$\sum_{i=0}^{n} y_{j,i}(t) = c_j + F^{-1}\left[\left(\frac{u}{s}\right)^{\beta} F\left[1 + 2\, y_{j,i} - \sum_{i=0}^{\infty} A_{j,i}\right]\right]. \quad (35)$$

After considering the comparison in Equation (35), we obtain

$$y_{j,0}(t) = c_j,$$

$$\begin{aligned} y_{j,1}(t) &= F^{-1}\left[\left(\frac{u}{s}\right)^{\beta} F\left[1 + 2\, y_{j,0} - A_{j,0}\right]\right] \\ &= \frac{\left(1 + 2c_j - c_j^2\right)(t - t^*)^{\beta}}{\Gamma(\beta + 1)}, \end{aligned}$$

$$
\begin{aligned}
y_{j,2}(t) &= F^{-1}\left[\left(\frac{u}{s}\right)^{\beta} F\left[2\, y_{j,1} - A_{j,1}\right]\right] \\
&= \frac{2\left(1-c_j\right)\left(1+2c_j-c_j^2\right)(t-t^*)^{2\beta}}{\Gamma(2\beta+1)} \\
&\quad - \frac{\left(1+2c_j-c_j^2\right)^2 \Gamma(2\beta+1)\,(t-t^*)^{2\beta}}{\Gamma^2(\beta+1)\,\Gamma(2\beta+1)}, \\
&\vdots
\end{aligned}
\tag{36}
$$

The series solution to equation (28) is provided by

$$
\begin{aligned}
y_j(t) &= c_j + \frac{\left(1+2c_j-c_j^2\right)(t-t^*)^{\beta}}{\Gamma(\beta+1)} \\
&\quad + \frac{2\left(1-c_j\right)\left(1+2c_j-c_j^2\right)(t-t^*)^{2\beta}}{\Gamma(2\beta+1)} \\
&\quad - \frac{\left(1+2c_j-c_j^2\right)^2 \Gamma(2\alpha+1)\,(t-t^*)^{2\beta}}{\Gamma^2(\beta+1)\,\Gamma(2\beta+1)} + \ldots.
\end{aligned}
$$

In this example, the suggested method is applied to the interval $[0,10]$. We selected dividing the interval $[0,5]$ into subintervals with a time step of $\Delta t = 0.1$.Figures 3 and 4 show the series solution of the MFTDM of the nonlinear fractional Riccati equations (26) and (27) for $\beta = 1, 0.7, 0.9$ and the exact. The graphical results show that the results produced using the MFTDM for $\beta = 1$ very closely correspond to the results of the exact solution.This emphasizes MFTDM applicability to many different kinds of nonlinear fractional differential equations, as well as its reliability and promise when compared to existing methods. Furthermore, as in the preceding instance, the numerical results produced by the MFTDM have the same course for various values of β. All results are obtained using Maple 16.

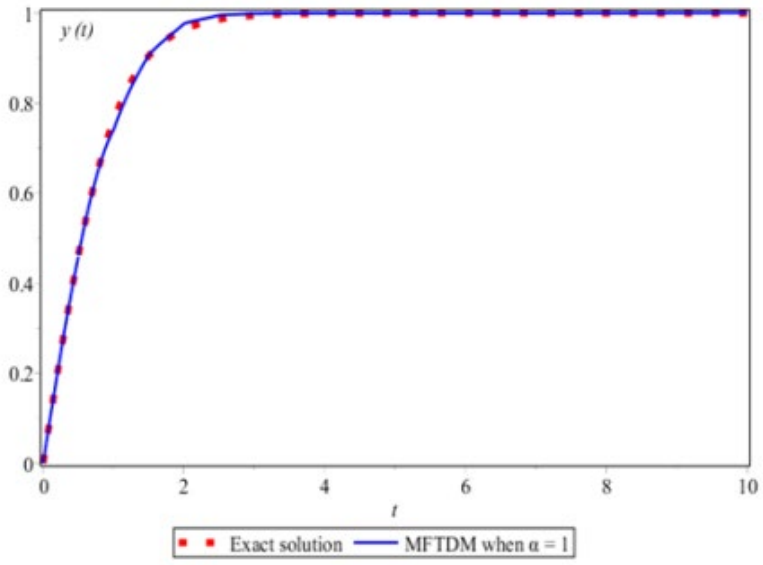

Figure: (1). Comparison between the exact and the MFTDM solutions of $y(t)$ for $\beta = 1$.

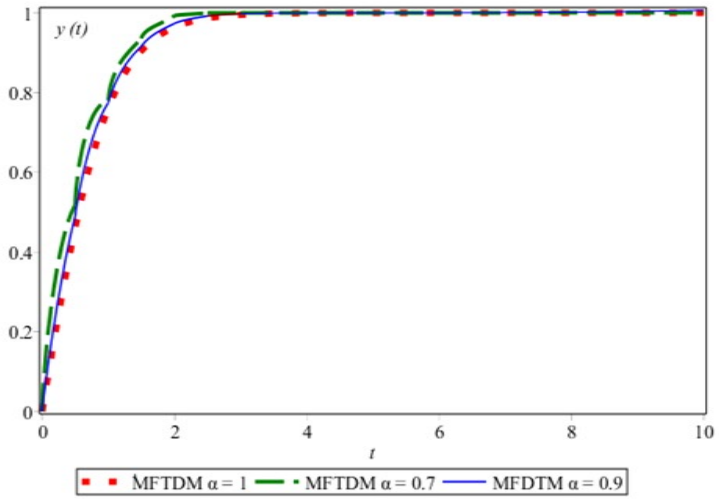

Figure: (2). The MFTDM solution of $y(t)$ for different values of β.

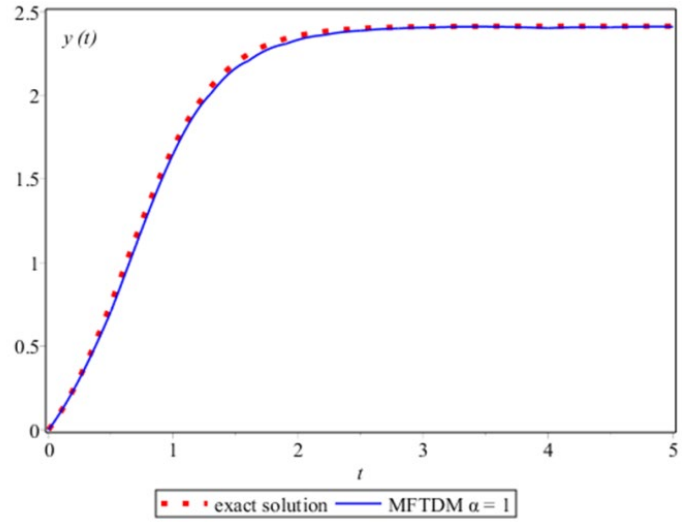

Figure: (3). Comparison between the exact and the MFTDM solutions of $y(t)$ for $\beta = 1$.

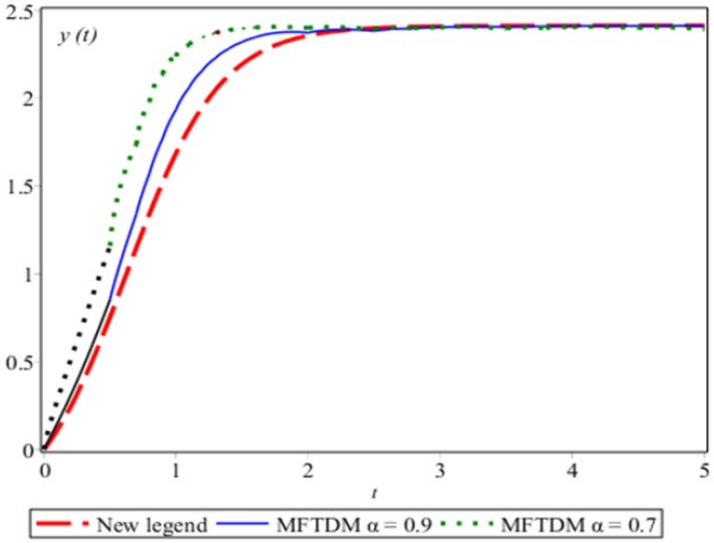

Figure: (4). The MFTDM solution of $y(t)$ for different values of β.

DISCUSSION

The graphical results show that the results produced using the MFTDM $\beta = 1$ very closely correspond to the results of the exact solution. This emphasizes the MFTDM applicability to many different kinds of nonlinear fractional differential equations, as well as its reliability and promise when compared to existing methods. Furthermore, as in the preceding instance, the numerical results produced by the MFTDM have the same course for various values of β. This is completely consistent with the research results of Al-Zoubi&Zurigat (2014).

CONCLUSION

A multi-step formable transform decomposition method (MFTDM) is suggested in this study to solve the nonlinear fractional-order Riccati problem.The MFTDM has been shown to solve fractional Riccati equations effectively, easily, and accurately. Approximate solutions quickly converge on exact solutions. This is completely consistent with the research results of Al-Zoubi&Zurigat (2014).Finally, we conclude that MFTDM is an excellent enhancement of existing numerical approaches.All results are obtained using Maple 16.

ACKNOWLEDGEMENT

The authors would like to thank the referees for their feedback.

Duality of interest: The author certifies that he has no competing interests with regard to this manuscript.

Author contributions: The author certifies that he has no competing interests concerning this manuscript.

Funding: This research received no funding from government, commercial, or non-profit organizations.

REFERENCES

Ali, M., Jaradat, I., &Alquran, M. (2017).New computational method for solving fractional Riccati equation. *J. Math. Comput.Sci*, *17*(1), 106-114.

Al-Zou'bi, H., & Al-Zurigat, M. (2014).Solving nonlinear fractional differential equations using multi-step homotopy analysis method. *Annals of the University of Craiova-Mathematics and Computer Science Series*, *41*(2), 190-199.

Beyer, H., &Kempfle, S. (1995). Definition of physically consistent damping laws with fractional derivatives. *ZAMM-Journal of Applied Mathematics and Mechanics/ZeitschriftfürAngewandteMathematik und Mechanik*, *75*(8), 623-635.

Burqan, A., Sarhan, A., &Saadeh, R. (2022).Constructing Analytical Solutions of the Fractional Riccati Differential Equations Using Laplace Residual Power Series Method. *Fractal and Fractional*, *7*(1), 14.

Cang, J., Tan, Y., Xu, H., & Liao, S. J. (2009).Series solutions of non-linear Riccati differential equations with fractional order. *Chaos, Solitons& Fractals*, *40*(1), 1-9.

Caputo, M. (1969).Elasticita de dissipazione, zanichelli, bologna, italy,(links). *SIAM journal on numerical analysis*.

Freihat, A. A., Zurigat, M., &Handam, A. H. (2015).The multi-step homotopy analysis method for modified epidemiological model for computer viruses. *AfrikaMatematika*, *26*, 585-596.

Ghorbani, A. (2009). Beyond Adomian polynomials: he polynomials. *Chaos, Solitons& Fractals*, *39*(3), 1486-1492.

Gorenflo, R., &Mainardi, F. (1997). *Fractional calculus: integral and differential equations of fractional order* (pp. 223-276). Springer Vienna.Jafari, H.; &Tajadodi, H. (2010). He's variational iteration method for solving fractional Riccati differential equation. *Int. J. Diff. Equ*, 2010**,** 764738.

Kapoor, M., Shah, N. A., Saleem, S., &Weera, W. (2022). An analytical approach for fractional hyperbolic telegraph equation using Shehutransform in one, two and three dimensions. *Mathematics*, *10*(12), 1961.

Kanwal, A., Phang, C., &Iqbal, U. (2018).Numerical solution of fractional diffusion wave equation and fractional Klein–Gordon equation via two-dimensional Genocchi polynomials with a Ritz–Galerkin method. *Computation*, *6*(3), 40.

Khan, N. A., Ara, A., &Alam Khan, N. (2013). Fractional-order Riccati differential equation: analytical approximation and numerical results. *Advances in Difference Equations*, *2013*, 1-16.

Mahdy, A. M. S., Mohamed, A. S., &Mtawa, A. A. H. (2015).Sumudu decomposition method for solving fractional-order Logistic differential equation. *Journal: JOURNAL OF ADVANCES IN MATHEMATICS*, *10*(7).

Miller, K. S., & Ross, B. (1993).An introduction to the fractional calculus and fractional differential equations. *(No Title)*.

Momani, S., & Al-Khaled, K. (2005).Numerical solutions for systems of fractional differential equations by the decomposition method. *Applied Mathematics and Computation*, *162*(3), 1351-1365.

Mtawal, A. A., &Alkaleeli, S. R. (2020).A new modified homotopy perturbation method for fractional partial differential equations with proportional delay. *Journal of Advances In Mathematics*, *19*, 58-73.

Mtawal, A. A., Muhammed, S. E., &Almabrok, A. A. (2020).Application of the alternative variational iteration method to solve delay differential equations. *International journal of Physical sciences*, *15*(3), 112-119.

Odibat, Z., &Momani, S. (2008). Modified homotopy perturbation method: application to quadratic Riccatidifferential equation of fractional order. *Chaos, Solitons& Fractals*, *36*(1), 167-174.

Podlubny, I. (1999). Fractional Differential Equations, *Academic Press, San Diego*.

Saadeh, R. (2021). Numerical algorithm to solve a coupled system of fractional order using a novel reproducing kernel method. *Alexandria Engineering Journal*, *60*(5), 4583-4591.

Saadeh, R. Z., & Ghazal, B. F. A. (2021). A new approach on transforms: Formable integral transform and its applications. *Axioms*, *10*(4), 332.

Saadeh, R., Qazza, A., Burqan, A., & Al-Omari, S. (2023). On Time Fractional Partial Differential Equations and Their Solution by Certain Formable Transform Decomposition Method. *CMES-Computer Modeling in Engineering & Sciences*, *136*(3), 3121-3139.

Sameehah, R. A., Ahmad, A. H., &Mbroka, S. H. (2021). Triple Shehu transform and its properties with applications. *African Journal of Mathematics and Computer Science Research*, *14*(1), 4-12.

Shawagfeh, N. T. (2002). Analytical approximate solutions for nonlinear fractional differential equations. *Applied Mathematics and Computation*, *131*(2-3), 517-529.

Wang, Q. (2007). Homotopy perturbation method for fractional KdV equation. *Applied Mathematics and Computation*, *190*(2), 1795-1802.

Zurigat, M., Momani, S., Odibat, Z., &Alawneh, A. (2010).The homotopy analysis method for handling systems of fractional differential equations. *Applied Mathematical Modelling*, *34*(1), 24-35.

Al-Mukhtar Journal of Basic Sciences 21 (2): 52-57, 2023
Doi: https://doi.org/10.54172/99p86m22

Research Article

Open Access

On Strongly Regular Relation of Canonical Hypergroup

Yasser A. AbouElwan[1*] and Maher. A. Alderawe[2*]

***Corresponding author:** yasserabouelwan@gmail.com Department of Mathematics, Faculty of Science, University of Omar Al-Mukhtar

Second Author: Department of Mathematics, Faculty of Science, University of Omar Al-Mukhtar

Received:
05 September 2023

Accepted:
30 December 2023

Publish online:
31 December 2023

Abstract

Burris and Sankappanavar established a connection between congruence in group G (ring R) and a normal subgroup of G (ideal of ring R). In this paper in the same manner, the connection between strongly regular relation defined on canonical hypergroup and normal subcanonical hypergroup of canonical hypergroup is established.

Keywords: canonical hypergroup, subcanonical hypergroup, normal subcanonical hypergroup, regular relation, strongly regular relation, and quotient of canonical hypergroup .

INTRODUCTION

The French mathematician Marty proposed the idea of hyperstructure, and particularly the idea of hypergroup, in 1934 (Marty, 1934). There are basic definitions and theories concerning the hyperstructures previously (AbouElwan & Alderawe, 2023; Davvaz *et al*., 2023) Several fields of other disciplines can benefit from the use of hyperstructures. There have been numerous books and articles written about the use of hyperstructures in the study of geometry, hypergraphs, binary relations, lattices, fuzzy sets, etc (AbouElwan & Alderawe, 2023; Davvaz, 2012; Burris & Sankappanavar, 1981; Vougiouklis, 1994). Canonical hypergroup as a special kind of hypergroup is indeed a natural generalization of the concept of abelian group. This kind of hypergroup is a basic additive hyperstructure of many hyperstructures.

By applying a specific kind of equivalence relations, semihypergroup can be connected to semigroup, hypergroup to the group and canonical hypergroup to abelian group. These equivalence relations are called strongly regular relations. More exactly, by given (a semihypergroup, a hypergroup, and a canonical hypergroup) and by using a strongly regular relation on them, (a semigroup, a group, and the abelian group) respectively can be constructed from their quotient hyperstructures. (Corsini & Leoreanu, 2003)

MATERIALS AND METHODS

The definitions and examples from this section will be utilized throughout the paper.
A hyperoperation o on a non-empty set H is a mapping o: H × H → P *(H), P *(H) is the power set of H, ∅∉ P *(H). Moreover, the pair (H, o) is called a hyper-groupoid. For every A and B ∈ P

*(H) and x ∈ H, the sets A o B, A o x and x o A are defined by A o B = ⋃{a o b | a ∈ A, b ∈ B}, A o x = A o {x} and x o A = {x} o A.

A hypergroupoid (H, o) is called a semihypergroup if for all a, b, c of H, we have a o (b o c) = (a o b) o c, this means that $\bigcup_{u \in b \circ c}$ a o u = $\bigcup_{v \in a \circ b}$ v o c. A semihypergroup (H, o) is called a hypergroup if for every a ∈ H, we have a o H = H o a = H, that is called the reproduction axiom. A hypergroup (H, o) is called a commutative hypergroup if for all a, b ∈ H, we have a o b = b o a. A non-empty subset K of a hypergroup (H, o) is called a subhypergroup of H if K is a hypergroup under o. Several books have been written on hyperstructure theory (AbouElwan & Alderawe, 2022; Velrajan & Asokkumar, 2010; Vougiouklis, 1994).

Let (H, o) be a semihypergroup and R be an equivalence relation on H. If A, B are non-empty subsets of H, then A$\overline{R}$B means that

∀a ∈ A, ∃b ∈ B such that aRb, and ∀b`∈ B, ∃a`∈ A such that a`Rb`.

Furthermore, A$\overline{\overline{R}}$B means that

∀a ∈ A, ∀b ∈ B, we have aRb.

In addition, the equivalence relation R on H is said to be:

1) Regular on the left (on the right) if ∀ x ∈ H, from aRb, it follows that (x o a)$\overline{R}$(x o b) ((a o x)$\overline{R}$(b o x) respectively).
2) Strongly regular on the left (on the right) if ∀ x ∈ H, from aRb, it follows that (x o a)$\overline{\overline{R}}$(x o b) ((a o x)$\overline{\overline{R}}$(b o x)respectively).
3) Strongly regular (Regular) if it is strongly regular (regular) on the right and on the left. (see 6).

Let (H, o) be a hypergroup, for an equivalence relation R on H, we use R(x) to denote the equivalence class of x to R and use H/R to denote the family of equivalence classes {R(x) | x ∈ H} of R. The reader can find the proofs of the following two theorems in (BDavvaz & Leoreanu-Fotea, 2007; Davvaz *et al*., 2022).

Theorem 2.1. If (H, o) is a hypergroup (a semihypergroup) and R is a regular relation on H, then the quotient H/R is a hypergroup (a semihypergroup) under the operation defined by

$$R(x) \otimes R(y) = \{R(z) \mid z \in x \circ y\}.$$

Theorem 2.2. If (H, o) is a hypergroup (a semihypergroup) and R is a strongly regular relation on H, then the quotient H/R is a group (a semigroup) under the operation defined by

$$R(x) \otimes R(y) = R(z), \forall z \in x \circ y.$$

Definition 2.3. A canonical hypergroup (M, +) is a non-empty set M together with a hyperoperation + which satisfies the following axioms:

i. ∀ x, y ∈ M, x + y = y + x,
ii. ∀ x, y, z ∈ M, x + (y + z) = (x + y) + z,
iii. ∃ 0 ∈ M (called neutral element of M) such that

$$0 + x = \{x\} = x + 0, \forall x \in M,$$

iv. ∀ x ∈ M, $\exists_1$ – x ∈ M such that

$$0 \in x + (-x) \cap (-x) + x,$$

v. the reversibility axiom:

$\forall$ x, y, z $\in$ M, z $\in$ x + y $\Rightarrow$ y $\in$ – x + z and x $\in$ z + (– y).

Let (M, +) be a canonical hypergroup, a non-empty subset N of (M, +) is called a subcanonical hypergroup of M if (N, +) is a canonical hypergroup itself. Equivalently, x – y $\subseteq$ N, $\forall$ x, y $\in$ N.

In particular, $\forall$ x $\in$ N, x – x $\subseteq$ N. Since 0 $\in$ x – x, it follows that 0 $\in$ N. Moreover, N is said to be normal if x + N – x $\subseteq$ N, for all x $\in$ M. In addition, a subcanonical hypergroup N of M is called a subgroup of M if (N, +) is a group, that is, if x + y is a singleton set for all x, y $\in$ N.

Example 2.4. Consider the set M ={0, a, b}. Define a hyperaddition + on M as in the following table

+	0	*A*	*b*	*c*
0	{0}	{*a*}	{*b*}	{*c*}
a	{*a*}	{0, *b*}	{*a, c*}	{*b*}
b	{*b*}	{*a, c*}	{0, *b*}	{*a*}
c	{*c*}	{*b*}	{*a*}	{0}

Then, (M, +) is a canonical hypergroup, {0, b} is a subcanonical hypergroup of M, and {0, c} is a subgroup of M.

Remark 2.5. If N be a subcanonical hypergroup of a canonical hypergroup (M, +), then the quotient is M/N = {x + N | x $\in$ M},

where x + N = {x + n | n $\in$ N}, we will use $\bar{x}$ instead of x + N.

Theorem 2.6.[11] If N be a subcanonical hypergroup of a canonical hypergroup (M, +). Then M/N is a canonical hypergroup with respect to the following hyperoperation

$$(x + N)\oplus(y + N) = \{z + N \mid z \in x + y\}, \text{ for all } x + N,\ y + N \in M/N.$$

Proof. Let $x_1, y_1, x_2, y_2 \in M$ such that $\bar{x}_1 = \bar{x}_2$ and $\bar{y}_1 = \bar{y}_2$ then $x_2 \in x_1 + N$ and $y_2 \in y_1 + N$. Let $z_2 \in x_2 + y_2 \subseteq (x_1 + N) + (y_1 + N)$. Since M is commutative, $z_2 \in z_1 + n$ for some $z_1 \in x_1 + y_1$ and for some n $\in$ N. That is, $z_2 + N = z1 + N$. Hence,

$$\bar{x}_2 \oplus \bar{y}_2 \subseteq \bar{x}_1 \oplus \bar{y}_1.$$

Also, since $x_1 \in x_2 + N$ and $y_1 \in y_2 + N$, by a similar argument, we get,

$$\bar{x}_1 \oplus \bar{y}_1 \subseteq \bar{x}_2 \oplus \bar{y}_2.$$

Hence, $\bar{x}_1 \oplus \bar{y}_1 = \bar{x}_2 \oplus \bar{y}_2$. Thus, $\oplus$ is well defined.

Let $\bar{x}, \bar{y}, \bar{z} \in$ M/N. If $\bar{u} \in (\bar{x} \oplus \bar{y}) \oplus \bar{z}$, then $\bar{u} \in \bar{p} \oplus \bar{z}$ for some $\bar{p} \in \bar{x} \oplus \bar{y}$. That is, $\bar{u} = \bar{a}$ for some a $\in$ p + z. Also $\bar{p} = \bar{b}$ for some b $\in$ x + y.

Now, a $\in$ p + z $\subseteq$ b + N + z = b + z + N. That is, a $\in$ v + N for some v $\in$ b + z $\subseteq$ (x + y) + z = x + (y + z). So, v $\in$ x + t for some t $\in$ y + z. This means that, $\bar{a} = \bar{v}$ and $\bar{v} \in \bar{x} \oplus \bar{t}$. Since $\bar{t} \in \bar{y} \oplus \bar{z}$, we have

$$\bar{u} = \bar{a} = \bar{v} \in \bar{x} \oplus \bar{t} \subseteq \bar{x} \oplus (\bar{y} \oplus \bar{z}).$$

This means that, $\bar{u} \in \bar{x} \oplus (\bar{y} \oplus \bar{z})$. Hence,

$$(\bar{x} \oplus \bar{y}) \oplus \bar{z} \subseteq \bar{x} \oplus (\bar{y} \oplus \bar{z}).$$

Similarly, we get

$$\bar{x}\oplus(\bar{y}\oplus\bar{z}) \subseteq (\bar{x}\oplus\bar{y})\oplus\bar{z}. \text{ Hence, } (\bar{x}\oplus\bar{y})\oplus\bar{z} = \bar{x}\oplus(\bar{y}\oplus\bar{z}).$$

Thus, the hyperoperation $\oplus$ is associative.

Consider the element $\bar{0} = 0 + N \in M/N$. Now, for any $x \in M$, we have

$$\bar{x}\oplus\bar{0} = \{\bar{z} \mid z \in x + 0\} = \bar{x}.$$

Similarly, $\bar{0}\oplus\bar{x} = \bar{x}$. Thus, $\bar{0}$ is the zero element of M/N.

Let $x \in M$, then $\bar{x}\oplus(-\bar{x}) = \{\bar{z} \mid z \in x + (-x) = x - x\}$. Since $\bar{0} \in x - x$, we get, $\bar{0} \in \bar{x}\oplus(-\bar{x})$. Similarly, $\bar{0} \in (-\bar{x})\oplus\bar{x}$. Let $\bar{x} \in M/N$, and suppose that $\bar{y} \in M/N$ such that $\bar{0} \in \bar{y}\oplus\bar{x}$, then $\bar{0} = \bar{a}$, where $a \in y + x$. That is, $y \in a - x \subseteq N - x$, and hence $\bar{y} = -\bar{x}$. Thus, the element $\bar{x} \in M/N$ has a unique inverse $-\bar{x} \in M/N$. Suppose that $\bar{z} \in \bar{x}\oplus\bar{y}$, then $\bar{z} = \bar{a}$, where $a \in x + y$. This implies,

$x \in a - y \subseteq z + N - y$. That is, $x \in r + N$, where $r \in z - y$. Thus, $\bar{x} = \bar{r} \in \bar{z}\oplus(-\bar{y})$. Similarly, we can show that $\bar{y} \in (-\bar{x})\oplus\bar{z}$. Since M is commutative, it is obvious that M/N is also commutative. Thus, M/N is a canonical hypergroup. ■

Theorem 2.7.[11] Let (M, +) be a canonical hypergroup, and let N be a normal subcanonical hypergroup of M. Then, (M/N, $\oplus$) is an abelian group.

RESULTS

Definition 3.1. Let $(M, +)$ be a canonical hypergroup, and ρ be an equivalence relation on M, then ρ is called:

1) Regular if for all $a, b \in M$, $a\rho b$ implies that for every $x \in M$, for every $u \in a + x$ there exists $v \in b + x$ such that $u\rho v$ and for every $v' \in b + x$ there exists $u' \in a + x$ such that $u'\rho v'$.
2) Strongly regular if for all $a, b \in M$, $a\rho b$ implies that for every $x \in M$, for every $u \in a + x$ and for every $v \in b + x$ one has $u\rho v$.

Proposition 3.2.[6] Let $(M, +)$ is a canonical hypergroup, and let N be a normal subcanonical hypergroup of M. Then, for all $x, y \in N$, the following are equivalent:

i. $y \in x + N$,

ii. $x - y \subseteq N$,

iii. $(x - y) \cap N \neq \emptyset$.

Proof.

($i \Longrightarrow ii$). Since $y \in x + N$, we have $y - x \subseteq x + N - x$, and since N is normal subcanonical hypergroup of M, we get $x + N - x \subseteq N$. Thus, $y - x \subseteq N$. That is, $-(y - x) \subseteq N$, and hence $x - y \subseteq N$.

($ii \Longrightarrow iii$). Is obvious.

($iii \Longrightarrow i$). Since $(x - y) \cap N \neq \emptyset$, there exists $a \in x - y$ and $a \in N$. Therefore, $-y + x \subseteq -y + a + y \subseteq N$. If $z \in -y + x$, then $z \in N$. Therefore, $-y \in z - x$. That is, $y \in x - z \subseteq x + N$. ■

Now, if $(M, +)$ is a canonical hypergroup, then we can establish the following connection between regular relations on M and subcanonical hypergroups of M, and establishe a similar connection between strongly regular relations on M and normal sub-canonical hypergroups of M as follows:

i. If ρ is a regular relation on M. Then the equivalence class $\rho(0)$ is a subcanonical hypergroup of M, where 0 is a neutral element of M. For $a, b \in M$, we have

$a\rho b$ iff $a \in b + \rho(0)$.

ii. If ρ is a strongly regular relation on M. Then the equivalence class $\rho(0)$ is a normal subcanonical hypergroup of M, where 0 is a neutral element of M. For $a, b \in M$, we have

$a\rho b$ iff $a - b \subseteq \rho(0)$.

Theorem 3.3. Let $(M, +)$ be a canonical hypergroup, and let N be a normal subcanonical hypergroup of M. If a, b are elements in M, then the binary relation ρ defined on M by:

$$a\rho b \quad \text{iff} \quad a - b \subseteq N,$$

is a strongly regular on M with $\rho(0) = N$.

Proof. Let $a, b, c \in M$. Clearly, $a \in a + 0$, implies

$$a - a \subseteq a + 0 - a \subseteq a + N - a \subseteq N.$$

So ρ is reflexive. Also, $a - b \subseteq N$ if and only if $b - a \subseteq N$. So ρ is symmetric. For transitivity, if $a - b \subseteq N$ and $b - c \subseteq N$ then by normality of N, we have

$$a - b + b - c = a - b + 0 + b - c \subseteq a + N - c \subseteq a - c + N \subseteq N,$$

$$a - c \subseteq N.$$

Thus ρ is an equivalence relation on M.

Next, to prove that the equivalence relation ρ is a strongly regular on M, suppose that $a\rho b$ then $a - b \subseteq N$, let $x \in M$, if $u \in a + x$ and $v \in b + x$, then

$u - v \subseteq a + x - (b + x) = a + x - (x + b) = a + (x - x) - b \subseteq a + (x + 0 - x) - b \subseteq a + N - b \subseteq N$, so $u\rho v$, thus

$$(a + x)\bar{\rho}(b + x).$$

Hence ρ is a strongly regular relation on M.

Now, to prove that $\rho(0)$ is a normal subcanonical hypergroup of M. Let $a, b \in \rho(0)$, then $a\rho 0$ and $b\rho 0$, since ρ is a strongly regular relation on M. this imply that

$$(a + b)\bar{\rho}(0 + 0),$$

this means that, for all $u \in a + b$ and $0 \in 0 + 0$, we have $u\rho 0$, it follows that

$$u \in \rho(0), \text{ so } a + b \subseteq \rho(0).$$

Since $a \in \rho(0)$ it follows that $-a \in \rho(0)$. Therefore $\rho(0)$ is a subcanonical hypergroup of M. For normality of $\rho(0)$, let $a \in \rho(0)$ and $x \in M$, then

$$(x + a)\bar{\rho}(x + 0),$$

this implies that $(x + a)\bar{\rho}x$,

it follows that $(x + a - x)\bar{\rho}(x - x)$,

then $(x + a - x)\bar{\bar{\rho}}0$, since $0 \in x - x$.

Therefore, $x + a - x \subseteq \rho(0)$.

Thus $\rho(0)$ is a normal subcanonical hypergroup of M.

Finally, to prove that $\rho(0) = N$, if $a \in \rho(0)$ then $a\rho 0$ implies $a - 0 \subseteq N$, so $a \in N$, thus $\rho(0) \subseteq N$. Conversly, if $a \in N$ then $a - 0 \subseteq N$, it follows that $a\rho 0$ implies $a \in \rho(0)$, thus $N \subseteq \rho(0)$. Hence, $\rho(0) = N$. ■

CONCLUSION

By strongly regular relation defined on a canonical hypergroup M, the equivalence class $\rho(0)$ is exactly a normal subcanonical hypergroup of M.

Duality of interest: The authors declare that they have no duality of interest associated with this manuscript.

Author contributions: Contribution is equal between authors.

Funding: No specific funding was received for this work.

REFERENCES

Marty, F. (1934). Sur une generalization de la notion de groups. In *8th congress Math. Scandinaves, Stockholm,(1934)*.

AbouElwan, Y., & Alderawe, M. (2023). On Homomorphisms and Congruences of Canonical Hypergroups. . *Global Libyan Journal* **59**, 1

AbouElwan, Y., & Qadous, S. (2022). On Canonical Hypergroup and Congruence of Semihypergroup. *Global Libyan Journal*, 1

Corsini, P., & Leoreanu, V. (2003). Applications of Hyperstructure Theory, Advances in Mathematics. *Kluwer Academic Publishers, Dordrecht*.

Davvaz, B. (2012). *Polygroup theory and related systems*. World scientific.

Davvaz, B., & Leoreanu-Fotea, V. (2007). *Hyperring theory and applications* (Vol. 347). International Academic Press, USA.

Davvaz, B., & Leoreanu-Fotea, V. (2022). *Hypergroup theory*.

Davvaz, B., Leoreanu-Fotea, V., & Vougiouklis, T. (2023). A Survey on the Theory of n-Hypergroups. *Mathematics*, *11*(3), 551.11.

Burris, S., & Sankappanavar, H. P. (1981). *A course in universal algebra* (Vol. 78, pp. xvi+-276). New York: Springer.

Velrajan, M., & Asokkumar, A. (2010). Note on isomorphism theorems of hyperrings. *International Journal of Mathematics and Mathematical Sciences*, *2010*.13.

Vougiouklis, T. (1994). *Hyperstructures and their representations*. Hadronic Press.

Al-Mukhtar Journal of Basic Sciences 21 (2): 58-62, 2023
Doi: https://doi.org/10.54172/rtn9cg93

Research Article **Open Access**

Approximate confidence intervals for the Population Proportion based on linear model

Nuri E. Mohamed

***Corresponding author:**
n.almadni@wau.edu.ly
Department of Mathematics, Faculty of Science-, Wadi Shati University, Gurdha, Libya

Received:
10 September 2023

Accepted:
29 November 2023

Publish online:
31 December 2023

Abstract

When the linear model errors are non-normal, one might be interested in making inferences concerning proportion. The goal of this article is to construct approximate confidence intervals for the proportion founded on the supposed linear model which covers a true value of a proportion that is close to a specific nominal value of the level of significant.

Keywords: Linear model, central limit theorem, slutsky's lemma, asymptotic distribution, confidence intervals**.**

INTRODUCTION

In this paper study was derived the asymptotic confidence intervals by the *z*-quantile and by the *t*-quantile, to construct approximate confidence intervals of the proportion based on linear models.

Then it was introduced to the used model:
suppose that the sum random variable X_i is a Poisson distribution can be splits into two separate Poisson random variables Y_i, Z_i with means λ_1, λ_2 respectively. It means.,

$X_i \sim (\lambda_1, \lambda_2)$, and since E($Y_i$) = Var($Y_i$) = λ_1, and $E(Z_i)$ = Var(Z_i) = λ_2, consequently

E(X_i) = Var(X_i) = $\lambda_1 + \lambda_2$. Further,
P(Yi | Xi) ~ Bin(X, p), where $p = \frac{\lambda_1}{\lambda_1+\lambda_2}$, $X_i > 0$ (B(n, p) denotes the
Binomial distibution with parameters n, p).

The remainder of the paper was organized as follows: Description of the assumed model is given in Sec 2. Estimation of linear model parameter were given in Sec. 3. Section 4 to provide confidence intervals for the proportion.

The Linear model

Suppose, there are m observations of two relevant components of data, i.e., (Y_i, X_i); i = 1,….,m are $m \times 2$ dimensional observed data since every observational item refrenced by the subscript i, as well as, $Y_i, X_i > 0$; $\forall i = 1, \dots, m$. The i^{th} observation represents unit, for example:

Xi ≡number of units for a product i; i = 1,….,m

Yi ≡number of damaged units for a product *i; i* = 1,….,*m*.

Consider the univariate linear model $Y_i = x_i p + \epsilon_i$, *i* = 1,….,*m*, with the following assumptions:

$E(Y_i) = x_i p$, $E(\epsilon_i) = 0$, also by variance relational to *xi* (*xi* is fixed variable), i.e, $Var(Y_i) = Var(\epsilon_i) = \sigma^2 x_i$, compressing the model in vector form (for the i^{th} observation) yields: $Y_i = Xp + \epsilon$, (*i* = 1,….,*m*), where

$Y = (Y_1, \dots Y_m)^T$, and the $m \times 1$ design vector.

$X = (x_1, \dots, x_m)^T$, then the heteroscedastic errors $(\epsilon_1, \dots \epsilon_m)^T = \epsilon$, through the expectations, $E(\epsilon) = \mathbf{0}_m$, and Var(∈) = σ²W, where **0**m =$(0, \dots, 0)^T$, and W = diag (x_i). The single model was weighted by the linear transformation

$$A_i Y_i = A_i\, x_i p + A_i\ \epsilon_i,$$

$$\tilde{Y}_i = \tilde{x}_i p + \tilde{\epsilon}_i,\ i = 1,\dots,m \qquad [2.1]$$

where, $A_i = \frac{1}{\sqrt{x_i}}$, given that $x_i > 0$, $\tilde{Y}_i = A_i\, Y_i = \frac{Y_i}{\sqrt{x_i}}$, $\tilde{x}_i = A_i\, x_i = \sqrt{x_i}$, $\tilde{\epsilon}_i = A_i\ \epsilon_i = \frac{\epsilon_i}{\sqrt{x_i}}$, it follows that $E(\tilde{\epsilon}_i) = 0$, and $Var(\tilde{\epsilon}_i) = \sigma^2$, $\forall i = 1, \dots, m$ (*homoscedastic errors*), as well as $Cov(\epsilon) = \sigma^2 I_m = Cov(\tilde{Y})$.such that *Im* is an Identity Matrix of elements $m \times m$, also the weighted response vector $\tilde{Y} = (\tilde{Y}_1, \dots, \tilde{Y}_m)^T$, and the weighted design vector $\tilde{X} = (\tilde{x}_1, \dots, \tilde{x}_m)^T$, as well as the weighted error vector $\tilde{\epsilon} = \left(\tilde{\epsilon}_1, \dots, \tilde{\epsilon}_m{}^T\right)$, where

$\sigma^2 = E\left(\tilde{Y}_i - \tilde{X}_i p\right)^2$

Estimation in linear models

Agreeing whether the demonstrate blunders are homoscedastic or heteroscedastic blunders we estimate the proportion *p*.

Heteroscedasticity

Since, error of the vector of the non-weighted ideal has covariance that is the variance proportional to the known invertible diagonal matrix *W;* so, it is the Generalized Least Squares Estimator, that is further the Best linear unbiased estimator. The covariance structure is given by

$$\mathrm{cov}(\epsilon) = \begin{bmatrix} \sigma^2 x_1 & \dots & 0 \\ \vdots & \ddots & \vdots \\ 0 & \dots & \sigma^2 x_m \end{bmatrix} = \sigma^2 W$$

x_i are fixed, $i = 1, \dots, m$ and $W^{-1}W = I_m$, as well as $X^T W = 1^T{}_m$, where $1_m = (1, \dots 1)^T$. So, we have

$$\hat{p}_{GLS} = (X^T(\sigma^2 W)^{-1} X)^{-1} X^T (\sigma^2 W)^{-1} Y = (X^T W^{-1} X)^{-1} X^T W^{-1} Y$$

Homoscedasticity

It is familiar and defined very well; that the Weighted Least Squares Estimator is the Best linear unbiased estimator, in addition, due to the reason that, the weighted errors are homoscedastic therefore, the Weighted Least Squares Estimator functional to the Model 2.1 concludes in the OLS Estimator, hence is also the greatest LUE , according to Gauss-Markov's theorem *(1-3)*, i.e., $\hat{p}_{WLS}$= $\hat{p}$. Since, $\mathrm{cov}(\tilde{\epsilon}) = \sigma^2 I_m$,

then

$$\hat{p}_{WLS} = \left(\tilde{X}^T(\sigma^2 I_m)^{-1}\tilde{X}\right)^{-1}\tilde{X}^T(\sigma^2 I_m)^{-1}\tilde{Y} = (X^T I_m X)^{-1}\tilde{X}^T I_m \tilde{Y}$$

$$= \left(\sum_{i=1}^{m}\left(\sqrt{x_i}\right)^2\right)^{-1}\sum_{i=1}^{m}\sqrt{x_i}\tilde{Y}_i = \frac{\sum_{i=1}^{m}\sqrt{x_i}\tilde{Y}_i}{\sum_{i=1}^{m}x_i} = \frac{\sum_{i=1}^{m}Y_i}{\sum_{i=1}^{m}x_i} = \hat{p},$$

$$\sqrt{x_i}\tilde{Y} = Y_i.$$

Asymptotic normal for the ratio $\hat{p}_m$

It supposed that the random errors $\tilde{\epsilon}_i$ are not Normally Distributed nonetheless are independently identical distributed random variables, $i = 1, \dots, m$, i.e.,$E(\tilde{\epsilon}_i) = 0$, and $\mathrm{Var}(\tilde{\epsilon}_i) = 0$. Furthermore, under a positive conditions on the project **X** we can demonstrate that in huge sample sizes, $\hat{p}$ obeys the asymptotic normal distribution.

And more additionally conditions on the couple of observations ***Xi, Yi*** are required, called (***Xi, Yi***) are independently identical distributed pairs of random variables, plus E(*Xi*) exist ⇒

($\tilde{X}_i$, $\tilde{Y}_i$**)** are then independently identical distributed random variables, furthermore $E\left(\tilde{X}^2{}_i\right)$ exists

$$i = 1, \dots, m\ , \tilde{X}_i = \sqrt{X_i}, \tilde{Y}_i = \frac{Y_i}{\sqrt{x_i}}, X_i > 0\ .$$

To arrive to the asymptotic distribution, one rephrases first the estimator $\hat{p}_m$as

$$\hat{p}_m = \left(\tilde{\boldsymbol{X}}^T\tilde{\boldsymbol{X}}\right)^{-1}\tilde{\boldsymbol{X}}^T\tilde{\boldsymbol{Y}} = \left(\sum_{i=1}^{m}\tilde{X}_i\,\tilde{X}_i\right)^{-1}\sum_{i=1}^{m}\tilde{X}_i\,\tilde{Y}_i$$

$$= \left(\sum_{i=1}^{m}X_i\right)^{-1}\sum_{i=1}^{m}\tilde{X}_i\,(\tilde{X}_i\,p + \tilde{\epsilon}_i) = \left(\sum_{i=1}^{m}X_i\right)^{-1}\left(\sum_{i=1}^{m}\tilde{X}_i\,p + \sum_{i=1}^{m}\tilde{X}_i\,\tilde{\epsilon}_i\right)$$

$$= p + \left(\sum_{i=1}^{m}X_i\right)^{-1} + \sum_{i=1}^{m}\tilde{X}_i\,\tilde{\epsilon}_i \qquad (3.1)$$

Consequently

$$\sqrt{m}(\hat{p}_m - p) = \left(\frac{1}{m}\sum_{i=1}^{m} X_i\right)^{-1} \frac{1}{\sqrt{m}}\left(\sum_{i=1}^{m} \sqrt{\tilde{X}_i}\,\tilde{\epsilon}_i\right) = \left(\frac{1}{m}\sum_{i=1}^{m} X_i\right)^{-1} \frac{1}{\sqrt{m}}\left(\sum_{i=1}^{m} \sqrt{X_i}\tilde{\epsilon}_i\right) \quad (3.2)$$

The asymptotic of the equation 3.2, requests to confirm, the denominator in 3.2 is reliable, and the numerator submits the CLT. It direct to see (by the LLN)

$$= \left(\frac{1}{m}\sum_{i=1}^{m} X_i\right)^{-1} \xrightarrow{p} \left(E(X_i)\right)^{-1},$$

Given that, E(Xi) > 0, and

$$= \left(\frac{1}{m}\sum_{i=1}^{m} x_i\right)^{-1} \to \mu^{-1}, \qquad \mu \text{ is a constant.}$$

Along with the numerator

$\frac{1}{\sqrt{m}}\sum_{i=1}^{m} \sqrt{X_i}\tilde{\epsilon}_i \xrightarrow{D} N\left(0, \sigma^2 E(X_i)\right)$, where, the marginal or asymptotic variance

$$\operatorname{cov}\left(\sqrt{X_i}\tilde{\epsilon}_i, \sqrt{X_i}\tilde{\epsilon}_i\right) = \operatorname{Var}\left(\sqrt{X_i}\tilde{\epsilon}_i\right) = E\left(X_i \operatorname{Var}(\tilde{\epsilon}_i \setminus \tilde{X}_i)\right) + \operatorname{Var}\left(E\left(\sqrt{X_i}\tilde{\epsilon}_i \setminus \tilde{X}_i\right)\right)$$
$$= \sigma^2 E(X_i).$$

As a result, following the use of the Slutsky's lemma (see [Knight,. 2000], pp. 119-120), the equation 3.2 can be rewritten as

$$\sqrt{m}(\hat{p}_m - p) \xrightarrow{D} N\left(0, \sigma^2 E(X_i)\left(E(X_i)\right)^{-2}\right) \equiv N\left(0, \sigma^2\left(E(X_i)\right)^{-1}\right) \quad (3.3)$$

Approximate Confidence Intervals for the Population Proportion *p*

From 3.3, the asymptotic variance,

$$\operatorname{Var}\left(\sqrt{m}(\hat{p}_m)\right) = E\left(\operatorname{Var}\sqrt{m}(\hat{p}_m) \setminus \boldsymbol{X}^T\right) + \operatorname{Var}\left(E\sqrt{m}(\hat{p}_m) \setminus \boldsymbol{X}^T\right) = \frac{\sigma^2}{E(X_i)},$$

$$\text{as } \operatorname{Var}\left(E\sqrt{m}(\hat{p}_m) \setminus \boldsymbol{X}^T\right) = 0, \boldsymbol{X} = (X_1, X_2, \dots, X_m)^T.$$

conclude that , the estimated $(1-\alpha)\%$ asymptotic confidence interval for the amount *p* is given by

$\left[\hat{p}_m \pm z_{1-\frac{\alpha}{2}}\, s.e(\hat{p}_m)\right]$, where, the standard error of $\hat{p}_m$

$$,s.e(\hat{p}_m) = \frac{s_m}{\sum_{i=1}^{m} X_i}, \qquad s^2{}_m = \frac{1}{m-1}\sum_{i=1}^{m}\left(Y_i - \hat{p}\,\tilde{X}_i\right)^2.$$

Further and since $\bar{X}_m$ and $s^2{}_m$ are consistent estimators for E(*Xi*) and σ^2 respectively, it follows that consistent estimator of the $\mathrm{Var}((\hat{p}_m))$ is $\frac{s^2 m}{\sum_{i=1}^{m} X_i}$ similarly, such as

$$\frac{\hat{p}_m - p}{\frac{s^2{}_m}{\sum_{i=1}^{m} X_i}} \sim t_{m-1} \xrightarrow{D} N(0,1)$$

Henceforth, the interval that is safety bounds provided by

$$\left[\hat{p}_m \pm t_{\left(m-1,1-\frac{\alpha}{2}\right)}\, s.e(\hat{p}_m)\right],$$

is the recommended more conservative confidence interval for *p*, where $s.e(\hat{p}_m) = \frac{s_m}{\sum_{i=1}^{m} x_i}$, as well as $t_{\left(m-1,1-\frac{\alpha}{2}\right)}$ is $\left(1-\frac{\alpha}{2}\right)$ percentile of the student t distribution with $(m-1)$ degrees of freedom.

CONCLUSION

Results obtained from this article two confidence intervals first is the asymptotic confidence interval and the second is the extra conservative asymptotic confidence interval for the population proportion which can give more reliable intervals to cover the true population proportion P. Hence we considered two confidence intervals, the asymptotic (following the normal quintile) in addition the proposed conservative (with the adjusted t-quintile) confidence intervals.

Duality of interest: The authors declare that they have no duality of interest associated with this manuscript..

Author contributions: The author did all the work related to the manuscript, including designing the research, collecting information, formulating theories and proofs, and preparing the entire paper.

Funding: There is no funding to support this manuscript

REFERENCES

A . Sen and M. Srivastava. Regression Analysis: Theory, Methods, and Application. *Springer-Verlage*, New York, Inc, (1990).

H. Stock, and W.C. Waston. Introduction to econometrics. Pearson Education, Inc, pp. 588-591, (2003) .

K.C. Knight,. Mathematical Statistics. Chapman & Hall/CRC. Texts in Statistical Science, pp. 120-149, (2000) .

Al-Mukhtar Journal of Basic Sciences 21 (2): 63-72, 2023
Doi: https://doi.org/10.54172/et373z10

Research Article Open Access

Hybrid Triple Quadrature Rule Blending Some Gauss-Type Rules with the classical or the Derivative-Based Newton-Cotes-Type Rules.

Haniyah A. M. Saed Ben Hamdin [1*] and Faoziya S. M. Musbah[2]

***Corresponding author:** h.saed1717@su.edu.ly, Mathematics Department, Faculty of Science, Sirte University, Sirte, Libya

Second Author: Mathematics Department, Faculty of Education, University of Bani Waleed, Bani Waleed, Libya

Received: 16 September 2023

Accepted: 30 November 2023

Publish online: 31 December 2023

Abstract

Hybrid numerical quadrature rules are widespread techniques for approximate computations of definite integrals. Such hybrid rules combine as many quadrature rules as long as they possess the same degree of precision. The revenue is a new mixed rule with a higher degree of precision than its constituted rules at least by two. Moreover, such mixed rules are quite simple and handy, because they do not involve any extra evaluations of the integrand. That is by relying on the same number of quadrature points of the constituted rules, the acquired hybrid rule performs more efficiently than its ingredients rules. In this paper; a triple hybrid quadrature rule has been constructed for the numerical integration of real definite integrals that do not possess a closed-form antiderivative. At First, a dual hybrid rule was produced by blending Milne's rule of Newton-Cotes type with the anti-Gaussian quadrature rule to prevail a dual rule of a degree of precision equal to five. Then the acquired dual rule is recombined with the composite derivative-based and mid-Point Newton–Cotes formula producing a hybrid triple rule of degree of precision equal to seven. The accomplished approach is satisfactory and efficient in the approximate evaluation of definite real integrals as confirmed analytically by the error analysis and numerically by some verification examples. To promote the degree of precision of the proposed triple approach, the numerical computations have been implemented in an adaptive environment.

Keywords: Hybrid Quadrature Rule, Milne's Rule, Anti-Gaussian Quadrature, Derivative-Based Newton-Cotes Quadrature Rules, Composite Mid-Point Newton-Cotes Quadrature Rules, Adaptive Quadrature Rule, Numerical Integration.

INTRODUCTION

Numerical quadrature rules have gained great popularity in numerical integration for certain classes of integrals that cannot be integrated analytically. The quadrature rules can be classified either as Newton-Cotes-type or Gauss-type (Atkinson, 2012; Burden and Faires, 2005). The pronounced difference between the two categories of quadrature rules is that the nodes for the Newton-Cotes rules are equally spaced points along the interval of integration. Whereas the Gauss rule picks the nodes differently and does not have to be equally distanced, and the corresponding weights are usually irrational numbers. A great feature of the Gauss-type rule is that

the weights are always positive which has a desirable effect on the stability of the quadrature rule. Unfortunately, such a feature cannot be guaranteed for Newton-Cotes rules, especially for a large number of quadrature points. Sermutlu (Sermutlu, 2005) conducted a comparative study between Newton-Cotes-Type and Gauss-Type quadrature rules based on several criteria such as degree of precision, running time, computational cost, coefficient of the leading term of the error, and stability. He claimed that the Gauss-type quadrature rules offer superior performance compared to the Newton-Cotes quadrature rules.

Modified families of closed, Mid-point, and open Newton-Cotes quadrature rules have been recently established by Burg *et al*. (Burg and Degney, 2013; Burg, 2012; Zafar *et al*., 2014), and are known as derivative-based Newton-Cotes formulae. Such formulae require the evaluations of the integrand and its derivative at a smaller number of quadrature points in comparison to the standard Newton-Cotes formulae. Burg *et al*. (Burg and Degney, 2013; Burg, 2012; Zafar *et al*., 2014) state that their modified Newton-Cotes formulae perform considerably well compared with the classical Newton-Cotes (Burg and Degney, 2013; Burg, 2012; Zafar *et al*., 2014; Dehghan *et al*., 2005 a; Dehghan *et al*., 2005b).

Moreover, numerical enhancements of the open and semi-open Newton-Cotes formulae were presented respectively by Dehghan *et al*. (Dehghan *et al*., 2005a; Dehghan *et al*., 2005b). Thus, they claim that the numerically enhanced rules are superior to the classical Newton-Cotes rules of open, closed, and semi-open types. Moreover, a recent approach was first introduced by Das and Pradhan in 1996 for numerical quadrature (Das and Pradhan, 1996). The core idea of their approach is joining a pair of quadrature rules of the same degree of precision to generate a new mixed rule with a better degree of precision. Then several formations of the mixed quadrature rules appeared for numerical computation of real definite integral (Das and Pradhan, 2012; Das and Pradhan, 2013a; Das and Pradhan, 2013b; Jena and Dash, 2011; Tripathy *et. al*., 2015; Patra *et. al.*, 2018). Furthermore, such an approach has been also implemented for the numerical computation of analytic functions (Mohanty, 2010). Such mixed rules have been proven valuable in solving different classes of integral equations either with regular or singular kernels (Jena and Nayak, 2015).

In this paper, a triple hybrid quadrature rule has been formalized for the numerical integration of real definite integrals that do not own closed-form anti-derivatives. The proposed approach blends Milne's rule with the anti-Gauss quadrature rule to generate a dual rule with a degree of precision equal to five. Then the accomplished dual hybrid rule is recombined with the composite derivative-based Newton-Cotes rule to produce a triple hybrid rule of degree of precision equal to seven. The proposed triple hybrid rule will be verified by some integral examples that do not hold an elementary anti-derivative.

The structure of this paper is as follows: The related literature review was reviewed in the introduction section. Then some preliminary concepts were introduced and the notations were used in this paper. In the third section; the dual and the triple hybrid quadrature rules have been established and an error analysis is presented analytically. To verify the acquired approach, some numerical results are shown in the results section followed by a discussion and conclusion.

Preliminaries Concepts

Here some basic definitions need throughout the paper.

Definition 1: An n-point Gaussian-quadrature rule is defined by the formula,

$$I_n(f) = \int_a^b f(x)\,dx \cong \sum_{i=1}^{n} w_i f(x_i) + EI_n(f), \tag{1}$$

where the points x_i are the quadrature points are known as nodes or abscissas, the factors w_i are the corresponding weights and $EI_n(f)$ is the error of the rule (1). The quadrature rule (1) is based on polynomials interpolation. The mechanism of the Gauss quadrature is based on the precision concept, that is the quadrature rule is exact for polynomial of degree less than or equal to $2n-1$. That is the formula (1) exactly integrates first n monomials functions $x^i, i = 0,1,2,\dots,n$. Thus we obtain a non-linear system of moment equations that can be solved yielding the nodes and the corresponding weights.

Definition 2 (Degree of Precision): The degree of precision of a quadrature rule is the highest degree of the polynomial $P_n = x^n$ such that the relevant rule is exact for all the monomials $x^i, i = 0,1,2,\dots,n$. Thus the quadrature rule is exact for all polynomials of degree $\leq n$ and the error does not vanish for $i = n+1, n+2, \dots$

MATERIALS AND METHODS

Here we outline the definitions of the quadrature rules that were implemented later through the formalization of the hybrid rules either the dual or the triple rules.

Anti-Gaussian Quadrature Rule

Definition 3 (Laurie, 1996): An $(n+1)$- the formula defines point Anti-Gaussian formula,

$$I_{aG(n+1)}(f) = \int_a^b f(x)\,dx \approx \sum_{i=1}^{n+1} w_i f(x_i), \tag{2}$$

where all the weights are positive and the abscissas are real and interlaced by those of the n-point Gaussian formula (1). This rule has $(2n-1)$ as the degree of precision and with the error of the same module but the opposite sign to the error of the n-point Gauss-Legendre quadrature rule (2).

For example, for $n = 2$, we have the 3-point anti-Gaussian formula $I_{aG3}(f)$ as,

$$I_{aG3}(f) = \frac{h}{13}\left\{16f(\rho) + 5\left[f\left(\rho - h\sqrt{\frac{13}{15}}\right) + f\left(\rho + h\sqrt{\frac{13}{15}}\right)\right]\right\}, \tag{3}$$

where $h = \left(\frac{b-a}{2}\right)$ and throughout the paper $\rho = \left(\frac{a+b}{2}\right) \in [a,b]$ denotes the mid-point of the integration interval. Thus, one has,

$$I_{Exact}(f) = \int_a^b f(x)\,dx = I_{aG3}(f) + E_{aG3}(f), \tag{4}$$

where $E_{aG3}(f)$ is the truncation error of the 3-point anti-Gauss quadrature rule. Thus from equation (4), one has

$$E_{aG3}(f) = I_{Exact}(f) - I_{aG3}(f).$$

This error can be derived by polynomials interpolation (Atkinson, 2012; Burden and Faires, 2005) or by Taylor expansion (Das and Pradhan, 1996) of the functions involved in $I_{aG3}(f)$ about the mid-point ρ of the integration interval $[a,b]$ to yield,

$$E_{aG3}(f) = -\frac{h^5}{135}f^{(4)}(\rho) - \frac{1016\,h^7}{675 \times 7!}f^{(6)}(\rho) - \frac{2144\,h^9}{1125 \times 9!}f^{(8)}(\rho) - \cdots \quad (5)$$

The degree of precision of the 3-point anti-Gauss quadrature rule $I_{aG3}(f)$ is three, and the local truncation error is of the fifth order.

Milne's Rule

Milne's rule is the three-point open Newton-Cotes quadrature rule, and is given by the following formula (Atkinson, 2012; Burden and Faires, 2005)*:*

$$\int_a^b f(x)\,dx \approx I_{Mil}(f) = \frac{4h}{3}\{2[f(a+h) + f(a+3h)] - f(a+2h)\}, \quad (6)$$

where the step-size $h = \left(\frac{b-a}{n+2}\right), n = 2$. Thus, one has,

$$I_{Exact}(f) = \int_a^b f(x)\,dx = I_{Mil}(f) + E_{Mil}(f), \quad (7)$$

where E_{Mil} is the truncation error of the Milne's rule. Thus from equation (7), one has

$$E_{Mil}(f) = I_{Exact}(f) - I_{Mil}(f).$$

This error can be derived by Taylor expansion of the functions involved in $I_{Mil}(f)$ about the mid-point ρ of the integration interval $[a, b]$ to yield,

$$E_{Mil}(f) = \frac{14h^5}{45}f^{(4)}(\rho) + \frac{656h^7}{3 \times 7!}f^{(6)}(\rho) + \frac{976\,h^9}{9!}f^{(8)}(\rho) + \cdots \quad (8)$$

Thus the degree of precision of Milne's rule $I_{Mil}(f)$ is three and the local truncation error is of the fifth order.

Composite Newton-Cotes-Type Derivative-Based and mid-point quadrature rule.

In the current work ,we used a derivative-based quadrature formula that only requires the integrand evaluations at the mid-point of the integration interval $[a, b,]$ and evaluations of odd derivatives at the end-points a and b. Such formula is given as (Burg and Degney, 2013),

$$\int_a^b f(x)\,dx = 2hf(\rho) - \frac{h^2}{6}[f'(a) - f'(b)] + \frac{7h^3}{360}[f'''(a) - f'''(b)] + \frac{62h^7}{3 \times 7!}f^{(6)}(\rho). \quad (9)$$

Thus the degree of precision of this rule is five and the local truncation error is of the seventh order. It should be noted that the weights of the first and third derivatives in equation (9) are of opposite sign. This formula can be put in composite form as (Burg and Degney, 2013).

$$\int_a^b f(x)\,dx = 2h\sum_{k=1}^{N/2} f(x_{2k-1}) - \frac{h^2}{6}[f'(a) - f'(b)] + \frac{7h^3}{360}[f'''(a) - f'''(b)] + \frac{31Nh^7}{3 \times 7!}f^{(6)}(\rho), \quad (10)$$

where the nodes $x_i = a + ih$ and the step-size $h = \left(\frac{b-a}{N}\right)$.

Formula (9) has great features that make it an efficient quadrature rule. For instance, consistently with using the composite formula (10), only derivative evaluations at the end-points are required. This advantageous feature is due to the desirable appearance of the opposite-sign weights of odd derivatives that are involved in the formula (9). Unfortunately, such a handy feature does not persist with the appearance of even derivatives in the composite formula (10)

for some values of N where the weights of derivatives are of the same signs (Burg and Degney, 2013).

Furthermore, the composite formula (10) is progressive concerning the weights of the involved derivatives, that is it can be easily extended to involve high-order odd-derivatives. Therefore to acquire higher accuracy of the formula (10), Burg and Degny (Burg and Degney, 2013) implemented the central difference approximations to the derivatives. Hence the weights for the low-derivative remain unchanged, thus one only needs to compute the weights for the arising derivatives.
Now after we introduce all the quadrature rules that we will use in this paper either of Gauss-type or Newton-Cotes-type, we will formulate our hybrid rules as shown next.

RESULTS AND ERROR ANALYSIS

Here study shows how to formalize the triple hybrid quadrature rule, such formulation has two stages. The first task is to generate the dual rule, and then generate the triple quadrature rule as shown next.

Establishment of the Dual Hybrid Rule Joining the 3-Point Anti-Gauss Rule with Milne's Rule.

Here we show how to mingle two quadrature rules to generate a dual rule of degree of precision seven. The ingredients rules of the hybrid dual rule are the 3-point anti-Gauss rule (3) and Milne's rule (6) both having the same degree of precision equal to five. The core idea of generating the hybrid quadrature rules is to linearly combine the ingredient quadrature rules in such a way that leads to the cancellation of the leading term in the remainder of the ingredient rules as we show next.
To attain a linear combination of the quadrature rules (3) and (6), we multiply equations (4) and (7) respectively by $\frac{1}{15}$ and $\frac{14}{5}$, then add the resulting equations, yielding the following dual hybrid quadrature rule as,

$$I_{DH}(f) = \frac{1}{43}[I_{Mil}(f) + 42\, I_{aG3}(f)]. \tag{11}$$

where $I_{Mil}(f)$ and $I_{aG3}(f)$ are respectively given by equations (6) and (3).
This error of $I_{DH}(f)$ denoted as $E_{DH}(f)$ can be generated by the following equation,

$$I_{Exact}(f) = I_{DH}(f) + E_{DH}(f). \tag{12}$$

Thus by Taylor expansions of the functions involved in $I_{DH}(f)$ about the mid-point ρ of the integration interval $[a, b]$ one has,

$$E_{DH}(f) = \frac{34976}{3375 \times 7!} h^7 f^{(6)}(\rho) + \frac{335984\, h^9}{5625 \times 9!} f^{(8)}(\rho) + \cdots \tag{13}$$

Hence the degree of precision of the dual hybrid $I_{DH}(f)$ is five and the local truncation error is of ninth order.

Establishment of the Triple Hybrid Rule.

Here study shows how to join the dual hybrid rule I_{DH} given by the equation (11) with the composite quadrature rule (10) of Newton-Cotes-Type and of the same degree of precision of I_{DH} to establish a triple quadrature rule with the degree of precision equal to seven. The formula (10) can be rewritten for $N = 6$ as,

$$\int_a^b f(x)\,dx = 2h[f(x_1)+f(x_3)+f(x_5)] - \frac{h^2}{6}[f'(a)-f'(b)] + \frac{7h^3}{360}[f'''(a)-f'''(b)] + \frac{62h^7}{7!}f^{(6)}(\rho), \qquad (14)$$

where $x_i = a + ih$. This equation can be rewritten as,

$$I_{Exact}(f) = \int_a^b f(x)\,dx = I_{CDM}(f) + E_{CDM}(f), \qquad (15)$$

where E_{CDM} is the truncation error of the composite quadrature rule (14). Given as,

$$E_{CDM}(f) = \frac{62h^7}{7!}f^{(6)}(\rho) + \cdots,$$

By following a similar analogy to the derivation of the dual hybrid rule, we will produce the triple hybrid rule. By a similar analogy of the derivation of the dual hybrid rule, an appropriate linear combination between the dual hybrid rule(11) and the composite quadrature rule (14). Such a linear mixture guarantees the cancellation of the leading term of the remainder of their ingredient rules. Hence, one has,

$$I_{TH}(f) = \frac{1}{31601}[34976\, I_{CDM}(f) - 3375\, I_{DH}(f)], \qquad (16)$$

and the corresponding truncation error of the triple rule I_{TH} is,

$$E_{TH}(f) = \mathcal{O}(h^9). \qquad (17)$$

Hence the degree of precision of the generated triple hybrid $I_{TH}(f)$ is seven and the local truncation error is of ninth order.

Numerical Results

Table (1) shows some integral examples that we consider in this paper with their non-elementary anti-derivative and their approximate values.

Table: (1). Some Integral examples with their non-elementary anti-derivative and their approximate values.

Integral	Exact Value	Approximate Value
$I_1 = \int_{-1}^{1} \frac{e^{e^{\left(\frac{x+3}{2}\right)}}}{2}dx$	$I_1 = E\mathrm{i}(e^2) - E\mathrm{i}(e)$ $\mathrm{Ei}(x) = -\int_{-x}^{\infty} \frac{e^{-y}}{y}dy$	≈ 255.676
$I_2 = \int_1^2 e^{-x^2}\,dx$	$I_2 = \frac{\sqrt{\pi}}{2}[erf(2) - erf(1)]$ $erf(x) = \frac{2}{\sqrt{\pi}}\int_0^x e^{-y^2}dy$	≈ 0.135257
$I_3 = \int_1^2 \frac{\sin x}{x}dx$	$I_3 = S\mathrm{i}(2) - S\mathrm{i}(1)$ $S\mathrm{i}(x) = \int \frac{\sin x}{x}dx$	≈ 0.6593329906
$I_4 = \int_0^1 \frac{dx}{1+x^4}$	$I_4 = \frac{\pi + 2\coth^{-1}(\sqrt{2})}{4\sqrt{2}}$	≈ 0.86697

Table (2) shows the approximate values of the four integrals I_1, I_2, I_3, and I_4 computed by the dual and the triple hybrid quadrature rules $I_{DH}(f)$ and $I_{TH}(f)$ and their ingredients rules $I_{MI}(f)$, $I_{CDM}(f)$ and $I_{aG3}(f)$. The obtained results have been enhanced to reach a certain degree of precision by implementing an adaptive quadrature algorithm as explained next.

Table: (2). Numerical results computed by the hybrid quadrature rules $I_{HD}(f)$ and $I_{TH}(f)$ compared with its constituent rules I_{MI}, $I_{CDM}(f,)$ and $I_{aG3}(f)$

Integral	$I_{MI}(f)$	$I_{aG3}(f)$	$I_{DH}(f)$	$I_{CDM}(f)$	$I_{TH}(f)$
	Relative Error	Relative Error	Relative Error	Relative Error	Relative Error
I_1	202.8302589	299.7667015	297.51236563	224.5599104	216.76855772
	0.20668986	0.17244816	0.163630999	0.1217007993	0.1521743547
I_2	0.135788265	0.134847269	0.1348691522	0.13532354	0.1353720733
	0.003925903	3.031182×10^{-3}	2.8693892×10^{-3}	4.900742×10^{-4}	8.488664×10^{-4}
I_3	0.659311367	0.6593440204	0.659343261	0.659326494	0.659328112
	2.811856×10^{-5}	2.140659×10^{-5}	2.025484×10^{-5}	5.175461×10^{-6}	2.72157×10^{-6}
I_4	0.85677642	0.8743924963	0.8739828201	0.866016272387	0.866785002
	1.17611×10^{-2}	8.557947×10^{-3}	8.0854108×10^{-3}	1.1035118×10^{-3}	2.16829×10^{-4}

Adaptive Quadrature

The adaptive algorithm was first introduced by Kuncir (Kuncir, 1962), to enhance the accuracy of any numerical quadrature rule depending on step-size parameter h. Adaptive quadrature routine allows us to rely on a low-order quadrature rule and, then improve the accuracy by implementing such a low-order rule on a finer mesh of the integration interval. The mechanism of the adaptive quadrature rule is to iteratively refine the step size of the relevant quadrature rule until a termination criterion is met and reaches the desirable degree of precision (Lyness, 1969). That is, the adaptive algorithm takes the following steps:

1. Set an allowed tolerance as $\varepsilon = 10^{-5}$and let $I_{Exact}(f) = E$.
2. At the mid-point $\rho = \frac{a+b}{2}$, subdivide the interval of integration $[a, b]$ into two subintervals $[a, \rho]$ and $[\rho, b]$.
3. Then implement the quadrature rule separately on each subinterval $[a, \rho]$ and $[\rho, b]$, to respectively obtain the approximate results R_1 and R_2.
4. Then estimate the error of the obtained approximate results as:
5. $|E - S_1|$ and $|E - S_2|$
6. If $|E - S_1| \leq \varepsilon$, the termination criterion is met for the subinterval, the adaptive routine will stop, the same for another subinterval $[\rho, b]$.

If $|E - S_i| > \varepsilon, i = 1,2$, then the subdivision processes are still ongoing till the termination criterion is met.

We build up an adaptive algorithm by Mathematica 13.1 to produce the results shown in Tables (3). This table shows that the approximate values of the four integrals I_1, I_2, I_3, and I_4 computed respectively by the dual $I_{DH}(f)$ and its ingredients rules $I_{MI}(f)$ and $I_{aG3}(f)$ in an adaptive environment.

Table: (3). Numerical results computed by the hybrid quadrature rules $I_{HD}(f)$ compared with its constituent rules $I_{MI}(f)$ and $I_{aG3}(f)$ in adaptive environment.

Integral	$I_{MI}(f)$	steps	$I_{aG3}(f)$	Steps	$I_{HD}(f)$	steps
I_1	255.675599	5	255.7257015	3	255.67606135	5
I_2	0.13525742	3	0.135257133	3	0.135257140	3
I_3	0.65932983	2	0.65932996	2	0.6593299577	2
I_4	0.86697254	3	0.866973326	3	0.866973308	2

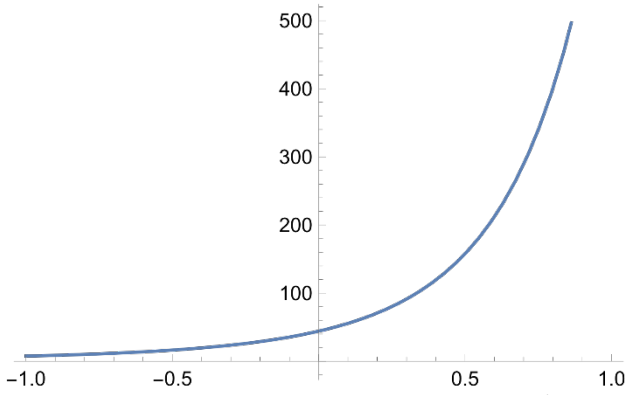

Figure (1): Plot of the integrand of $\int_{-1}^{1} \frac{e^{e^{\left(\frac{x+3}{2}\right)}}}{2} dx$

DISCUSSION

The error analysis of the proposed dual and triple hybrid rules analytically confirms that the degree of precision of such generated rules is higher than their ingredient quadrature rules as shown by equations (13) and (17). Also, the numerically observed results agree with the analytic error analysis. Moreover, the obtained numerical values for the four integrals I_1, I_2, I_3, and I_4 by implementing the dual hybrid rule $I_{DH}(f)$ are better than those attained by its ingredients $I_{MI}(f)$ and $I_{aG3}(f)$ as shown in Table (2). Also, the obtained numerical values of the four integrals I_1, I_2, I_3, and I_4 by using the triple hybrid rule $I_{TH}(f)$ are better than those obtained by its ingredients $I_{CDM}(f)$ and $I_{DH}(f)$ as shown in Table (2). Apart from the integral I_1, all the numerical values of I_2, I_3, and I_4 are reasonably very well although we use a quite few quadrature points. The slow convergence of the integral I_1 is due to the large variation of the integrand on the integration interval, because the integrand has sharp variation from the value 40 at $x = -1$ to the value 500 at the value $x = 1$ as shown in Figure 1. Thus, we easily tackle this issue by implementing the obtained quadrature rule in an adaptive environment with the allowed tolerance set to $\varepsilon = 10^{-5}$. Hence we achieve accurate results that coincide with the exact ones up to four digits only in two steps for the adaptive algorithm for the integrals I_3 and I_4 as shown in Table (3).

CONCLUSION

To conclude triple and dual hybrid quadrature rules have been constructed by blending Gauss-type rules with the classical or the modified Newton-Cotes-type rules that incorporate odd derivatives. Such a mixture incorporates the advantages of both types of quadrature rules to gain better accuracy, thus there is no need to increase the number of quadrature points that may bring instability issues to the numerical process. The acquired results have been enhanced by the adaptive quadrature algorithm. The analytic error analysis and the numerical computations both confirm the efficiency of the proposed approaches. A similar analogy can be adopted to generate hybrid quadrature rules of high-order accuracy by blending as many quadrature rules provided that they are of the same degree of precision.

Duality of interest: The authors declare that they have no duality of interest associated with this manuscript.

Author contributions: Contribution is equal between authors.

Funding: No specific funding was received for this work.

REFERENCES

Atkinson K. E.. (2012). *An introduction to numerical analysis*. Second edition. Wiley Student Edition.

Burden, R. L. and Faires J. D. (2005), Numerical Analysis. Eighth edition. Thomson, Brooks/Cole.

Burg E. C. and E. Degny. (2013) Derivative-Based Midpoint Quadrature Rule. *Applied Mathematics*. 4(1A): 228-234. https://dx.doi.org/10.4236/am.2013.41A035

Burg E. C.. (2012) Derivative-based closed Newton–Cotes numerical quadrature. *Applied Mathematics and Computation*. 218(13): 7052-7065. DOI: https://doi.org/10.1016/j.amc.2011.12.060

Das R. N. G. (2013a) Pradhan. Application of mixed quadrature rules in the adaptive quadrature routine. *General Mathematics Notes.*18: 46-63.

Das R. N. G. Pradhan, (1996). A mixed quadrature for approximate evaluation of real and definite integrals. *Int. J. Math. Educ. Sci. Technology*. 27(2), 279-283. DOI: https://doi.org/10.1080/0020739960270214

Das R. N. G. Pradhan. (2012) On the use of mixed quadrature in adaptive quadrature routine. *Global Journal of Mathematics and Mathematical Sciences*. 2:45-56.

Das R. N. G. Pradhan. (2013b) Numerical computation of integrals with singularity in the adaptive integration scheme involving a mixed quadrature rule. *Bulletin of Pure and Applied Sciences*. 32: 29-38.

Dehghan M., J. Masjed-Jamei, M R. (2005a) Eslahchi. On numerical improvement of open Newton–Cotes quadrature rules. *Appl. Math. Comput.* 175:618-627. DOI: https://doi.org/10.1016/j.amc.2005.07.030

Dehghan M., J. Masjed-Jamei, M R. (2005b) Eslahchi. The semi-open Newton–Cote's quadrature rule and its numerical improvement. *Appl. Math. Comput*. 171:1129-1140. DOI: https://doi.org/10.1016/j.amc.2005.01.137

Jena S. D. Nayak. (2015) Hybrid quadrature for numerical treatment of nonlinear Fredholm integral Equation with separable kernel. *International journal of applied mathematics and statistics*. 53: 83-89.

Jena S. R R. B. Dash. (2011) Study of Approximate Value of Real Definite Integral by Mixed Quadrature Rule Obtained from Richardson Extrapolation. *International Journal of Computational Science and Mathematics.* 3(1): 47-53.

Kuncir F. G., (1962) Algorithm 103: Simpson's rule integrator. *Communication of the ACM*, 16 (3)343-348. DOI: https://doi.org/10.1145/367766.368179.

Laurie D. P.. (1996) Anti-Gaussian Quadrature formulas. *Math. Comp., A. M. S*. 65: 739-747.

Lyness J. N., (1969) Notes on the Adaptive Simpson Quadrature Routine. Journal *of the ACM*, 16 (3) 483-495. DOI: https://doi.org/10.1145/321526.321537.

Mohanty S. K. R. B. Dash. (2010) A mixed quadrature using Birkhoff-Young rule modified by Richardson extrapolation for numerical integration of Analytic functions. *Indian Journal of Mathematics and Mathematical Sciences* 6 (2): 221-228.

Patra P., D. Das, B. Dash. (2018) A comparative study of Gauss–Laguerre quadrature and an open-type mixed quadrature by evaluating some improper integrals. *Turkish Journal of Mathematics*. 42(1).

Sermutlu E.. (2005) Comparison of Newton–Cotes and Gaussian methods of quadrature. *Applied Mathematics and Computation*. 171:1048-1057. DOI: https://doi.org/10.1016/j.amc.2005.01.102

Tripathy A. K. R. B. Dash A. Baral. (2015) A mixed quadrature blending Lobatto and Gauss-Legendre three-point rule for approximate evaluation of the real definite integral. *International Journal of Computing Science and Mathematics.* 6(4): 366-377. DOI: https://doi.org/10.1504/IJCSM.2015.071809

Zafar F., S. Saleem E. C. (2014) Burg. New Derivative Based Open Newton-Cotes Quadrature Rules. *Hindawi Publishing Corporation*. *Abstract and Applied Analysis*. DOI: https://doi.org/10.1155/2014/109138

Al-Mukhtar Journal of Basic Sciences 21 (2): 73-83, 2023
Doi: https://doi.org/10.54172/307bb178

Research Article

Open Access

Synthesis and Antimicrobial Activity of Zinc (II) Complexes of Schiff Bases Derived from 2-Aminobenzoic Acid

Hana B. Shawish[1*] and Hawa M. Alsul[2*]

***Corresponding author:**
h.shawish@sci.misuratau.edu.ly
Department of Chemistry, Faculty of Science, Misurata University, Libya.

Second Author:
h.shawish@sci.misuratau.edu.ly
Department of Chemistry, Faculty of Science, Misurata University, Libya.

Received:
18 September 2023

Accepted:
28 December 2023

Publish online:
31 December 2023

Abstract

Research in Schiff base complexes has been among the mostintriguing areas in coordination chemistry. Mononuclear zinc Schiffbase complexes of the type [Zn(L1) (H2O)2] and [Zn(HL2)2] anddinuclear complexes of the type [Zn2(L1) Q(OAc) (H2O)] and [Zn2(L2) Q(OAc) (H2O)] (where H2L1= 2-2((2hydroxybenzylidene) amino) benzoic acid, H2L2 = 2 -((4-hydroxy-3methoxybenzylidene) amino) benzoic acid and HQ= 8hydroxyquinoline) are described. The complexes were investigatedbyusing various spectroscopic methods including elemental analysis, mass spectra, 1H-NMR spectra, Fourier transform infrared (FT-IR) and UV−visible spectra. Using the diffusion method, the Schiff bases and Schiff base zinc complexes were screened in vitro against four bacteria (S. aureus, K. pneumonia, and Acinetobacter spp. and E. coli).

Keywords: 2-aminobenzoic acid; Zinc (II) complexes; 8-hydroxyquinoline Ligand, Spectrophotometry; Antibacterial

INTRODUCTION

Schiff base metal complexes have been playing an important role in coordination chemistry development due to the simple and direct synthesis of quite different ligands, reactivity, versatility and richness of the chemistry, stability of the complexes and their fascinating potential applications (Abu-Dief & Mohamed, 2015; Gupta & Sutar, 2008). Schiff base complexes play vital roles in modern coordination chemistry in addition to the improvement of bioinorganic chemistry (Deghadi *et al.*, 2022), catalysis (Dalia *et al.*, 2018; Cozzi, 2004) and magnetism (Rani *et al.*, 2018). Schiff base type ligands in coordination chemistry are flexible ligands that can confer better coordination tendency to a metal center in different coordination modes. They commonly coordinate to metal centers through azomethine nitrogen with other donor atoms from carbonyl moiety yielding mono or polynuclear complexes. However, the chelation capacity of the Schiff base ligand can be increased by introducing additional donor atoms ((Rani *et al.*, 2018; Abdel-Rahman *et al.*, 2019)). Among Schiff bases ligands, N, O type ligands have attracted considerable attention because of the stability that they give to their complexes by chelation (El-t Ashoor & Shawish, 2015; Lazzarini *et al.*, 2016).

Schiff bases that are derived from 2-aminobenzoic acid have gained significant attention.These ligands coordinate with the metal ions as anionic NO and NOX (whereX = O, N, or S) chelating lig-

ands. In the NO mode, the coordination occursthrough the imine nitrogen and oxygen atomsof the carboxylic group to form mononuclear complexes with the ligand binding to the metal center forming one six-membered ring (Abdel-Rahman *et al*., 2019; Jirjees *et al*., 2021). Whereas, the NOX donor ligands coordinate to the metal center through the imine nitrogen, oxygen of the carboxylic group and the X atom attached to the aldehyde/ketone skeletal forming mononuclear or dinuclear complexes (Wu *et al*., 2020).

Interest has centered on zinc(II) complexes with N, O bidentatedonor ligands due to the ability of zinc to bind tohard donors. Generally, Zinc in biological systems is mainly coordinated with nitrogen and oxygen of amino acid residues (Pellei *et al*., 2021). Moreover, certain zinc complexes with N, O type ligands exhibit considerable biological activities. Dasgupta *et al*., It has been reported that Zn (II) complexes with acyl hydrazone Schiff base ligands exhibit anti-cancer activity towards (human colorectal carcinoma) HCT116, (human hepatocellular carcinoma) HepG2, and (human non-small lung carcinoma) cell lines A549. (Dasgupta *et al*., 2020).

In this study, the aim was to present the synthesis and structural characterization of zinc (II) complexes with Schiff base derivatives of 2-aminobenzoic acid.The Schiff bases (H_2L^1 and H_2L^2) react with zinc(II) acetate dihydrate to afforda mononuclear zinc complex. However, the reaction of these Schiff bases with $Zn(OAc)_2.2H_2O$ in the presence of 8-hydroxyquinoline afforded binuclear complexes and the antibacterial activity of the complexes has been evaluated.

MATERIALS AND METHODS

Reagents and solvents

All reagents and solvents were obtained from commercial sources and used without further purification. 2-aminobenzoic acid, salicylaldehyde and 3-methoxy 4-hydroxybenzaldehyde have been acquired from Alfa Aesar, 8-hydroxyquinoline was supplied from Riedel-De Haen, zinc (II) acetate dihydrate was supplied from Merck. The ligands H_2L^1 and H_2L^2have beensynthesized according to thepreviously published procedure (El-Ajaily *et al*., 2016)

Physical measurements

The equipment used for elemental analysis was the Perkin Elmer Model 2400. PerkinElmer FT-IR Spectrometer (Frontier) where used for infrared spectra. The UV-Vis spectra for the metal complexes in the DMSO solution were recorded in the 200–800 nm range on an Agilent Technologies Cary 60 UV-Vis spectrophotometer. Mass spectra (EI) were recorded using a micromassautospec spectrometer. JEOL JNM-ECA Series FT NMR was used to document 1H-NMR spectra.

Synthesis of the complexes

Synthesis of the complexes $[ZnL^1(H_2O)_2]$ (C1) and $[Zn(HL^2)_2]$ (C2)

A solution of $Zn(CH_3COO)_2.H_2O$ (0.5 mmol, 0.1097 g) in 20 mL of methanol was added to a solution of the ligand H_2L^1 (1 mmol, 0.241 g) or H_2L_2 (1 mmol, 0.271 g) dissolved in 20 mL of methanol. The mixture was heated to reflux for 4 hours. The resulting precipitates were filtered then washed with water, methanol and then dried at room temperature.

Synthesis of the complexes$[ZnL^1Q(OAc)(H_2O)]$ (C3) and $[Zn(L^2)Q(OAc)(H_2O)]$ (C4)

In a 5 mL methanol solution, 1 mmol (1.45g) of 8-hydroxyquinoline was mixed with either 1 mmol (0.241g) of Schiff base ligand H_2L^1 or 1 mmol (0.271g) of H_2L^2Schiff base ligand, dissolved in 20 mL methanol. Next, a solution of $Zn(CH_3COO)_2.H_2O$ (1mmol, 0.219g) in 20 mL methanol was added. The mixture was heated and stirred for 5 hours. The resulting suspension was filtered washed with methanol then dried in air.

Antibacterial study

The Schiff bases H_2L^1 and H_2L^2, along with zinc (II) complexes, were tested against bacterial strains: Acinetobacter spp., Staphylococcus aureus, Streptococcus, Klebsiella pneumonia, and Escherichia coli by using the agar-well diffusion method (Bauer, 1996). The antibacterial efficiencywas tested using the DMSO as solvent. The tested compounds were added to agar plates, which were then incubated at 37 °C for 24 hours. The inhibition zones were measured in millimeters, and the experiment was repeated twice to ensure accuracy.

RESULTS

The mononuclear zinc (II) complexes C1 and C2 are prepared from a typical synthetic procedure, in which $Zn(OAc)_2.2H_2O$ is reacted with Schiff bases H_2L^1 and H_2L^2 in methanol aqueous (Scheme 1), while the dinuclear mixed ligand complexes C3 and C4 are prepared with the Schiff bases in the presence of 8-hydroxyquinoline as a co-ligand (Scheme 2). The prepared complexes are air stable, soluble in DMSO, DMFand almost insoluble in water and other common organic solvents as well. The physical properties and analytical data of the prepared complexes are summarized in Table 1. The elemental analysis results of the prepared complexes are in good agreement with the results required by the proposed formula.

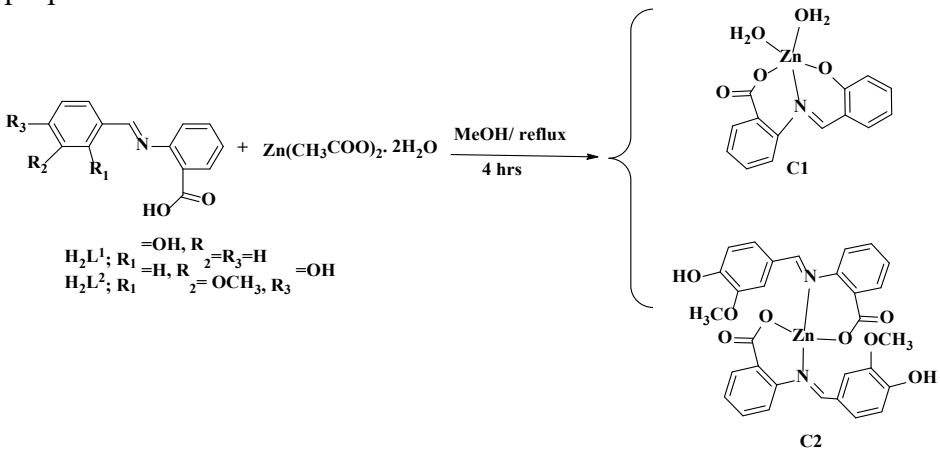

Scheme (1). Schematic routes of the synthesis of complexes C1 and C2

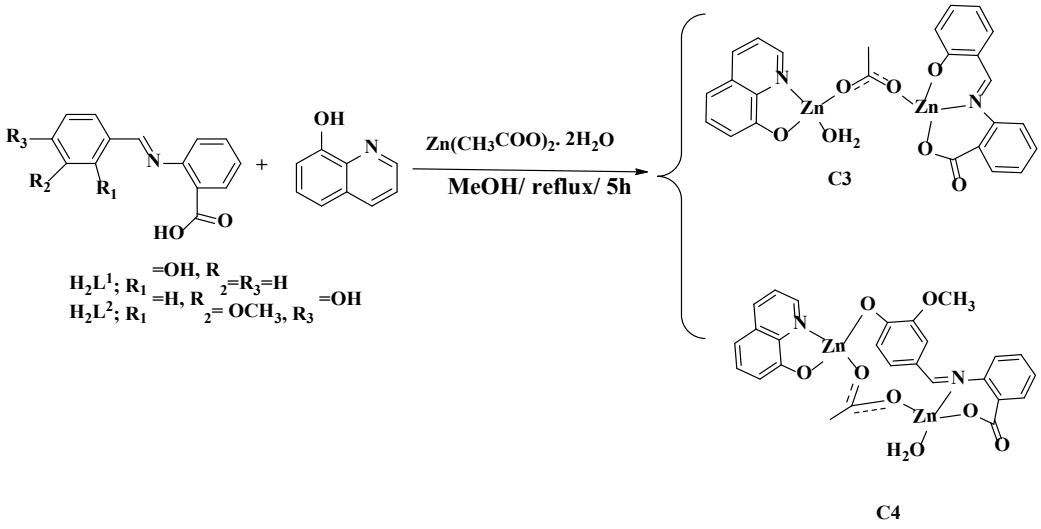

Scheme (2). Schematic routes of the synthesis of complexes C3 and C4

Table (1). Analytical data of the ligand–metal complexes

Compound	Molecular Formula	Colour	Melting Point °C	Yield (%)	Anal.Calc. (Found)%		
					N	H	C
$[ZnL^1(H_2O)_2]$(C1)	$C_{14}H_{14}NO_5Zn$	Pale yellow	280	68	4.11 (4.01)	4.40 (4.02)	49.36 (49.10)
$[Zn(HL^2)_2]$(C2)	$C_{30}H_{40}N_2O_8Zn$	Pale yellow	285	72	4.62 (4.60)	3.99 (4.06)	59.47 (59.44)
$[ZnL^1Q(OAc)(H_2O)]$(C3)	$C_{25}H_{20}N_2O_7Zn_2$	Yellow	Up to 300	44	4.74 (4.78)	3.41 (3.80)	50.79 (51.02)
$[ZnL^2Q(OAc)(H_2O)]$(C4)	$C_{26}H_{22}N_2O_8Zn_2$	Pale yellow	Up to 300	48	4.51 (4.35)	3.57 (3.43)	50.27 (50.12)

IR spectra of the prepared complexes were compared with those of their free Schiff bases H_2L^1 and H_2L^2(Table 2). The bands at 1688 and 1690 cm^{-1} in the spectra of free H_2L^1 and H_2L^2 ligands can be attributed to the C=O stretching of the carboxylic group. However, these bands disappeared in the spectra of the zinc complexes and new bands at around 1540 cm^{-1} and 1370-1407 cm^{-1} which attributed to $v_{as}(COO^-)$ and $v_s(COO^-)$, respectively (Refat *et al*., 2013; Dubey & Mishra, 2011). Also, the IR spectra of the free ligands presented distinguishing bands at 1615 and 1593 cm^{-1} for the CH=N, whichwere moved downfield to 1593 and 1589 cm^{-1} upon complexation of ligands H_2L^1 and H_2L^2, respectively,hence elucidating the coordination of N atom ofthe CH═N group to the central zinc (II) ion (Aldawood, 2013) . coordination of the phenolic oxygen to zinc (II) ion in C1, C3, and C4 complexes is confirmed by the shift of the strong band at about 1244 cm^{-1} in the H_2L^1 and at 1279 cm^{-1} in H_2L^2, which is ascribed to C-O stretching vibrations, to lower frequency at 1232 cm^{-1} (Uba, 2023).

Table (2). IR spectra of the ligands and theirzinc complexes

compound	Stretching frequency (cm^{-1})								
	$\upsilon_{C=O}$	$\upsilon_{C=N}$	$\upsilon_{asyCOO-}$	υ_{syCOO-}	υ_{C-O}	$\upsilon_{C=N}$ Quinoline	υ_{C-O} Quinoline	υ_{asyCOO^-} acetate	υ_{syCOO^-} acetate
H_2L^1	1688	1615	-	-	1244	-	-	-	-
H_2L^2	1690	1589	-	-	1279	-	-	-	-
C1	-	1593	1542	1406	1232	-	-	-	-
C2	-	1591	1540	1407	1272	-	-	-	-
C3	-	1593	1541	1372	1231	1467	1109	1499	1390
C4	-	1593	1543	1387	1235	1467	1110	1499	1387

This band did not shift in the IR spectrum of complex C2, which appeared at 1275 cm^{-1}. This confirms that the phenolic OH group is not coordinating with Zn. (II) (Fugu *et al*., 2013) Moreover, the IR spectra of the mixed complexes C3 and C4 displayed new bands at 1109 and 1467 cm^{-1} assignable to v(C-O) and v(C=N), respectively in the co-ligand 8-hydroxyquinoline. (Shivankar *et al*., 2003; Bufarwa & Abdel-Latif, 2022) Another new band appeared only in the IR spectra of C3 and C4 at 1499 and 1390 cm^{-1}assigned for $v_{as}(COO^-)$ and $v_s(COO^-)$ in the acetate group, indicating the involvement of acetate as a bridging ligand (Nakamoto, 2009). When used in conjunction with other spectroscopic information, ^1H NMR is a valuable tool for identifying coordination sites in zinc (II) complexes. The chemical shifts of the Schiff base ligands and their zinc complexes

$[ZnL^1(H_2O)_2]$ (C1), $[Zn(HL^2)_2]$ (C_2), $[ZnL^1Q(OAc)(H_2O)]$ (C_3) and $[Zn(L^2)Q(OAc)(H_2O)]$ (C_4)are presented in Table 3. Figure 1 shows the ^1H NMR spectra for the ligands and their prepared zinc complexes. The singlet band appeared at 10.25 and 9.77 ppm for the free Schiff bases H_2L^1 and H_2L^2 respectively, and is assigned to the phenolic proton.

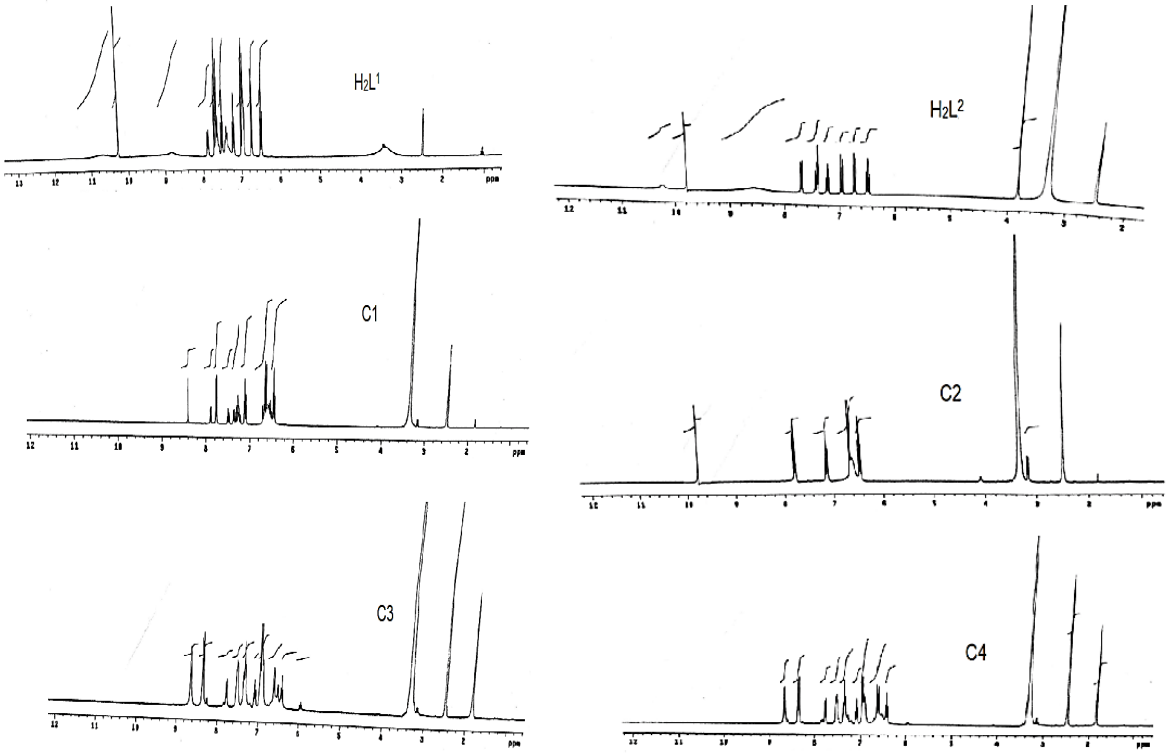

Figure (1). ^1H NMR spectra for the ligands and their prepared zinc complexes

Table (3). ^1H NMR spectral data (δ, ppm) of H_2L^1, H_2L^2, and their Zn (II) complexes

compound	Chemical shifts, δ (ppm)					
	COOH	OH	C=N	Aromatic	CH_3 (acetate)	OCH_3
H_2L^1	10.90	10.25	8.86	7.71- 6.49	-	-
H_2L^2	10.30	9.77	8.84	6.49–7.69	-	3.84
C1	-	-	8.47	7.90- 6.42	-	-
C2	-	9.85	7.89	6.44 –7.77	-	3.18
C3	-	-	8.64	6.43-7.19	1.85	-
C4	-	-	8.66	6.41-7.78	1.85	

This signal is absent from the spectra of complexes C1, C3, and C4, showing that coordination of the ligands H_2L_1 and H_2L_2 to Zn (II) was through the oxygen atom of these ligands with deprotonation (Nishal *et al*., 2014). Also, the singlet at 10.90 and 10.30 ppm in the free ligands H_2L^1 and H_2L^2 respectively, which is attributed to the proton of the carboxylic group, disappeared in the ^1H NMR spectra of all complexes. The coordination of the carboxylic oxygen with the zinc center is likely confirmed. In all complexes, the azomethine proton signal in the ^1H NMR spectra is shifted upfield compared to the free ligands, indicating coordination through the azomethine nitrogen. Ad-

ditionally, the singlet at 1.85 ppm corresponds to the CH_3 of the acetate moiety in the C3 and C4 complexes, integrating as three hydrogens (Abu-Dief *et al*., 2019).

Electronic spectra of the zinc(II) complexes and the free Schiff bases were recorded in DMSO (1×10^{-5} M) at room temperature.The study results are depicted in Figure 2 and Table 4.The Schiff base H_2L^1 exhibits two absorption bands at 261 and 315 nm, respectively attributed to ($\pi \rightarrow \pi^*$) and ($n \rightarrow \pi^*$) transitions of the azomethine and carboxylic chromophore.Similarly, the ligand H_2L^2 exhibits two bands that appeared at 280 and 313 nm which are attributed to the ($\pi \rightarrow \pi^*$) and ($n \rightarrow \pi^*$), respectively. On complexation, this band was shifted to a higher wavelength region, proposing the coordination of azomethine nitrogen and carboxylic oxygen with Zn (II) ion (Belal *et al*., 2015). Furthermore, complexes C3 and C4 exhibit a broadband at 398 nm, which is assigned to metal-ligand charge transfer (MLCT) transitions. This is expected for zinc complexes (Abdel-Rahman *et al*., 2017). The mass spectra of the complexes showed different patterns of fragmentation, as expected. The results were consistent with the molecular formulas of the compounds. Figure 3 displays the mass spectra of the C1, C2, C3, and C4 complexes. These spectra showed molecular ion peaks at m/z = 341, 607, 593, and 622, respectively. These peaks matched the calculated weights of 340.64, 592.21, 605.91, and 621.23.

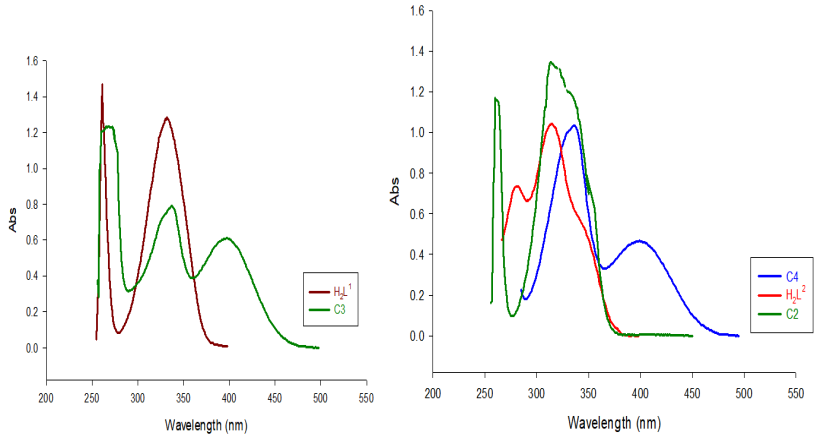

Figure (2). Electronic spectra of the ligands andtheir zinc (II) complexes

Table (4). Electronic spectra data of the ligands and their zinc (II) complexes

Compound	Absorbance (nm)	Assignment
H_2L^1	259	$\pi \rightarrow \pi^*$
	331	$n \rightarrow \pi^*$
H_2L^2	260, 281	$\pi \rightarrow \pi^*$
	315	$n \rightarrow \pi^*$
C1	266	$\pi \rightarrow \pi^*$
	338	$n \rightarrow \pi^*$
	396	M→ L
C2	272	$\pi \rightarrow \pi^*$
	336	$n \rightarrow \pi^*$
C3	268	$\pi \rightarrow \pi^*$
	336	$n \rightarrow \pi^*$
	403	M→ L
C4	336	$n \rightarrow \pi^*$
	405	M→ L

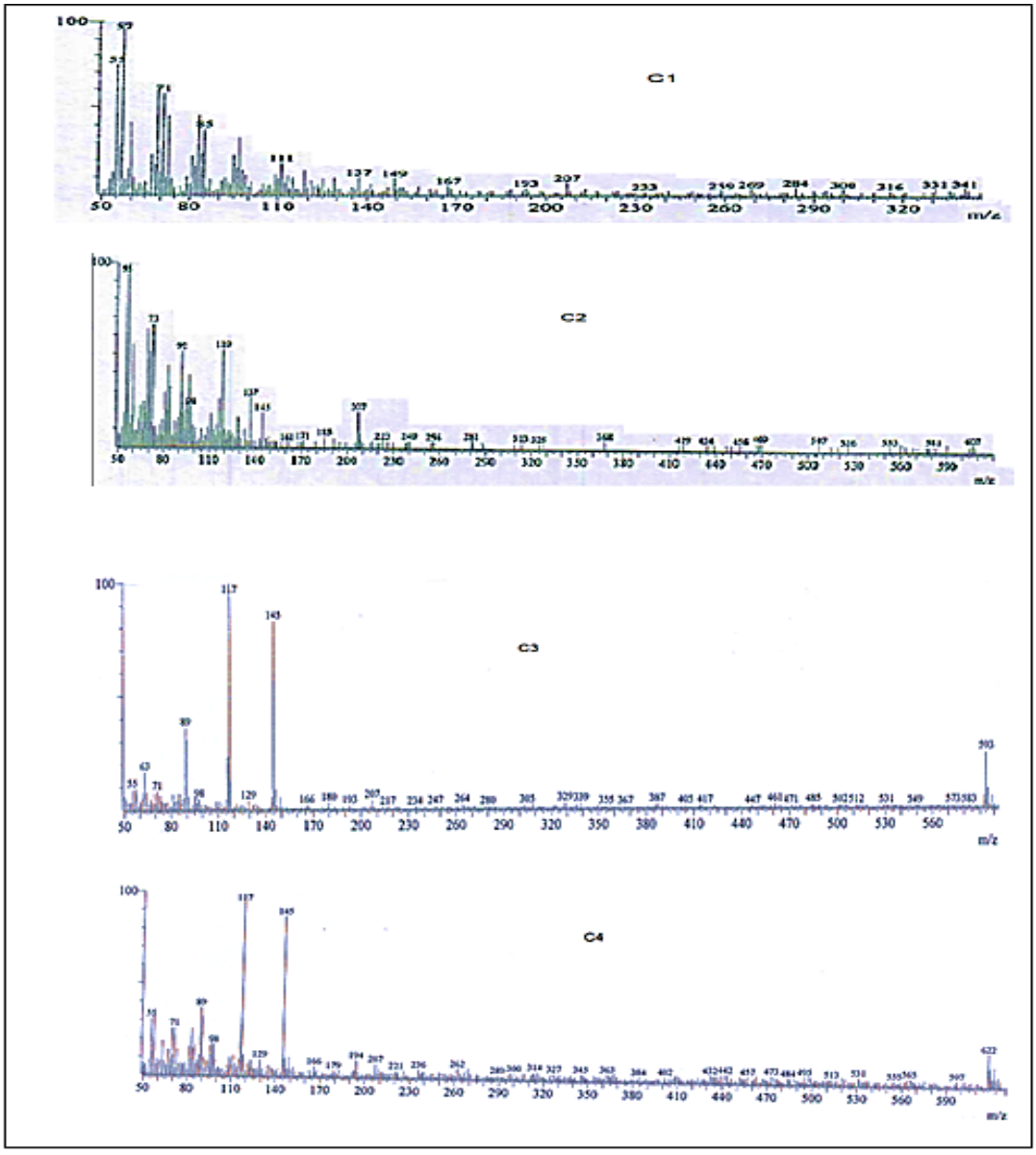

Figure (3). Mass spectra of zinc complexes

The antibacterial potential of the ligands and their zinc (II) complexes is investigated. For antibacterial testing, Gram-negative strains (Escherichia coli, Streptococcus Klebsiella pneumonia, and Staphylococcus aureus) and Gram-positive strains (Acinetobacter Spp.) were used. Table 5 summarizes the results of the antibacterial activity. The ligands had low activity against each bacterial species, however, the zinc complexes performed better than the original ligands. All prepared zinc complexes showed notable antibacterial activity against the *Streptococcusaureus* bacterial strain with an inhibition zone range of 14-20. However, the zinc complex $[ZnL^{1}(H_2O)_2]$ (C1) With an inhibition zone diameter of 20mm, showed demonstrated activity against the Staphylococcus aureus strain. This result can be comparable with results reported in the literature (Joseyphus & Nair, 2008; Zabin *et al*., 2018).

Table (5). shows the antibacterial activity of ligands and their zinc complexes.

Compound	Bacterial Zone of Inhibition (mm)			
	Gram Positive		Gram Negative	
	Staphylococcus aureus	*Escherichia coli*	*Acinetobacter Spp.*	*Klebsiella pneumonia*
DMSO(control)	6	6	6	6
H_2L^1	6	11	7	7
H_2L^2	6	11	10	7
C1	20	17	19	15
C2	14	6	11	10
C3	16	14	14	10
C4	19	14	19	14

CONCLUSION

Schiff bases derived from 2-aminobenzoic acid were synthesized and characterized as zinc (II) complexes. Schiff base ligands coordinate with the Zn (II) ion in various ways, including as a dibasic tridentate ONO chelating ligand and as a negative ON bidentate ligand. According to the antibacterial study, Zinc (II) complexes have better antibacterial properties than free Schiff base ligands.

ACKNOWLEDGEMENT

The authors would like to thank Misurata University for their assistance with this study.

Duality of interest: The authors declare that they have no duality of interest associated with this manuscript.

Author contributions: Contribution is equal between authors.

Funding: No specific funding was received for this work.

REFERENCES

Abdel-Rahman, L. H., El-Khatib, R. M., Nassr, L. A., & Abu-Dief, A. M. (2017). DNA binding ability mode, spectroscopic studies, hydrophobicity, and in vitro antibacterial evaluation of some new Fe (II) complexes bearing ONO donors amino acid Schiff bases. *Arabian Journal of Chemistry*, *10*, S1835-S1846.

Abdel-Rahman, L. H., Abu-Dief, A. M., Shehata, M. R., Atlam, F. M., & Abdel-Mawgoud, A. A. H. (2019). Some new Ag (I), VO (II) and Pd (II) chelates incorporating tridentate imine ligand: Design, synthesis, structure elucidation, density functional theory calculations for DNA interaction, antimicrobial and anticancer activities and molecular docking studies. *Applied Organometallic Chemistry*, *33*(4), e4699.

Abu-Dief, A. M., Abdel-Rahman, L. H., Shehata, M. R., & Abdel-Mawgoud, A. A. H. (2019). Novel azomethine Pd (II)-and VO (II)-based metallo-pharmaceuticals as anticancer, antimi-

crobial, and antioxidant agents: Design, structural inspection, DFT investigation, and DNA interaction. *Journal of Physical Organic Chemistry*, *32*(12), e4009.

Aldawood, A. Y. (2013). Mono Nuclear and Oxalato-Bridged Binuclear Transition Metal Complexes with a Tridentate Schiff Base Ligand and their Applications as Anticancer Reagents. *International Journal of Chemistry*, *35*(1), 1431.

Bauer, A. W. (1996). Antibiotic susceptibility testing by a standardized single disc method. *Am. J. of Clinc. Path.*, *45*, 149-158.

Belal, A. A. M., El-Deen, I. M., Farid, N. Y., Zakaria, R., & Refat, M. S. (2015). Synthesis, spectroscopic, coordination and biological activities of some transition metal complexes containing ONO tridentate Schiff base ligand. *Spectrochimica Acta Part A: Molecular and Biomolecular Spectroscopy*, *149*, 771-787.

Bufarwa, S. M., & Abdel-Latif, S. A. (2022). Spectroscopic, thermal, and conductometric investigation of some (arylazo) quinolin-8-ol and their complexes with the divalent ions of Mn, Ni, Cu, and Zn.

Casas, J. S., Garcıa-Tasende, M. S., & Sordo, J. J. C. C. R. (2000). Main group metal complexes of semicarbazones and thiosemicarbazones. A structural review. *Coordination Chemistry Reviews*, *209*(1), 197-261.

Cozzi, P. G. (2004). Metal–Salen Schiff base complexes in catalysis: practical aspects. *Chemical Society Reviews*, *33*(7), 410-421.

Dalia, S. A., Afsan, F., Hossain, M. S., Khan, M. N., Zakaria, C., Zahan, M. E., & Ali, M. (2018). A short review on chemistry of schiff base metal complexes and their catalytic application. *Int. J. Chem. Stud*, *6*(3), 2859-2867.

Dasgupta, S., Karim, S., Banerjee, S., Saha, M., Saha, K. D., & Das, D. (2020). Designing of novel zinc (II) Schiff base complexes having acyl hydrazone linkage: study of phosphatase and anti-cancer activities. *Dalton Transactions*, *49*(4), 1232-1240.

Deghadi, R. G., Elsharkawy, A. E., Ashmawy, A. M., & Mohamed, G. G. (2022). Can one novel series of transition metal complexes of oxy-dianiline schiff base afford advances in both biological inorganic chemistry and materials science?. *Comments on Inorganic Chemistry*, *42*(1), 1-46.

Dubey, U. K., & Mishra, S. K. (2011). Synthesis, spectroscopic (IR, electronic, FAB-mass, and PXRD), magnetic, and antimicrobial studies of new iron (III) complexes containing Schiff bases and substituted benzoxazole ligands. *Journal of Coordination Chemistry*, *64*(13), 2292-2301.

El-Ajaily, M. M., Al-Barki, N. S., & Maihub, A. A. (2016). Mixed Schiff Bases Chelates: Synthesis and Spectroscopic Investigation. *Asian Journal of Advanced Basic Sciences*, *4*(2), 123-130.

El-t Ashoor, S., & Shawish, H. B. (2015). Synthesis, X-ray crystallography and DFT studies of Ni (II) complex with tetradentate. *Science and Education*, *3*(1), 7-11.

Fugu, M. B., Ndahi, N. P., Paul, B. B., & Mustapha, A. N. (2013). Synthesis, characterization, and antimicrobial studies of some vanillin schiff base metal (II) complexes. *Journal of Chemical and Pharmaceutical Research*, *5*(4), 22-28.

Kumar, S., Dhar, D. N., & Saxena, P. N. (2009). Applications of metal complexes of Schiff bases-A review.K.C.

Gupta, K. C., & Sutar, A. K. (2008). Catalytic activities of Schiff base transition metal complexes. *Coordination Chemistry Reviews*, *252*(12-14), 1420-1450.

Inci, D. (2020). A new ternary Cu (II) complex with 4, 7-dimethyl-1, 10-phenanthroline and NOO-type tridentate Schiff base ligand: Synthesis, crystal structure, biomacromolecular interactions, and radical scavenging activities. *Applied Organometallic Chemistry*, *34*(12), e6016.

Joseyphus, R. S., & Nair, M. S. (2008). Antibacterial and antifungal studies on some schiff base complexes of zinc (II). *Mycobiology*, *36*(2), 93-98.

Jirjees, V. Y., Al-Hamdani, A. A. S., Wannas, N. M., A. R, F., Dib, A., & Al Zoubi, W. (2021). Spectroscopic characterization for new model from Schiff base and its complexes. *Journal of Physical Organic Chemistry*, *34*(4), e4169.

Lazzarini, I. C., Carrella, L., Rentschler, E., & Alborés, P. (2016). One dimensional Mn (III) Schiff-base complex organization through very strong symmetrical H-bond interaction. *Inorganica Chimica Acta*, *453*, 692-696.

Nakamoto, K. (2009). *Infrared and Raman spectra of inorganic and coordination compounds, part B: applications in coordination, organometallic, and bioinorganic chemistry*. John Wiley & Sons.

Nishal, V., Singh, D., Kumar, A., Tanwar, V., Singh, I., Srivastava, R., & Kadyan, P. S. (2014). A new zinc–Schiff base complex as an electroluminescent material. *Journal of Organic Semiconductors*, *2*(1), 15-20.

Niu, M., Cao, Z., Xue, R., Wang, S., Dou, J., & Wang, D. (2011). Structural diversity of Cu (II) compounds of Schiff bases derived from 2-hydroxy-1-naphthaldehyde and a series of aminobenzoic acid. *Journal of Molecular Structure*, *996*(1-3), 101-109.

Pellei, M., Del Bello, F., Porchia, M., & Santini, C. (2021). Zinc coordination complexes as anticancer agents. *Coordination Chemistry Reviews*, *445*, 214088.

Rani, V. S. V., Dhanasekaran, T., Jayathuna, M., Narayanan, V., & Jesudurai, D. (2018). Synthesis, characterization of Cu (II) Schiff base complexes: optical and magnetic studies. *Materials Today: Proceedings*, *5*(2), 8784-8788.

Refat, M. S., Sharshar, T., Elsabawy, K. M., & Heiba, Z. K. (2013). Physicochemical impact studies of gamma rays on “aspirin” analgesics drug and its metal complexes in solid form: Synthesis, spectroscopic and biological assessment of Ca (II), Mg (II), Sr (II) and Ba (II) aspirinate complexes. *Journal of molecular structure*, *1047*, 37-47.

Shivankar, V. S., Vaidya, R. B., Dharwadkar, S. R., & Thakkar, N. V. (2003). Synthesis, characterization, and biological activity of mixed ligand Co (II) complexes of 8-hydroxyquinoline and some amino acids. *Synthesis and reactivity in inorganic and metal-organic chemistry*, *33*(9), 1597-1622.

Şenol, C., Hayvali, Z., Dal, H., & Hökelek, T. (2011). Syntheses, characterizations and structures of NO donor Schiff base ligands and nickel (II) and copper (II) complexes. *Journal of Molecular structure*, *997*(1-3), 53-59.

Uba, B. (2023). Antibacterial and antifungal activities of Schiff base and its metal (Ii) complexes of Fe (Ii), Ni (Ii) and Co (Ii) derived from 2-hydroxy-1-naphthaldehyde and 2-amino-3-methylpyridine. *Microbes and Infectious Diseases*, *4*(1), 312-322.

Wu, R., Bi, C., Zhang, X., Zong, Z., Fan, C., Zhang, X., ... & Fan, Y. (2020). Syntheses, crystal structure and biological evaluation of three novel Cu (II) complexes with Schiff base derived from fluorinated amino acid and Salicylaldehyde. *Applied Organometallic Chemistry*, *34*(1), e5264.

Zabin, S. A., Jammali, M., & Alzahrani, A. A. (2018). The bivalent Cu, Ni and Zn complexes of unsymmetrical ONO tridentate Schiff base ligands derived from 2-aminobenzoic acid: antimicrobial and molluscicidal activity. *J Org Inorg Chem*, *4*(2), 6.

Al-Mukhtar Journal of Basic Sciences 21 (2): 84-90, 2023
Doi: https://doi.org/10.54172/m3552n48

Research Article

Open Access

Size structure and dynamics of the threatened Laurus nobilis L population in Shahat, AL-Jabal AL-Akhdar, Libya

Mabroka A. G.Abdalrhim

***Corresponding author:** mabrokagbrial@yahoo.com
Department of Botany, Faculty of Arts and Science - Al marj, Benghazi University, Benghazi, Libya

Received:
21 September 2023

Accepted:
29 December 2023

Publish online:
31 December 2023

Abstract

The fragrant evergreen leaves of the bay tree, also known as laurel (Laurus nobilis L., Lauraceae), are a large shrub that is extensively used in Mediterranean cooking. The present work aimed to study the size structure of Lauru snobilis populations concerning their soil conditions. Twenty-one terraces (25m × 25m) were selected at Shahat of Al-Jabal Al-Akhder at three different levels. The height-to-diameter ratio was more than unity for Laurus nobilis. This means that the diameter of these species tends to expand vertically rather than horizontally. Five forms of size distribution along the different elevations were recognized. In the present study, it was found that Laurus nobilis exhibited more or less J-shaped distribution along elevation levels (downstream and midstream). Laurus nobilis exhibited more or less symmetrical distribution (bell-shaped) along the elevation level (upstream). The negatively skewed distribution of Laurus nobilis indicated the dominance of mature individuals over the juvenile ones. The field observations were consistent with the results of the investigation of soil properties.

Keywords: Population dynamic; Size distribution; Laurus nobilis L; Shahat, AL-Jabal AL-Akhdar, Libya .

INTRODUCTION

The Greeks established the ancient city of Shahat, Cyrene (Qurina), in the northeastern Libyan district of Al-Jabal Al-Akhdar. Overall, recent vegetation studies revealed a high degree of plant diversity. Furthermore, the vast majority of Al-Jabal Al-Akhdar's wild plants are used in biotechnology and medicine. There are medicinal plants all over the nation, although they are concentrated in the areas of Al-Jabal Al-Akhdar (UNEP, 2002). However, a shift in the vegetation within this delicate ecosystem may result from various factors, including desertification, increased rates of dry land degradation, overgrazing, urbanization, and the destruction of natural vegetation (MEA, 2005; El-Barasi *et al*., 2013). Along with extensive human activity, large areas have been reclaimed. Without a doubt, these activities have had a negative impact on species diversity as well as size structure. The ages, sizes, and morphologies of the individuals that make up a plant population can be used to characterize its structure (Harper & White, 1974). The characterize population structure, plant size, and reproductive traits in *Laurus nobilis* commonly known as bay leaves. Its leaves and extracts are used to treat eructation, flatulence, and gastrointestinal issues, as well as to suppress bacterial and fungal infections and high blood sugar. Moreover, it has antioxidant, anti-inflammatory, anticonvulsive, and antiepileptic qualities (Gómez-Coronado & Barbas, 2003;

Ouchikh *et al*., 2011; Ramos *et al*., 2012). The most prevalent phenolic compounds in bay leaves have been reported to be flavonoids, including derivatives of myrcetin, luteolin, apigenin, kaempferol, and quercetin (Lu *et al*., 2011). The current study set out to examine the dynamics and population structure of *Laurus nobilis* in various habitats in Shahat, North-Eastern Libya.

MATERIALS AND METHODS

Location of study area:

The study area is located in the Mediterranean Sea Cost of Libya between latitude 32°35′52.84" N and longitude 21°28′22" E (Al-Jabal Al-Akhder South project, 2005) Cyrene is located about 10Km east of the city of Al-Bayda, in the northeast of Libya. It is found on the second terrace of Al- Jabal Al- Akhdar, at an elevation of around 600 meters, its height is between (555: 578) meters it lies between Latitude 32°49′23.952 ′N And longitude 021°51′11.1888 ′E on the North East region, Al Jabal Al-Akhdar (Newport & Haddor, 1963). The study area is shown in Figure 1.

Climate of the area:

The distinctive features of the climate of the study area are a concentration of rainfall during the cool winter season and summer drought climate data for the study area. December and January have the highest mean monthly rainfall totals, at 63 and 62 mm, respectively. The annual rainfall average is roughly 566 mm, albeit highly variable in terms of location. Just before spring, humidity rises, with a peak of 33% in March. In June, the mean maximum monthly temperature reaches 38ºC; in January and December, it drops to 21ºC and 22ºC, respectively. January and December have the lowest mean minimum monthly temperatures, with 5ºC and 6ºC, respectively (Shahat Metrological Station). Figure 2 (El-Tantawi, 2005).

Collections and population frequency:

Twenty one quadrates (each of 25x25m) were selected to represent the main habitats of *Laurus nobilis* populations along Shahat. The population structure of these species was evaluated in terms of size distribution. The size index of each individual was calculated as the mean of its height and diameter [(H+D)/2]. The size estimates were then used to classify the population into 7 size classes. The size classes (m/ ind.) are (1=0<1, 2=1.1-2, 3=2.1–3, 4=3.1–4, 5=4.1–5, 6=5.1–6 and 7= 6.1–7) (Shaltout *et al*., 2015).

Soil analysis:

In each location, one composite soil sample was collected from soil profiles (0 – 25cm), air dried then physical and chemical parameters of such soil samples were analyzed (Gupta, 2000; Brown, 1998; Allen *et al*., 1974; Blanchar *et al*., 1965).

RESULTS

Size distribution analysis of *Laurus nobilis* population using tree height and diameter, the size was estimated by measuring the height and mean diameter were shown in Table 1. Generally, the height to diameter ratio was more than unity for *Laurus nobilis*. The relationships between the individual heights and diameters of the *Laurus nobilis* population are simple linear with r^2 values of 0.616 Figure 3. The population downstream had highest height-to-diameter ratio (5.32), except the population upstream had the lowest (3.22).

In the present study, it was found that *Laurus nobilis* exhibited more or less J-shaped distribution along elevation levels I (downstream and midstream). *Laurus nobilis* exhibited more or less symmetrical distribution (bell-shaped) along the elevation level (upstream). The distribution of *Laurus nobilis* was negatively skewed, indicating that mature individuals outnumbered juvenile ones. Due

to the population's high proportion of larger individuals relative to smaller ones, this distribution is indicative of a declining population. The distribution pattern suggests that there is no recruitment to support the smallest size categories. Furthermore, the study area's high mortality rate is caused by human disturbance, as evidenced by the diminishing numbers of both small and large trees Figure 4.

Soil chemical and physical analysis in different elevation levels indicated that at Shahat, soils elevation downstream were characterized by the highest values of E.C (0.344 ds/m) as well as bicarbonate, sulfate, and sodium (0.75, 5.22 and 6.6 m.eq./L. respectively) Table 2. Soils at midstream were values of clay (58.24), but the lowest value was E.C, silt and chloride (0.144 m.eq./L., 37.51 and 0.71 m.eq./L. respectively). Clay and E.C content in soil showed significant variations between the three levels.

Figure (1): Location map indicating the study

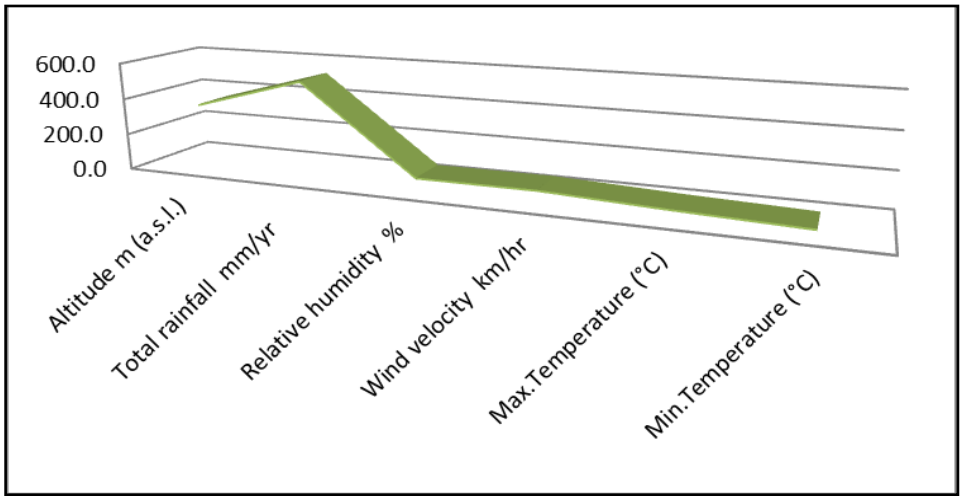

Figure (2): Meteorological data of Shahat station.

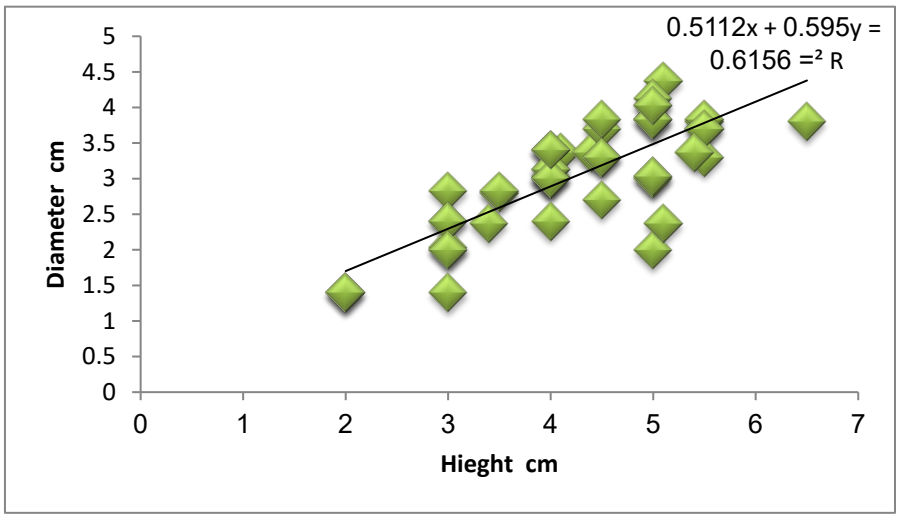

Figure (3): **The** relationships between height, diameter and size index

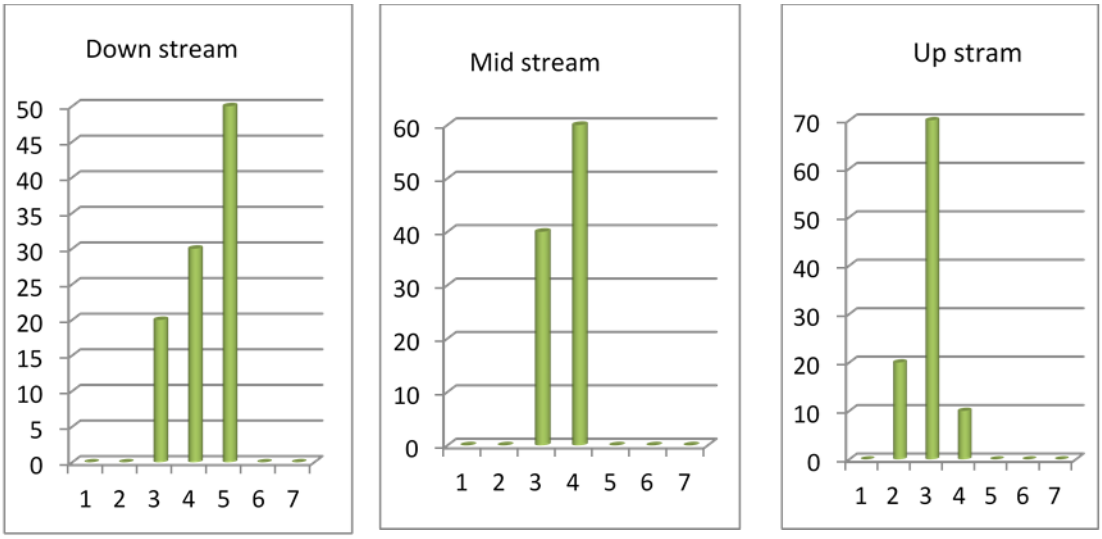

Figure (4): Size frequency distribution of *Laurus nobilis* populations. The ranges of size classes are: 1>1 , 2=1.1-2, 3=2.1-3 ,4=3.1-4 ,5=4.1-5, 6=5.1-6, 7=6.1-7.

Table (1): Size distribution analysis of *Laurus nobilis* population (H: Height, D: Diameter, r: simple linear correlation coefficient between height and diameter and size index

Sites	Species	H (m)	D (m)	H/D	r^2	Size index (m)
Downstream	*Laurus nobilis* L.	5.5 ± 0.844	2.1 ± 0.255	2.6 ± 0.532	0.616	5.32 ± 0.811
Midstream	*Laurus nobilis* L.	4.6 ± 0.721	2.2 ± 0.255	2 ± 0.322	0.616	4.56 ± 0.723
Upstream	*Laurus nobilis* L.	3.4 ± 0.511	2.5 ± 0.361	1.4 ± 0.111	0.616	3.22 ± 0.577

Table (2): Soil chemical and physical analysis in each of the three habitats recognized in the study area.

Soil variables	Elevation levels			F – value
	Downstream	Midstream	Upstream	
pH value	8.4±0.32	7.5±0.21	7.5±0.22	0.317
E.C ds/m	0.344±0.247	0.144±0.76	0.283±0.236	2.88*
Sand (%)	26.8±3.77	29.55±6.22	33.22±6.11	0.252
Silt (%)	40.1±7.16	37.51±6.3	42.2±9.1	1.95
Clay (%)	37.1±9.52	58.24±11.22	33.6±12.04	2.97*
CO3-m.eq./L.)	0.0±0.0	0.0±0.0	0.0±0.0	0.0
HCO3-(m.eq./L.)	0.75±0.22	0.55±0.64	0.45±0.44	0.112
SO4 -(m.eq./L.)	5.22±4.3	1.55±1.32	0.75±2.3	0.832
CI ٦(m.eq./L.)	0.76±0.12	0.71±1.1	0.94±3.1	1.22
Ca^{+2} (m.eq./L.)	0.51±1.14	0.91±0.44	0.16±0.6	0.163
Mg^{+2} (m.eq./L.)	0.02 ±0.15	0.05±0.88	0.31±0.69	0.362
Na^{+} (m.eq./L.)	6.6±5.79	3.18±0.46	1.44±1.52	0.944
K^{+} (m.eq./L.)	0.09±1.99	0.29±0.58	0.33±0.42	0.937

*= significant at P= 0.05

DISCUSSION

Laurus nobilis was observed in three different habitats (upstream, midstream, and downstream) in this study. Its presence was more significant in the first three habitats (downstream), according to the current study. Accordingly, compared to species with smaller morphological variations, those with larger morphological variations would be more adapted to wide environment gradients (Pang & Jiang, 1995). The height-to-diameter ratio provides insight into the plant's growth habit; changes in this ratio are primarily caused by spacing (Wonn & O'Hara, 2001), indicating a tendency for these species' diameters to expand vertically as opposed to horizontally. This ratio in the current study marginally exceeds unity, indicating that people have a tendency to expand (Galal, 2011).

Furthermore, the distribution of *Laurus nobilis* was negatively skewed, suggesting that mature individuals predominate over juvenile ones. Due to the population's high proportion of larger individuals relative to smaller ones), this distribution is indicative of a declining population. Variations in growth rates brought on by age differences, genetic variation, resource heterogeneity, and competition can also contribute to size differences within the plant population (Weiner, 1985). The population's size structure in the wadi beds was close to the distribution's negative skew, suggesting that mature individuals predominated over juvenile ones. Because there are more large individuals in the population than small ones (limited regeneration capacity), this distribution has been associated with declining populations (Weiner, 1984). The study conducted soil analysis at various elevation levels and found that plant cover and vegetation variables were positively correlated with altitude at Shahat. Additionally, soils at elevation downstream had the highest values of sodium, bicarbonate, sulfate, and E.C. The highest concentrations of clay, silt, and chloride were found in midstream soils, while the lowest concentrations were found in E.C.

CONCLUSION

In summary, the overall demographic makeup of *Laurus nobilis* populations in the studied region is distinguished by a greater proportion of elderly individuals relative to younger ones. Genetic, environmental, or dominance-and-suppression competition can be sources of discontinuous variation. Because only the smaller plants are negatively impacted by this type of competition, it could be regarded as asymmetric (Abdalrhim, 2021). Since human activity contributes significantly to the worsening of the situation, species may be able to adapt to and survive climate change (Mawdsley *et al*., 2009).

Duality of interest: The authors declare that they have no duality of interest associated with this manuscript.

Author contributions: The author did all the work related to the manuscript

Funding: There is no funding to support this manuscript

REFERENCES

Abdalrhim, M. A. (2021). Size Structure of Arbutus pavarii and Juniperus phoenicea Populations in Al-Marj Plain, Libya. *International Journal of Multidisciplinary Sciences and Advanced Technology*, 1:10–16.

Allen, S. E., Grimshaw, H. M., Parkinson, J. A., & Quarmby, C. (1974). *Chemical analysis of ecological materials*. Blackwell Scientific Publications.

Blanchar, R. W., Rehm, G., & Caldwell, A. C. (1965). Sulfur in plant materials by digestion with nitric and perchloric acid. *Soil Science Society of America Journal*, *29*(1), 71-72.

Brown, J. R. (1998). *Recommended chemical soil test procedures for the North Central Region* (No. 1001). Missouri Agricultural Experiment Station, University of Missouri--Columbia.

El-Barasi, Y. M. M., & Saaed, M. W. B. (2013). Threats to plant diversity in the north eastern part of Libya (El-Jabal El-Akahdar and Marmarica Plateau). *Journal of Environmental Science and Engineering. A*, *2*(1A), 41.

El-Tantawi, A. M. (2005). Climate change in Libya and desertification of Jifara Plain. *PhD Diss., University of Johannes Gutenberg, Mainz, Germany*.

Galal, T. M. (2011). Size structure and dynamics of some woody perennials along elevation gradient in Wadi Gimal, Red Sea coast of Egypt. *Flora-Morphology, Distribution, Functional Ecology of Plants*, *206*(7), 638-645.

Gómez-Coronado, D. J., & Barbas, C. (2003). Optimized and validated HPLC method for α-and γ-tocopherol measurement in Laurus nobilis leaves. New data on tocopherol content. *Journal of agricultural and food chemistry*, *51*(18), 5196-5201.

Gupta, P. K. (2000). Soil plant water and fertilizer analysis. Agrobios pub. *Bikaner. India*.

Harper, J., & White, J. (1974). The demography of plants. *Annual review of ecology and systematics*, *5*(1), 419-463.

Lu, M., Yuan, B., Zeng, M., & Chen, J. (2011). Antioxidant capacity and major phenolic compounds of spices commonly consumed in China. *Food Research International*, *44*(2), 530-536.

Mawdsley, J. R., O'MALLEY, R. O. B. I. N., & Ojima, D. S. (2009). A review of climate-change adaptation strategies for wildlife management and biodiversity conservation. *Conservation Biology*, *23*(5), 1080-1089.

MEa, M. E. A. (2005). Ecosystems and Human Well-Being: wetlands and water synthesis.

Newport, T. G., & Haddor, Y. (1963). *Ground-water Exploration in Al Marj Area, Cyrenaica, United Kingdom of Libya*. US Government Printing Office.

Ouchikh, O., Chahed, T., Ksouri, R., Taarit, M. B., Faleh, H., Abdelly, C., ... & Marzouk, B. (2011). The effects of extraction method on the measured tocopherol level and antioxidant activity of L. nobilis vegetative organs. *Journal of Food Composition and Analysis*, *24*(1), 103-110.

Pang, G., & Jiang, D. (1995). Population genetic diversity and data analysis. *Scientia Silvae Sinicae*, *31*, 543-550.

Ramos, C., Teixeira, B., Batista, I., Matos, O., Serrano, C., Neng, N. R., ... & Marques, A. (2012). Antioxidant and antibacterial activity of essential oil and extracts of bay laurel Laurus nobilis Linnaeus (Lauraceae) from Portugal. *Natural Product Research*, *26*(6), 518-529.

Saad, A. M. A., Shariff, N. M., & Gairola, S. (2011). Nature and causes of land degradation and desertification in Libya: Need for sustainable land management. *African Journal of Biotechnology*, *10*(63), 13680-13687.

United Nations Environment Programme (UNEP) With a Foreword by Kofi Annan, UN Secretary-General. (2002). Global environment outlook 3: past, present and future perspectives. *Environmental Management and Health*, *13*(5), 560-561.

Shaltout, K. H., Fawzy, M., Ahmed, D. A., Awad, M. H. A., El-Barasi, Y. M., & Al-hasi, S. M. (2015). Impact of waste water discharge on the plant diversity and community structure of Al-Marj Plain, Libya. *Feddes repertorium*, *126*(1-2), 6-15.

Wonn, H. T., & O'Hara, K. L. (2001). Height: diameter ratios and stability relationships for four northern Rocky Mountain tree species. *Western Journal of Applied Forestry*, *16*(2), 87-94.

Weiner, J. (1985). Size hierarchies in experimental populations of annual plants. *Ecology*, *66*(3), 743-752.

Weiner, J., & Solbrig, O. T. (1984). The meaning and measurement of size hierarchies in plant populations. *Oecologia*, *61*, 334-336.

Al-Mukhtar Journal of Basic Sciences 21 (2): 91-97, 2023
Doi: https://doi.org/10.54172/kwpp4n86

Research Article

Open Access

Assessment of Content Cations Present in Groundwater Samples Collected from Wells of Ajdabya City and its Environs

Amal. S. Eltwati*[1] and Manal. H. Elgaddi[2]

***Corresponding author:** ammalsaleh1983@gmail.com
Department of Chemistry, University of Ajdabya, Ajdabya, Libya.

Second Author: ammalsaleh1983@gmail.com
Department of Chemistry, University of Benghazi, Benghazi, Libya.

Received:
23 September 2023

Accepted:
25 November 2023

Publish online:
31 December 2023

Abstract

The purpose of this study was aimed to evaluate the quality of the drinking water in fifteen wells from Ajdabya City and its surrounding areas. By measuring the conductivity, total dissolved solids, major calcium (Ca2+), magnesium (Mg2+), sodium (Na+), potassium(K+), lithium(Li+), and total hardness (TH) in the groundwater. According to this study, the conductivity, total dissolved solids, and cation concentrations were rose in the majority of the groundwater samples except in forth wall of Zuwaytinah area, which was in limiting value (EC = 770), (TDS =340), (TH =360), (Ca2+ =160). Meanwhile rest the chemical analysis were higher than limiting value (Na+= 390), (k+ 60) and (Li+ =60) when compared to the WHO and Libyan drinking water standards.

Keywords: Groundwater; Cations; Flame photometry; Titration; Ajdabya City.

INTRODUCTION

Water is the source of life on Earth for all living organisms, as Allah Almighty says in the Munificent Quran ﴿And, We made from water every living thing﴾ (The Prophets:30). The two main sources of it are surface water and groundwater (Dawood & Sanad, 2014; AZAZA et al., 2012), and about one-third of people on Earth use groundwater for drinking (Nickson et al., 2005). One valuable natural water resource that is suitable for residential use and is easily accessible is groundwater (Najafi et al., 2020). In arid and semiarid regions, groundwater has traditionally been the preferred source of drinking water (Loh et al., 2020). Subterranean water is the world's primary source of drinking water and is also utilized as a backup supply for the industrial and agricultural sectors (Mishra & Bhatt, 2008)). Elements exist in aquatic systems as suspended, colloidal ions, dissolved ions and complexes, and solid in sediments. The ionic strength, pH, redox potential, biological processes, and activities all have a significant impact on the concentrations of these ions (Arjonilla et al., 1994).

Numerous techniques for analyzing ions (anions and cations) in water have been documented in the literature. Water cation analysis has historically been done using flame atomic absorption spectrophotometry (Aberoumand & Deokule, 2009). Flame atomic emission is another name for flame photometry. The study of species in the form of atoms is known as spectrometry, and it primarily relies on the ionization of salts containing alkali metals that are drawn into a non-luminous flame.

When alkali metal salt absorbs enough energy from a flame, it vaporizes and emits light with a distinctive wavelength that can be seen by a change in color intensity (Chikhale & Chikhale, 2017).

The present study aims to evaluate a simple, fast, and accurate method for the determination of pH, electrical conductivity, and cations, which included (total hardness, calcium ion, magnesium ion, sodium ion, and potassium ion) in different sites of wells water samples of groundwater, which collected in the year 2019 from Ajdabya City in Libya and its Environs.

MATERIALS AND METHODS

Sample Collection:

In this study, fifteen groundwater samples were taken from three different areas in Ajdabya City and its surroundings: The Sultan and Zuwaytinah areas. Five samples from various well sites were taken from each locality. 500 ml plastic bottles were used to collect the samples. The water samples were later brought to the lab. A water quality parameter test was conducted right away. After that, nitric acid was added to the models in order to preserve the metal content for as long as possible during storage.

Materials

Sodium Hydroxide (NaOH) Guangdong, 515021, China. Ammoniachloride (NH_4Cl) Riedei-DeHaen Germany. Ethylenediaminetetraaceticdisodium ($EDTA_2Na$) Riedel-DeHaen Germany. Ammonia NH_3. Deionized water was used for preparation of solutions. And the reagents which used are Powder Eriochrome Black T and powder murexide MERK company Germany.

Electrical Conductivity and Total Dissolved Solids:

The conductivity and TDS measurements were carried out using (Conductivity / Temp / TDS meter Goldpoint Company Ltd (Taiwan)). Then, the samples were measured when the laboratory was reached, and stabilize the sample temperature at 25.

Determination of Total Hardness

The total hardness (TH) was measured by the Lind method, in this method we took 5-10ml of the groundwater sample, then the volume was completed with distilled water to 50ml and titrated with (Na2EDTA) solution 0.01N after raising the pH of the sample solution to 10 by adding 1ml of ammonia regulator solution. Then add a suitable amount of Erichrom Black-T powder as a dry indicator until the color changes to blue. Then we took the average of the reading. [10] The total hardness is calculated according to the following equation:

$$\text{Total Hardness} = \frac{\text{VNa2EDTA} \times \text{NNa2EDTA} \times 1000 \times \text{M.W as CaCO3}}{\mathbf{V}\text{sampl}}$$

Determination of Calcium ion:

Calcium ion was calculated by taking 5-10ml of the filtered groundwater sample and then softening the complete volume with distilled water to 50 ml in a correction method using the standard solution (Na2EDTA) 0.01N, then the pH raised to 13-14 by adding 2ml of NaOH 0.1N and used the Murexid as a dry powder 0.2 g indicator to change the color to solid blue (APHA, 1926). Calcium ions calculated according to the following equation:

$$\text{Calcium Hardness} = \frac{\text{V}_{\text{Na2EDTA}} \times \text{N}_{\text{Na2EDTA}} \times 1000 \times \text{M.W as CaCO3}}{\text{V}_{\text{Sample}}}$$

Determination of Magnesium ion:

Magnesium ion was estimated by the difference between total hardness and hardness of calcium as expressed in the following equation:

Magnesium hardness Mg (mg / L) = Total hardness $CaCO_3$ (mg/L) - Calcium hardness (mg / L)

Determination of ions (Na^+, K^+, Ba^{+2} and Li^+):
The Concentrations of different ions (Na^+, K^+, Ba^{+2}, and Li^+) were measured using flame photometer equipment. The device depends on the Flame Photo Meter on a solution containing metal ions in the flame.

RESULTS

The chemical parameters measured to electrical conductivity, total dissolved solids and some cations from groundwater wells were precisely analyzed and compared with the regulatory standards set by the World Health Organization and Libyan Standards Specification. According to the amount the cations Na+, and K+ were measured using Flame Photometer. Whereas Ca2+, Mg2+, and total hardness which determined by titration methods. The results reveal that the mean values of cation concentrations in groundwater samples studies were quite variable which are illustrated in Tables (1-6). From the results, that illustrated in Table 1, the conductivity and total dissolved solids of well samples in Ajdabya City were not within the allowable limit to Libya Standard Specification NO.82 for drinking water (750 -1200) (500-1000), all of which have high values (1309- 2810) (1083-1570). As noted in Table 2 the conductivity and total dissolved solids of wells water samples in the Zuwaytinah area were higher than the permissible limit. Except in well NO. 4, which the conductivity average and total dissolved solids values are approximately 770 mg/L and 340 mg/L respectively. Table 3 shows the conductivity and total dissolved solids of wells water samples in the Sultan area were very high values (3390-1361) (2243- 1077).

Table 1: The analytical results of wells water samples for conductivity and total dissolved solids (mg/L) in Ajdabya City.

Well site	1	2	3	4	5
EC	2810 ±0.153	1309 ±0.0743	1487 ±0.0653	1438 ±0.0272	1979 ±0.0840
TDS	1570 ±0.0048	1083±0.0574	1284±0.0761	1103±0.0032	1489±0.0659

Mean ± SD

Table 2: The analytical results of wells water samples for conductivity and total dissolved solids (mg/L) in Zuwaytinah area.

Well site	1	2	3	4	5
EC	1530±0.077	1155±0.603	1430±0.541	770±0.0967	3530±2,0455
TDS	1150±0.073	1030±0.037	1109±0.033	340±0.0043	1993 ±0.0436

Mean ± SD

Table 3: The analytical results of wells water samples for conductivity and total dissolved solids (mg/L) in Sultan area.

Well site	1	2	3	4	5
EC	3256 ±1.069	2690±0,322	3390±2.851	1876±0.0438	1361±0.0711
TDS	1860±0.055	1498±0.0908	2243±0.377	1366±0.0421	1077±0.033

Mean ± SD

The maximum concentrations of total hardness of wells water samples in Table 4 at Ajdabya City were not within the allowable limit according to Libya Standard Specification NO.82 for drinking water (200-500 mg/L). Except for groundwater samples of well site NO. 2, the amount of water

hardness was nearly 450 mg/L, which was match of the allowable limit. Table 5 recorded the amount of total hardness of wells water samples in the Zuwaytinah area was higher than the permissible limit. Except in wells NO. 2 and 4 which were average of total hardness values approximately 472 mg/L and 380 mg/L respectively.

Table 6 also showed the concentration of water hardness in the Sultan area's well samples, all of which were found to be over the allowable limit. Variations in the amount of heavy rain, leachate drainage from agricultural fields, and the use of well water for farming and gardening all had an impact on the total hydrocarbon (TH) content of groundwater. Water samples are classified as soft (>1–70 mg/L), moderately hard (75–150 mg/L), hard (150–300 mg/L), and extremely hard (> 300 mg/L) based on TH (Boyd, 2003). The groundwater wells under analysis had levels of lead above the permissible 500 mg/L drinking water limit. The water samples were deemed excessively hard and not fit for domestic use or consumption. Table 7 shows the comparison of the Libya standard NO.82 limits for Cations in water with WHO limits (mg/L).

Table 4: The analytical results of wells water samples for cations concentration (mg/L) in Ajdabya City.

Well site	TH	Ca	Mg	Na	K	Li
1	1226±0.588	812±0.011	414±0.009	390±0.965	60±0.003	10±0.007
2	450±0.065	226±0.022	224±0.0744	230±0.005	10±0.011	10±0.0322
3	592±0.081	320±1.012	272±0.090	320±0.076	200±0.015	30±0.099
4	632±0.172	360±0.0134	272±0.011	280±0.524	20±0.006	30±0.0322
5	773±0.987	426±0.832	347±0.004	340±0.099	20±0.0943	20±0.066

Mean ±SD. TH = Total Hardness

Table 5: The analytical results of wells water samples for cations concentration (mg/L) in Zuwaytinah area.

Well site	TH	Ca	Mg	Na	K	Li
1	747±0.0867	162±0.0944	585±0.0521	720±0.0965	100±1.094	60±0.0063
2	472±0.076	226±0.073	246±0.098	430±0.134	90±0.055	60±0.0433
3	735±0.0023	226±0.986	509±0.0547	570±0.861	80±0.997	60±0.033
4	380±0.943	160±1.009	220±0.022	390±0.654	60±1.066	60±0.643
5	3448±2.985	746±0.873	2702±0.512	4050±0.032	300±0.009	300±0.055

Mean ±SD. TH = Total Hardness

Table 6: The analytical results of wells water samples for cations concentration (mg/L) in Sultan area.

Well site	TH	Ca	Mg	Na	K	Li
1	1853±0.044	426±0.0941	1427±0.991	3500±2.054	200±0.006	200±0.031
2	1226±0.0376	240±0.33	986±0.721	600±0.0766	240±0.741	60±0.132
3	3228±1.381	692±0.806	2536±1.873	7150±2.965	350±0.0464	80±0.0877
4	772±0.055	226±0.070	546±0.543	640±0.135	40±0.733	30±0.125
5	720±0.0041	182±0.866	538±0.114	510±0.955	40±0.883	30±0.667

Mean ±SD. TH = Total Hardness

Table 7: Comparison of the Libya standard NO.82 limits for Cations in water with WHO limits (mg/L).

Major Ion	Libya standard NO.82 (mg/L)	WHO limit (mg/L)
TDS	500-1000	1000
TH	200-500	500
Ca^{2+}	75-200	200
Mg^{2+}	30-150	150
Na^{+}	20-200	200
K^{+}	10-40	100
Li^{+}	0-0.7	-

DISCUSSION

(812 mg/L). In addition, the present data illustrated that the lowest concentration of Ca2+ was found in wells NO. 1 and 4 of the Zuwaytinah area which were 162 mg/L and 160 mg/L respectively. While the other wells were not within the permissible limit. Whereas Ca2+ values in the Sultan area as shown in Table 6 find that all wells were not within the permissible limit, except well NO. 5 Ca2+ amount was within the permissible limit which was approximately 182 mg/L. The abundance of Ca2+ in water is mostly due to its usual presence in Earth's crust (Deshpande et al., 2012). Most of the groundwater wells had a high distribution of Ca2+, exceeding the WHO-recommended limit for drinking water (WHO, 2004). The main water chemistry of the groundwater wells may reflect the geology of the area. The total concentration of Ca2+ is the main factor that increases the hardness of water (Sadat-Noori et al., 2014). According to study results of magnesium concentration of wells water samples in Ajdabya City, note that all readings were higher than the permissible limit which is (30 mg/L -150 mg/L). Where the reading of the analytical results is nearly (224mg/L-414 mg/L). The highest values of magnesium ions in the Zuwaytinah area, which ranging 220mg/L to 2702mg/L. In addition, the present data illustrated that the highest concentration of Mg2+ in the Sultan area was found in all wells, which were nearly from 538 mg/L to 2536mg/L. The abundance of Mg2+ in the groundwater wells referred to the dissolution of all solids and rocks but mostly from limestone, dolomite, and gypsum, which are found in large quantities in some brines (Basem et al., 2010; Chenini et al., 2010).

Sultan area of all wells water samples were above of permitted limit which ranging from (20mg/L – 200mg/L). The presented information shows that potassium ion concentration in all wells water samples of Ajdabya City was within the permissible limit which is (10mg/L – 40mg/L). except in well NO. 1 the result obtained was nearly 60mg/L which overtook permissible limit. According to the results obtained in the present work, the K+ content in the Zuwaytinah area was not within permissible limits in all wells water samples. Whereas, found that the amount of K+ of both wells NO. 4 and 5 in of Sultan area which were within the permitted limit. while the highest average values of K+ content were found in wells NO. 1, 2, and 3 which outran the permitted limit. Potassium may primarily come from rock weathering in addition to solid and liquid wastes (Tikle et al., 2012; Belkhiri & Narany, 2015).

Tables delineate that Li+ concentration in Ajdabya City, Zuwaytinah area, and Sultan area of all wells water samples was above the permitted limit which ranging from (0 mg/L – 0.7 mg/L). Groundwater is a major source of freshwater in the Arab world, and in most cases, fresh groundwater originates from leakage and vertical precipitation of fresh rainwater, rivers, and lakes through cracks, fractures, and sedimentary rock layers into the aquifer. Groundwater is saltier than surface

water, salt concentrations may be higher than some of the taste, color, and hardness of the water below the surface of the earth, whether in saturated areas is the area filled with their water, or unsaturated which are directly below the surface of the earth and contain geological materials that makeup water and air in the spaces between the soil granules. Ions seeped out of rocks and soils and dissolved in water as a result of weathering and water circulation. The main elements affecting the geochemistry of the water are the geological formations, the water-rock interaction, and the relative mobility of ions (Yousef et al., 2009). It is important to consider major ions and their ratios when attempting to deduce how rock chemistry affects water composition (Shaltami et al., 2017).

CONCLUSION

In summary, most the results obtained in this study was higher than the Libya standard and WHO limit. Groundwater is saltier than surface water, salt concentrations may be higher than area to another. That are primarily come from rock nature in addition to solid and liquid wastes.

Duality of interest: The authors declare that they have no duality of interest associated with this manuscript.

Author contributions: Contribution is equal between authors.

Funding: No specific funding was received for this work.

REFERENCES

Aberoumand, A., & Deokule, S. S. (2009). Determination of elements profile of some wild edible plants. *Food Analytical Methods*, *2*, 116-119.

American Public Health Association. (1926). *Standard methods for the examination of water and wastewater* (Vol. 6). American Public Health Association.

Arjonilla, M., Gomez-Parra, A., & Forja, J. M. (1994). Sediment analysis does not provide a good measure of heavy metal bioavailability to Cerastoderma glaucum (Mollusca: Bivalvia) in confined coastal ecosystems. *Bulletin of Environmental Contamination and Toxicology;(United States)*, *52*(6).

Azaza, F. H., Ameur, M., Bouhlila, R., & Gueddari, M. (2012). Geochemical characterization of groundwater in a Miocene Aquifer, Southeastern Tunisia. *Environmental & Engineering Geoscience*, *18*(2), 159-174.

Basem, S., Sami Abu, F., & Alfred, Y. (2010). Assessment of groundwater quality in the Gaza Strip, Palestine using GIS mapping. *Journal of Water Resource and Protection*, *2010*.

Belkhiri, L., & Narany, T. S. (2015). Using multivariate statistical analysis, geostatistical techniques and structural equation modeling to identify spatial variability of groundwater quality. *Water Resources Management*, *29*, 2073-2089. Boyd, C. E. (2003). Guidelines for aquaculture effluent management at the farm-level. *Aquaculture*, *226*(1-4), 101-112.

Chikhale, H. U., & Chikhale, P. U. (2017). Flame photometric estimation of sodium and potassium ion present in water sample of Darna and Godavari River. *Int J of Sci & Eng Res*, *8*, 131-136.

Chenini, I., Farhat, B., & Ben Mammou, A. (2010). Identification of major sources controlling groundwater chemistry from a multilayered aquifer system. *Chemical Speciation & Bioavailability*, *22*(3), 183-189.

Dawood, D. H., & Sanad, M. I. (2014). Determination of ions (anion and cation) by ion chromatography in drinking water from talkha territory and some its villages, Dakahlia, Egypt. *Journal of Agricultural Chemistry and Biotechnology*, *5*(9), 215-226.

Deshpande, S. M., Aher, K. R., & Gaikwad, G. D. (2012). Assessment of Groundwater Quality and its Suitability for Drinking Uses in Warora tehsil, District Chandrapur, India. *Int. J. Rec. Tren. Sci. Technol*, *4*(3), 2249-8109.

Loh, Y. S. A., Akurugu, B. A., Manu, E., & Aliou, A. S. (2020). Assessment of groundwater quality and the main controls on its hydrochemistry in some Voltaian and basement aquifers, northern Ghana. *Groundwater for Sustainable Development*, *10*, 100296.

Mishra, A., & Bhatt, V. (2008). Physico-chemical and microbiological analysis of under ground water in VV Nagar and near by places of Anand District, Gujarat, India. *Journal of Chemistry*, *5*, 487-492.

Najafi Saleh, H., Valipoor, S., Zarei, A., Yousefi, M., Baghal Asghari, F., Mohammadi, A. A., ... & Mousavi Khaneghah, A. (2020). Assessment of groundwater quality around municipal solid waste landfill by using Water Quality Index for groundwater resources and multivariate statistical technique: a case study of the landfill site, Qaem Shahr City, Iran. *Environmental geochemistry and health*, *42*, 1305-1319.

Nickson, R. T., McArthur, J. M., Shrestha, B., Kyaw-Myint, T. O., & Lowry, D. (2005). Arsenic and other drinking water quality issues, Muzaffargarh District, Pakistan. *Applied geochemistry*, *20*(1), 55-68.4-

Sadat-Noori, S. M., Ebrahimi, K., & Liaghat, A. M. (2014). Groundwater quality assessment using the Water Quality Index and GIS in Saveh-Nobaran aquifer, Iran. *Environmental Earth Sciences*, *71*, 3827-3843.

Shaltami, O. R., Fares, F. F., Salloum, F. M., Elghazal, R., & El Feituri, M. A. (2017). Assessment of surface water quality for drinking and irrigation purposes in Ain Apollo, Shahat city, NE Libya. In *2nd Libyan Conference on Chemistry and its Applications (LCCA-2), Benghazi, Libya, Proceeding Book* (pp. 127-134).

Tikle, S., Saboori, M. J., & Sankpal, R. (2012). Spatial distribution of ground water quality in some selected parts of Pune city, Maharashtra, India using GIS. *Current World Environment*, *7*(2), 281.

World Health Organization. (2004). *Guidelines for drinking-water quality* (Vol. 1). World Health Organization.

Yousef, A. F., Salem, A. A., Baraka, A. M., & Aglan, O. S. (2009). The impact of geological setting on the groundwater occurrences in some Wadis in Shalatein–Abu Ramad Area, South Eastern Desert, Egypt. *Eur Water Pub (EWRA)*, *25*(26), 53-68.

Al-Mukhtar Journal of Basic Sciences 21 (2): 98-104, 2023
Doi: https://doi.org/10.54172/4kk1ad33

Research Article

Open Access

Synthesis, Characterization (I.R, Elemental analysis, Molar Conductivity), and Antibacterial Investigation of Complex produced by the reaction between Co (II) ion with mixed ligands of (Amoxicillin and Salen)

Hana. A. Binhamad [1], Reem. M. El-seifat[2], Rehab. A. Hesien[1] and Saleh. M. Bufarw*[1]

***Corresponding author:** saleh.bufarwa@omu.edu.ly Department of Chemistry, Omar Al-Mukhtar University, Libya

First author: saleh.bufarwa@omu.edu.ly Department of Chemistry, Omar Al-Mukhtar University, Libya

Second Author: saleh.bufarwa@omu.edu.ly Natural Resources and Environmental Sciences, Omar Al-Mukhtar University, Libya.

Third author: saleh.bufarwa@omu.edu.ly Department of Chemistry, Omar Al-Mukhtar University, Libya

Received:
30 September 2023

Accepted:
26 December 2023

Publish online:
31 December 2023

Abstract

The complex of cobalt (II) was prepared with the mixed ligand (amoxicillin and salen), and the formed complex was characterized using infrared (I.R.) spectroscopy, elemental analysis of (C%, H%, N%, and M%), molar conductivity methods, and melting point to characterize the complex. The results indicated that the complex is relatively insoluble in aqueous solutions and has significant antibiotic activity against colon bacteria. They also showed that the mixed complex formed has an octahedral structure and has a good electrolytic nature.

Keywords: Amoxicillin- Salen, Co complex, Infrared spectra, antibiotic.

INTRODUCTION

Metal complexes of drugs have changed many of the toxicological, pharmacological, physical, and chemical properties of those drugs (Wu et al., 2003). Dosage forms and drug distribution are strongly tied to a medication's physicochemical properties, and these properties are influenced by the complex formation mechanism in one way or another, which may be beneficial or maybe the opposite. These properties include the complex's solubility, energy absorption, stability, and chemical reaction mechanics (Nogueira Silva et al., 2008; Eze et al., 2014). Some studies have shown that the dissolution of some compounds is faster and the bioavailability is greater than that of the physical mixture, and it has been found that the processing properties such as physical state, flow ability, stability, etc. for complexes are better than those of free drugs (Marcolino et al., 2011).

Numerous metallic drug complexes were created to increase their potency, and after they had undergone a few successful clinical trials, they were analyzed and evaluated. (Mustapha et al.,2014) Amoxicillin is a β-lactam antibiotic that inhibits carboxypeptidase and transpeptidase enzymes, preventing the synthesis of peptidoglycan. Amoxicillin's bio-functional activity, like that of other penicillin, is based on the β-lactam ring (Hrioua et al., 2021). Blocking the activity of beta-lactamases, which are produced by certain bacteria, is currently the most advanced approach. These enzymes make the bacteria resistant to beta-lactam antibiotics. Metallic particles have gained a lot of attention due to their high surface-area-to-volume ratio and usefulness in biological applications. (Khatoon et al., 2017; Khatoon et al., 2018). Amoxicillin is a drug with a molecular weight of 419.45 gm.mole^{-1} and the chemical formula $C_{16}H_{19}N_3O_5S.3H_2O$. It is a crystalline powder that is an almost white or off-white powder that is only moderately soluble in alcohols like methanol ethanol and water (Martindale, 2009). Its UV maximum wavelength (λ_{max}) is 229,272 nm in 0.1N HCl and 230,274 nm in ethanol (O'Neil & Budavari, 2006). Amoxicillin complexes were synthesized with Ni (II), Cu (II), Zn (II), and Ag (I) ions and analyzed using C, H, and N elemental analysis as well as IR spectroscopy. The complexes exhibited enhanced biological activity for the drug (Imran et al., 2006).

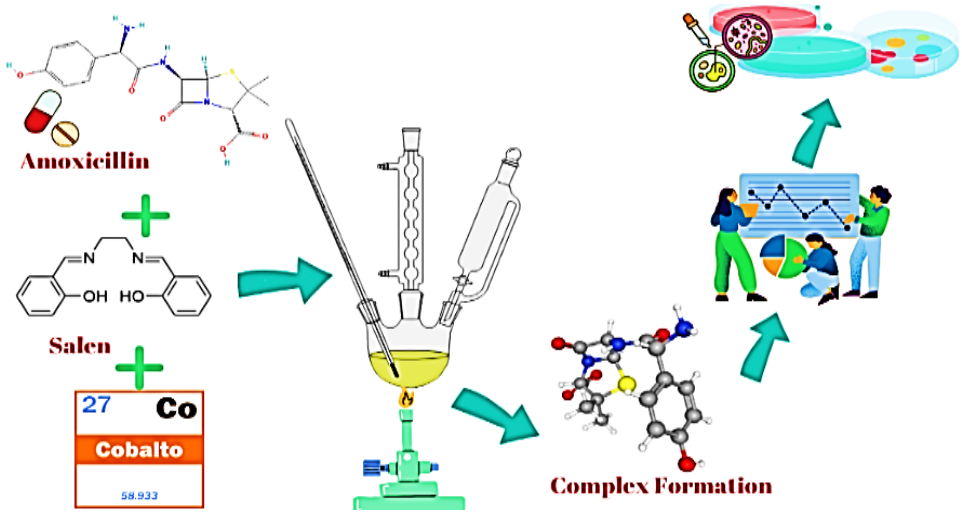

Fig (1). Graphical Abstract

In many kinds of literature, the efficacy of amoxicillin metallic complexes has been discussed (Abou-Hussein & Linert, 2014; Chohan et al., 2004). Studies conducted on the metal complexes of amoxicillin showed that it has great physiological and pharmacological importance, as the drug complexes are stronger than the drugs themselves (Anacona et al., 2002). The stability of complexes in aqueous and non-aqueous solutions has been investigated using a variety of physical and chemical approaches, such as spectroscopic methods (Ravichandran et al., 2014), potentiometric methods (Sonkamble, 2014), and methods of measuring conductivity (Rezayi et al,. 2011). In a previous study, researchers synthesized several complexes of amoxicillin with some transition metals. These complexes were analyzed using elemental analysis, IR, and mass spectra. The stability constant (K_f) of these chelates fell within the range of 10-7 to 10-14, and the molar ratio of the complexes was found to be Metal: Drug = 1:1, 1:2. (Zayed & Abdallah, 2005), In a recent study, mixed complexes of the β-lactam antibiotics ampicillin, amoxicillin, and cephalexin were prepared using solutions containing Co (II) and glycine anions (Gly). These complexes, named [Co Gly Ampicillin, Co Gly Amoxicillin, and Co Gly Cephalexin], were analyzed by pH-metric titration at 20 °C in an alkaline medium. (Alekseev & Samuilova, 2008). Salen is very important as a ligand as it easily binds to metal ions, forming complexes of various geometries due to the N_2 and O_2 donor

sites it contains. (Clarke & Storr, 2014; Atwood & Harvey, 2001). This study was aimed to synthesis, characterization (I.R, Elemental analysis, Molar Conductivity), and antibacterial investigation of complex produced by the reaction between Co (II) ion with mixed ligands of (Amoxicillin and Salen).

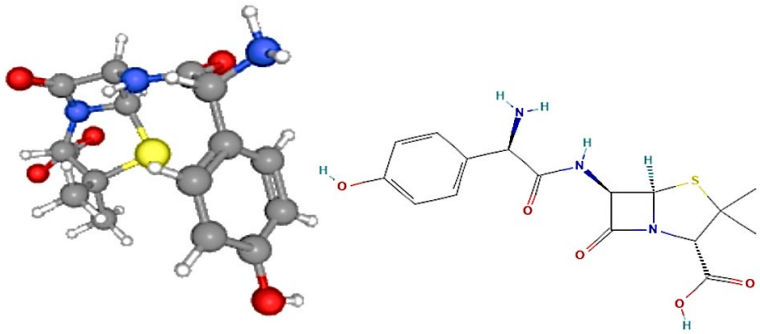

Fig 2: Chemical structure of amoxicillin (AMX)

MATERIALS AND METHODS

Amoxicillin-containing antibiotics were bought from commercial sources. 500 mg of amoxicillin capsules. Other chemicals used in this study are analytical-grade reagents and high purity from Fluka company. All buffer solutions from Sigma–Aldrich.

Synthesis of Salen ligand

To prepare Salen, 0.601 g (0.01 mol) of ethylene diamine and 2.44 g (0.02 mol) of salicylaldehyde were mixed in 50 ml of ethanol. The resulting mixture was re-condensed for 60 minutes. The red crystals formed were isolated by filtration. The crystals were then washed with ethanol and dried at room temperature in a dark place (Tsumaki, 1938).

Synthesis of the Metal-AMX Complexes

A solution of 25 ml methanol was used to dissolve 3 mmol of amoxicillin, followed by adding a solution containing 1 mmol of Co (II) metal chloride in 25 ml of methanol. The ligand was added in a 1:1:1 mole ratio, and the pH was adjusted to 8–9 by adding 1 M methanolic ammonia solution. The mixture was heated at 60–70 ºC with constant stirring for about 2 hours. It was then left overnight, filtered, and washed with residual anhydrous calcium chloride and methanol. The collected yield was 62.7% (Refat et al., 2014; Bufarwa & Abdel-Latif, 2022).

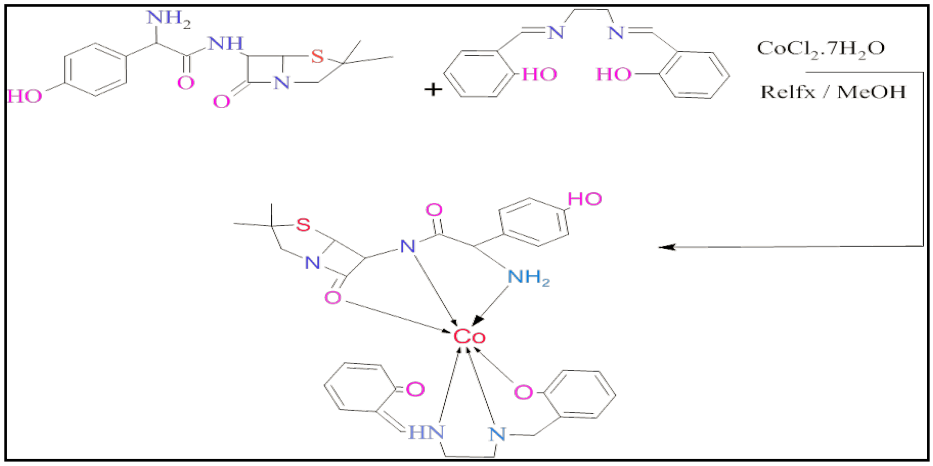

Fig 3: Preparation of [Co (AMX)(S)]

Molar Conductance

The conductivity of a 10^{-3} M complex solution in DMF was measured on a model HACH meter to determine its molar conductance.

Melting point measurements

To determine the melting points of the complex, we used the Stuart Scientific electrothermal melting point apparatus with glass capillary tubes in Celsius degrees.

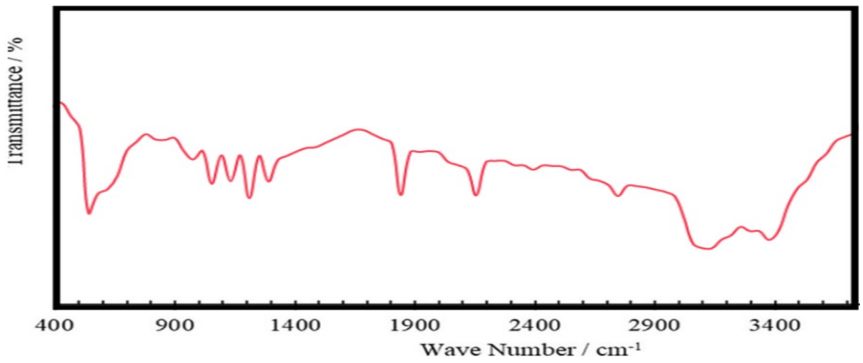

Fig 4: FT-IR of [Co(AMX)(S)]

RESULTS AND DISCUSSION

Elemental analysis of the solid complex was conducted to compare the calculated and found values for carbon, hydrogen, and nitrogen. Table 1 shows the obtained elemental analysis values. Conductivity measurement of the prepared complex also revealed that chloride ions are present outside the coordination sphere.

Table 1: The proposed formula, color, melting point, conductivity, and elemental analysis of the complex

Compound	M. wt. (g/mol)	Yield %	Color	Conductivity µS	M.P	Anal. Calc. (Found)%			
						N	H	C	Co
[Co (AMX)(S)] $C_{31}H_{37}CoN_5O_5S$	650.65	62.7	Red	121	248	54.75 (57.22)	5.38 (5.73)	9.88 (10.76)	8.52 (9.06)

FT-IR spectra: Studying the infrared spectrum is very important to determine the status of the chelation process as well as the location of coordination. Figure 3 shows the FT-IR spectra of the mixed complex of amoxicillin (AMX) and salen (S) with the cobalt (II) ion. At 1400cm^{-1}, the benzene ring's stretching vibration band v(C=C) is exhibited (Hrioua *et al*., 2021). While the bands of the hydroxyl and ammonium groups still appear unchanged, as they have not undergone any displacement because they did not enter as ligands in the formation of the complex (Gasheva *et al*., 1984). The stretching and vibration bands between metal ions and oxygen of the carbonyl group are responsible for the occurrence of bands at 500-600 cm^{-1}. Similarly, the vibration bands between amino groups and metal ions are classified as v(M-N) stretching bands between 400 and 500 cm^{-1} (Reiss *et al*., 2015). The distinctive band at about 3300 cm-1 indicates the presence of water molecules outside the coordination sphere in AMX complexes.

Antibacterial activity

The disk diffusion method has been used to examine the antibacterial effectiveness of the cobalt complexes (AMX.S) against ***E. coli*** (Bonev *et al*., 2008). The type of the metal ion and the chelate stability are likely to be blamed for the antibacterial action of AMX-salen complexes (Hrioua *et al*., 2021). Antibiotics made of metal complexes are very effective against resistant strains. Due to their potential to affect drug-induced metallo-enzyme inhibition, cobalt ions remain an area of interest in bioinorganic research for their impact on pathogens, influenza, cancers, and inflammation (Saleh *et al*., 2023).

Table 2: Inhibitor zone of antibacterial by different concentrations of complex

Concentration µg/L	Inhibitor zone diameter (in mm)	
	AMX	[Co(AMX)(S)]
10	-	10.76
25	-	15.68
50	12.4	19.43

CONCLUSION

The mixed amoxicillin ligands were studied in the form of capsules and the salen ligand with the cobalt binary ion, and some properties were studied to confirm the formation of a complex of mixed ligands of this type. The results showed that the complex formed has an octahedral form, and is an electrolyte in nature because the two chloride atoms are outside the coordination sphere of the complex, and are stable under normal conditions. It was observed that as the concentration of the complex increased, its effectiveness against E. coli bacteria increased.

Duality of interest: The authors declare that they have no duality of interest associated with this manuscript.

Author contributions: Contribution is equal between authors.

Funding: No specific funding was received for this work.

REFERENCES

Abou-Hussein, A. A., & Linert, W. (2014). Synthesis, spectroscopic, coordination and biological activities of some organometallic complexes derived from thio-Schiff base ligands. *Spectrochimica Acta Part A: Molecular and Biomolecular Spectroscopy*, *117*, 763-771.

Anacona, J. R., Ramos, N., de Delgado, G. D., & Roque, E. M. (2002). Coordination Behavior of Sulfathiazole: Crystal Structure of [Cu (en) 2 (OH2) 2][Sulfathiazole] 2· 2H2O (en= ethylenediamine): Antibacterial activity. *Journal of Coordination Chemistry*, *55*(8), 901-908.

Alekseev, V. G., & Samuilova, I. S. (2008). Complex formation in systems cobalt (II)-glycine-beta-lactam antibiotics. *Russian journal of Inorganic chemistry*, *53*, 327-329.

Atwood, D. A., & Harvey, M. J. (2001). Group 13 compounds incorporating salen ligands. *Chemical reviews*, *101*(1), 37-52.

Bonev, B., Hooper, J., & Parisot, J. (2008). Principles of assessing bacterial susceptibility to antibiotics using the agar diffusion method. *Journal of antimicrobial chemotherapy*, *61*(6), 1295-1301.

Bufarwa, S. M., & Abdel-Latif, S. A. (2022). Spectroscopic, thermal, and conductometric investigation of some (arylazo) quinolin-8-ol and their complexes with the divalent ions of Mn, Ni, Cu, and Zn.

Chohan, Z. H., Pervez, H., Rauf, A., Khan, K. M., & Supuran, C. T. (2004). Isatin-derived antibacterial and antifungal compounds and their transition metal complexes. *Journal of Enzyme Inhibition and Medicinal Chemistry*, *19*(5), 417-423.

Clarke, R. M., & Storr, T. (2014). The chemistry and applications of multimetallic salen complexes. *Dalton Transactions*, *43*(25), 9380-9391.

Eze, F. I., Ajali, U., & Ukoha, P. O. (2014). Synthesis, physicochemical properties, and antimicrobial studies of Iron (III) complexes of ciprofloxacin, cloxacillin, and amoxicillin. *International journal of medicinal chemistry*, *2014*.

Gasheva, L. M., Kalinkova, G., Minkov, E., & Krestev, V. (1984). IR spectroscopic investigations of amoxicillin trihydrate, included in the technological models sirup granules in ethylcellulose. *Journal of Molecular Structure*, *115*, 323-326.

Hrioua, A., Loudiki, A., Farahi, A., Bakasse, M., Lahrich, S., Saqrane, S., & El Mhammedi, M. A. (2021). Recent advances in electrochemical sensors for amoxicillin detection in biological and environmental samples. *Bioelectrochemistry*, *137*, 107687.

Hrioua, A., Loudiki, A., Farahi, A., Laghrib, F., Bakasse, M., Lahrich, S., ... & El Mhammedi, M. A. (2021). Complexation of amoxicillin by transition metals: Physico-chemical and antibacterial activity evaluation. *Bioelectrochemistry*, *142*, 107936.

Imran, M., Iqbal, J., Mehmood, T., & Latif, S. (2006). Synthesis, characterization and in vitro screening of amoxicillin and its complexes with Ag (I), Cu (II), Co (II), Zn (II) and Ni (II). *Journal of Biological Sciences*, *6*(5), 946-949.

Khatoon, U. T., Rao, G. N., Mohan, K. M., Ramanaviciene, A., & Ramanavicius, A. (2017). Antibacterial and antifungal activity of silver nanospheres synthesized by tri-sodium citrate assisted chemical approach. *Vacuum*, *146*, 259-265.

Khatoon, U. T., Rao, G. N., Mohan, M. K., Ramanaviciene, A., & Ramanavicius, A. (2018). Comparative study of antifungal activity of silver and gold nanoparticles synthesized by facile chemical approach. *Journal of environmental chemical engineering*, *6*(5), 5837-584

Marcolino, V. A., Zanin, G. M., Durrant, L. R., Benassi, M. D. T., & Matioli, G. (2011). Interaction of curcumin and bixin with β-cyclodextrin: complexation methods, stability, and applications in food. *Journal of agricultural and food chemistry*, *59*(7), 3348-3357.

Martindale, C. (2009). *The complete drug reference* (Vol. 1). S. C. Sweetman (Ed.). London: Pharmaceutical press.

Mustapha, A. N., Ndahi, N. P., Paul, B. B., & Fugu, M. B. (2014). Synthesis, characterization and antimicrobial studies of metal (II) complexes of ciprofloxacin. *Journal of chemical and Pharmaceutical Research*, *6*(4), 588-593.

Nogueira Silva, J. J., Pavanelli, W. R., Salazar Gutierrez, F. R., Alves Lima, F. C., Ferreira da Silva, A. B., Santana Silva, J., & Wagner Franco, D. (2008). Complexation of the anti-Trypanosoma cruzi drug benznidazole improves solubility and efficacy. *Journal of Medicinal Chemistry*, *51*(14), 4104-4114.

O'Neil, M. J, Budavari, S. (2006). The Merck Index, Merck Research Laboratories, Merck and Co. Inc, Rahway, USA. 83.

Ravichandran, R., Rajendran, M., & Devapiriam, D. (2014). Antioxidant study of quercetin and their metal complex and determination of stability constant by spectrophotometry method. *Food chemistry*, *146*, 472-478.

Refat, M. S., Al-Maydama, H. M., Al-Azab, F. M., Amin, R. R., & Jamil, Y. M. (2014). Synthesis, thermal and spectroscopic behaviors of metal–drug complexes: La (III), Ce (III), Sm (III) and Y (III) amoxicillin trihydrate antibiotic drug complexes. *Spectrochimica Acta Part A: Molecular and Biomolecular Spectroscopy*, *128*, 427-446.

Reiss, A., Samide, A., Ciobanu, G., & Dabuleanu, I. (2015). Synthesis, spectral characterization and thermal behaviour of new metal (II) complexes with Schiff base derived from amoxicillin. *Journal of the Chilean Chemical Society*, *60*(3), 3074-3079.

Rezayi, M., Ahmadzadeh, S., Kassim, A., & Heng, L. Y. (2011). Thermodynamic studies of complex formation between Co (Salen) ionophore with chromate (II) ions in AN-H2O binary solutions by the conductometric method. *Int. J. Electrochem. Sci*, *6*, 6350-6359.

Saleh, M., Reem, M., Attitalla, I. H., & Saleh, A. (2023). Algal Bioremediation: Heavy Metals Removal And Evaluation Of Biological Activities In Sewage Plant. *Journal of Survey in Fisheries Sciences*, 1355-1365.

Sonkamble, S. (2014). Metal-ligand stability constants of Fe (III), Cd (II), Co (II), Ni (II), Zn (II) metal ion complexes with Lorazepam in aquo-organic media at 0.1 M ionic strength pH metrically. *Appl. Sci. Res*, *5*(4), 171-175.

Tsumaki, T. (1938). Nebenvalenzringverbindungen. IV. über einige innerkomplexe Kobaltsalze der Oxyaldimine. *Bulletin of the Chemical Society of Japan*, *13*(2), 252-260.

Wu, G., Wang, G., Fu, X., & Zhu, L. (2003). Synthesis, crystal structure, stacking effect and antibacterial studies of a novel quaternary copper (II) complex with quinolone. *Molecules*, *8*(2), 287-296.

Zayed, M. A., & Abdallah, S. M. (2005). Synthesis and structure investigation of the antibiotic amoxicillin complexes of d-block elements. *Spectrochimica Acta Part A: Molecular and Biomolecular Spectroscopy*, *61*(9), 2231-2238.